

Fused combiners for photonic crystal bers

Noordegraaf, Danny; Lægsgaard, Jesper; Broeng, Jes; Skovgaard, Peter M. W.

Publication date:
2012

Document Version
Publisher's PDF, also known as Version of record

[Link back to DTU Orbit](#)

Citation (APA):
Noordegraaf, D., Lægsgaard, J., Broeng, J., & Skovgaard, P. M. W. (2012). Fused combiners for photonic crystal bers. Kgs. Lyngby: Technical University of Denmark (DTU).

DTU Library

Technical Information Center of Denmark

General rights

Copyright and moral rights for the publications made accessible in the public portal are retained by the authors and/or other copyright owners and it is a condition of accessing publications that users recognise and abide by the legal requirements associated with these rights.

- Users may download and print one copy of any publication from the public portal for the purpose of private study or research.
- You may not further distribute the material or use it for any profit-making activity or commercial gain
- You may freely distribute the URL identifying the publication in the public portal

If you believe that this document breaches copyright please contact us providing details, and we will remove access to the work immediately and investigate your claim.

Fused combiners for photonic crystal fibers

Ph.D. Thesis
Danny Noordegraaf

January 2nd, 2012

 **DTU Fotonik**
Department of Photonics Engineering

DTU Fotonik
Department of Photonics
Engineering
Technical University of Denmark
Building 345V
DK-2800 Kgs. Lyngby
Denmark

 **NKT** Photonics

NKT Photonics A/S
Department of Fiber
Technology
Blokken 84
DK-3460 Birkerød
Denmark

Preface

This thesis is a part of the formal requirements to obtain the Ph.D. degree at the Technical University of Denmark. The work was carried out from April 2008 to January 2012. The project is a collaboration between NKT Photonics A/S and the Department of Photonics Engineering at the Technical University of Denmark.

The major part of the work took place at NKT Photonics A/S in Birkerød, Denmark. Some of the work was carried out abroad during short stays. The work on beam combining of high-power fiber lasers was carried out at the labs of Rofin in Hamburg, Germany. Characterization of fused fiber bundles, the so called hexabundles, was done at the University of Sydney. Insight into the use of the astrophotonics components was obtained at the Australian Astronomical Observatory in Epping, Sydney, Australia, and at the Anglo-Australian Telescope, Coonabarabran, Australia.

The project was financed by NKT Photonics and the Danish Agency for Science, Technology and Innovation. The project was supervised by

- Peter M. W. Skovgaard, Ph.D., NKT Photonics A/S, Birkerød, Denmark.
- Jes Broeng, Ph.D., NKT Photonics A/S, Birkerød, Denmark.
- Jesper Lægsgaard, Associate Professor, DTU Fotonik, Technical University of Denmark, Kgs. Lyngby, Denmark.

Copenhagen, January 2nd 2012

Danny Noordegraaf

Contents

Preface	iii
Acknowledgements	ix
Abstract	xi
Resumé (Danish abstract)	xiii
Publication list	xv
Award	xix
1 Introduction	1
2 Optical fibers	5
2.1 Step-index fibers	5
2.1.1 Fiber optical modes	6
2.1.2 Double-clad fibers	8
2.2 Photonic crystal fibers	9
2.2.1 Air-clad photonic crystal fibers	10
2.3 Modeling of optical fibers	11
2.4 Fusion splicing of optical fibers	13
2.5 Tapering of optical fibers	14
2.5.1 Tapering of single-mode fibers	14
2.5.2 Tapering of multi-mode fibers	16
3 High power fiber lasers and amplifiers	19
3.1 Double-clad active fibers	20
3.1.1 Double-clad fiber lasers	20

3.1.2	Double-clad fiber amplifiers	20
3.1.3	Air-clad fibers	21
3.2	Fused combiners for double-clad fibers	21
3.3	Fiber coupled laser diodes	25
3.4	Power limitations of fiber lasers and amplifiers	25
3.5	High-power beam combining	26
4	Pump combiners for air-clad fiber lasers	29
4.1	Pump combiner fabrication	29
4.2	Air-clad fiber laser	32
4.3	Gain switched air-clad fiber laser for supercontinuum generation	34
4.3.1	Gain switched air-clad fiber laser	35
4.3.2	Supercontinuum generation with air-clad fiber laser	36
5	Signal combiners for beam combining of fiber lasers	39
5.1	Signal combiner fabrication	39
5.2	High-power connector	41
5.3	Optical testing of the signal combiner	42
5.4	High-power fiber lasers	43
5.5	High-power beam combining	43
6	Pump/signal combiners for air-clad fiber amplifiers	47
6.1	Mode field diameter preserving fiber tapers	48
6.1.1	Air-hole based 6 μm MFD feed-through	48
6.1.2	Air-hole based 15 μm MFD feed-through	51
6.1.3	F-doped rod based 15 μm MFD feed-through	53
6.2	Pump/signal combiner fabrication	55
6.3	Pulse amplification with active air-clad fiber	58
6.4	Supercontinuum generation with fiber amplifier	61
7	Combiners for astrophotonics	65
7.1	Hexabundles	67
7.1.1	7 port hexabundles	69
7.1.2	Cladding etch of 7 port hexabundles	69
7.1.3	Degree of fusing of the 7 port hexabundles	72
7.1.4	61 port hexabundle	73
7.2	Photonic lanterns	74
7.2.1	Photonic lantern fabrication	75
7.2.2	7 port photonic lantern	77

7.2.3	61 port photonic lantern	84
7.2.4	19 port photonic lantern with multi-mode delivery fiber	87
8	Conclusion	93
A	Formula derivations	97
A.1	Minimum single-mode fiber taper length for a linear taper profile	97
A.2	Minimum multi-mode fiber taper length for a linear taper profile	98
	List of Acronyms	99
	Bibliography	101

Acknowledgements

First of all I would like to thank all of my supervisors for their support, suggestions, guidance, and for making this project possible. Peter Skovgaard for building the components group, his contagious enthusiasm and visions for creating new components. Jes Broeng for creating some fantastic optical fibers and never ending support. Jesper Lægsgaard for always helping out with theoretical difficulties.

I would also like to extend a very special thanks to Martin D. Maack for his pioneering work within pump combiners for photonic crystal fibers, for all his help in developing new components, and for always kindly sharing his experimental and theoretical knowledge.

Thanks to all the people involved in the development of the components for astrophotonics. A special thanks to Professor Joss Bland-Hawthorn from the University of Sydney, for his visions for creating components for astrophotonics. Jon Lawrence from the Australian Astronomical Observatory for the telescope testing of the components that were fabricated in this Ph.D. project. Also, a special thanks to both Joss and Jon for hosting a very pleasant stay in Australia in July 2011. I would also like to thank Roger Haynes for testing the very first prototype photonic lanterns. Julia Bryant for demonstrating the astronomer way of characterizing the hexabundles during my stay in Sydney. Sergio Leon-Saval for kindly providing the simulations on the 7 port photonic lanterns. Chris Springob for accompanying me on the visit to the Anglo-Australian Telescope.

Also thanks to all the people involved in the laser combiner project. Frank Becker and Stefan Belke from Rofin for providing the high-power fiber lasers and aiding in the testing of the signal combiners at the Rofin laser facilities in Hamburg, Germany. Mats Blomqvist from Optoskand for providing the high-power connectors.

Thanks to my former fellow Ph.D. students Christina B. T. Olausson,

Jens Kristian Lyngsøe and Marko Laurila for always helping out and for their great company on a number of travels abroad. Also thanks to my fellow Ph.D. student Casper Larsen for his great work on the supercontinuum generation with gain-switched fiber lasers. Also a very special thanks to all the people at NKT Photonics who have been involved in the various projects that I have been a part of, and to all the always positive and helpful people in the lab.

Finally, I would also like to thank Eva, my family and all my friends for their help and support during this Ph.D. study.

Abstract

The work presented in this Ph.D. thesis focuses on the fabrication of fused combiners for high-power fiber lasers and amplifiers. The main focus of the Ph.D. project was to further develop the fused pump combiners for air-clad photonic crystal fibers (PCFs), and implement a signal feed-through in these combiners. Such a pump/signal combiner enables the fabrication of all spliced fiber amplifier systems based on the PCFs technology. Amplifier systems interfaced only by standard multi-mode (MM) and single-mode (SM) fibers are easy to use, since all-spliced systems can be made and bulk optics are avoided. Pump/signal combiners were realized in two versions; one with a 12 μm mode field diameter (MFD) signal feed-through and one with a 15 μm MFD feed-through.

A signal combiner for combining the SM output from multiple fiber lasers into a single MM fiber was also realized. The component was based on a tapered fiber bundle approach and was tested up to 2.5 kW of combined output power.

Two components for the field of astrophotonics have also been developed. The first was a fused fiber bundle, designed to be placed in the focal plane of a telescope. By measuring the spectral content out of the individual fibers in the bundle, more detailed observations of large astronomical objects can be achieved. The second component was a further development of the MM to SM converters or photonic lanterns. These components were developed for the field of astrophotonics, where the transformation of MM starlight into an ensemble of SM fibers enables filtering with advanced fiber Bragg gratings (FBGs).

Resumé (Danish abstract)

Denne Ph.D. afhandling omhandler fremstilling af fiber koblere til høj-effekts fiber lasere og forstærkere. Hovedfokus i afhandlingen ligger på en videreudvikling af pumpe koblere til air-clad fotoniske krystal fibre (PCF), og implementeringen af en signal gennemførsel i disse koblere. En pumpe/signal kobler muliggør fremstilling af fiber baserede splidsede fiber forstærker-systemer baseret på PCF teknologien. Forstærker systemer hvis interface udelukkende består af standard multi-mode og single-mode fibre, er nemme at anvende fordi fuldt splidsede systemer kan konstrueres uden brug af linse optik. Pumpe/signal koblere blev i projektet fremstillet i to versioner; en med en $12\ \mu\text{m}$ mode field diameter (MFD) signal gennemførsel og en med en $15\ \mu\text{m}$ MFD gennemførsel.

En signal kobler, der kombinerer lyset fra flere single-mode (SM) fiber lasere over i en enkelt multi-mode (MM) fiber blev også fremstillet. Komponenten er baseret på en taperet fiber bundt fremgangsmåde og blev testet op til 2.5 kW kombineret udgangs effekt.

To komponenter til astrofotonik blev også fremstillet. Den første var et fiber bundt, designet til at blive placeret i fokal planet af et teleskop. Ved at måle det spektrale indhold i de enkelte fibre, opnås en mere detaljeret observation af store astronomiske objekter. Den anden komponent var videreudvikling af en MM til SM kobler. Disse komponenter blev udviklet til brug indenfor astrofotonik, hvor koblingen af MM stjernelys til en samling af SM fibre muliggør filtrering med avancerede Bragg gitre.

Publication list

Journal publications

1. **D. Noordegraaf**, M. D. Maack, P. M. W. Skovgaard, S. Agger, R. H. Sandberg, T. Feuchter, J. Broeng, C. L. Thomsen, and J. Lægsgaard, “Pump/signal combiner for air-clad fibers and the application within pulse amplification and supercontinuum generation,” Submitted to *Opt. Express*.
2. C. Larsen, S. T. Sørensen, **D. Noordegraaf**, K. P. Hansen, K. E. Mattsson, and O. Bang, “Zero dispersion dependencies in CW and Quasi-CW pumped supercontinuum generation,” Submitted to *IEEE Phot. Tech. Letters*.
3. **D. Noordegraaf**, P. M. W. Skovgaard, R. S. Helmsby, M. D. Maack, J. Bland-Hawthorn, J. Lawrence, and J. Lægsgaard, “19 port photonic lantern with multi-mode delivery fiber,” Accepted for publication in *Opt. Letters*.
4. **D. Noordegraaf**, M. D. Maack, P. M. W. Skovgaard, M. H. Sørensen, J. Broeng, and J. Lægsgaard, “Mode field diameter preserving fiber tapers,” *Opt. Lett.* **36**, 4524–4526 (2011).
5. K. P. Hansen, C. B. Olausson, J. Broeng, **D. Noordegraaf**, M. D. Maack, T. T. Alkeskjold, M. Laurila, T. Nikolajsen, P. M. W. Skovgaard, M. H. Sørensen, M. Denninger, C. Jakobsen, and H. R. Simonson, “Airclad fiber laser technology,” *Opt. Engineering* **50** (2011).
6. C. Larsen, **D. Noordegraaf**, P. M. W. Skovgaard, K. P. Hansen, K. E. Mattsson, and O. Bang, “Gain-switched CW fiber laser for improved supercontinuum generation in a PCF,” *Opt Express* **19**, 14883–14891 (2011).

7. J. Bland-Hawthorn, J. Bryant, G. Robertson, P. Gillingham, J. O'Byrne, G. Cecil, R. Haynes, S. Croom, S. Ellis, M. Maack, P. Skovgaard, **D. Noordegraaf**, "Hexabundles: imaging fiber arrays for low-light astronomical applications," *Opt. Express* **19**, 2649–2661 (2011).
8. C. B. Olausson, L. Scolari, L. Wei, **D. Noordegraaf**, J. Weirich, T. T. Alkeskjold, K. P. Hansen, A. Bjarklev, "Electrically tunable Yb-doped fiber laser based on a liquid crystal photonic bandgap fiber device," *Opt. Express* **18**, 8229–8238 (2010).
9. **D. Noordegraaf**, P. M. W. Skovgaard, M. D. Maack, J. Bland-Hawthorn, R. Haynes, and J. Lægsgaard, "Multi-mode to single-mode conversion in a 61 port Photonic Lantern," *Opt. Express* **18**, 4673–4678 (2010).
10. **D. Noordegraaf**, P. M. Skovgaard, M. D. Nielsen, and J. Bland-Hawthorn, "Efficient multi-mode to single-mode coupling in a photonic lantern," *Opt. Express* **17**, 1988–1994 (2009).

Conference contributions

1. C. Larsen, **D. Noordegraaf**, K. P. Hansen, K. E. Mattsson, O. Bang, "Photonic crystal fibers for supercontinuum generation pumped by a gain-switched CW fiber laser," Accepted for presentation at Photonics West (2012).
2. C. Larsen, P. M. W. Skovgaard, **D. Noordegraaf**, K. P. Hansen, K. E. Mattsson, O. Bang, "Supercontinuum generation in a photonic crystal fiber pumped by a gain-switched high-power fiber laser," in *CLEO/Europe and EQEC 2011 Conference Digest*, OSA Technical Digest (CD) (Optical Society of America, 2011), paper CD7.2.
3. J. Broeng, M. Laurila, **D. Noordegraaf**, C. B. Olausson, K. P. Hansen, M. D. Maack, T. T. Alkeskjold, J. K. Lyngsøe, M. Denninger, C. Jakobsen, H. R. Simonsen, "Photonic crystal fibres in the market," in *Opto-Electronics and Communications Conference* (2011).
4. **D. Noordegraaf**, M. D. Maack, P. M. W. Skovgaard, J. Johansen, F. Becker, S. Belke, M. Blomqvist, and J. Lægsgaard, "All-fiber 7x1 signal combiner for incoherent laser beam combining," *Proc. SPIE* **7914**, 79142L (2011).

5. J. Bland-Hawthorn, J. Bryant, G. Robertson, P. Gillingham, J. O'Byrne, G. Cecil, R. Haynes, S. Groom, S. Ellis, M. D. Maack, P. M. W. Skovgaard, and **D. Noordegraaf**, "Hexabundles: imaging fibre arrays for low-light astronomical applications," Proc. SPIE **7735**, 773541 (2010).
6. C. B. Olausson, L. Scolari, L. Wei, **D. Noordegraaf**, J. Weirich, T. T. Alkeskjold, K. P. Hansen, and A. Bjarklev, "Electrically Tunable Liquid Crystal Photonic Bandgap Fiber Laser," Proc. SPIE **7580**, 75801D (2010).
7. **D. Noordegraaf**, P. M. W. Skovgaard, M. D. Maack, J. Bland-Hawthorn, R. Haynes, and J. Lægsgaard, "Efficient MM to SM conversion in a 61 port photonic lantern," Proc. SPIE **7580**, 75802D (2010).
8. **D. Noordegraaf**, M. D. Maack, P. M. W. Skovgaard, S. Agger, T. T. Alkeskjold, and J. Lægsgaard, "7+1 to 1 pump/signal combiner for air-clad fiber with 15 μm MFD PM single-mode signal feed-through," Proc. SPIE **7580**, 75801A (2010).
9. **D. Noordegraaf**, M. D. Nielsen, P. M. W. Skovgaard, S. Agger, K. P. Hansen, J. Broeng, C. Jakobsen, H. R. Simonsen, and J. Lægsgaard, "Pump combiner for air-clad fiber with PM single-mode signal feed-through," in *Conference on Lasers and Electro-Optics/International Quantum Electronics Conference*, OSA Technical Digest (CD) (Optical Society of America, 2009), paper CThGG6.

Award

Danny Noordegraaf was awarded the 2011 Annual Award of the Danish Optical Society.

Statement from the jury (English):

Danny is at the end of a successful industrial Ph.D. project, in which he has developed some of the world's most advanced fiber based couplers. These couplers address industrial lasers (especially high-power lasers based on photonic crystal fibers) and telescopes (where the couplers represent a breakthrough within astronomical research). Danny has played a main role in the development of the components, and Danny has proven to be a very competent and cooperative person.

We especially wish to emphasize Danny's ability to combine academic research and industrial development. He sets a good example for young researchers within optics in Denmark, and a person that we in the Danish Optical Society can rightfully acknowledge.

Danny's educational background is from the Technical University of Denmark, where he received a Master of Engineering within Applied Physics. His master project was made at the Department of Photonics Engineering at DTU ("Long period gratings in liquid crystal photonic bandgap fibers", for which he was awarded the grade 13). The current industrial Ph.D. study is a collaboration between the department of photonics engineering at DTU and NKT Photonics A/S.

Statement from the jury (Danish):

Danny står ved afslutningen af et succesfuldt erhvervs Ph.D. projekt, hvor han har udviklet verdens mest avancerede lysleder-koblere. Disse koblere adresserer bla. industrielle lasere (specielt høj effekts-lasere baseret på fotoniske krystal fibre) og teleskoper (hvor koblerene repræsenterer et genembrud indenfor astronomisk forskning). Danny's rolle har været (og er fortsat) som hovedansvarlig for denne udvikling - og Danny har udmærket sig som en ekstraordinær kompetent og samarbejdsvillig person.

Vi ønsker specielt at fremhæve Danny's evne til at kombinere den akademisk forskning og den industrielle udvikling. På dette punkt er han et værdigt forbillede for yngre forskere indenfor optik i Danmark - og en person vi i Dansk Optisk Selskab med rette kan fremhæve og anerkende.

Danny's uddannelsesmæssige baggrund er fra DTU, hvor han er civilingeniør fra teknisk-fysik retningen. Hans speciale blev udført på DTU Fotonik ("Long period gratings in liquid crystal photonic bandgap fibers", hvor han fik karakteren 13). Det nuværende erhvervs Ph.D. studium er i samarbejde med DTU Fotonik og NKT Photonics A/S.

Chapter 1

Introduction

The first low-loss optical fibers were demonstrated in the 1970's by researchers at Corning Glass Works [1, 2]. These were solid thin glass fibers, with a high refractive index core and a low index cladding. Guiding of light in the core of these waveguides is possible by the principle of total internal reflection (TIR). Today, these fibers are widely used within optical communication, and transporting an ever increasing amount of data traffic around the world [3].

Optical fibers are also used to realize fiber lasers and amplifiers. For this application, the core of the fiber is doped with an active element such as erbium or ytterbium. Fiber lasers have a number of advantages over solid state lasers or gas lasers. A fiber is easily cooled, it has a high efficiency, it allows for easy beam delivery, and a high beam quality can be achieved with single-mode (SM) fibers. The fiber can either be core pumped or cladding pumped [4, 5]. The cladding pumped configuration is used for reaching high power levels and requires the fiber to be of a double-cladding design. This means a small SM core in the center of the fiber, surrounded by a bigger multi-mode (MM) waveguide for confining the pump light. The advantage of the double-clad design is that a large pump area and high numerical aperture (NA) enable pumping with low-cost multi-mode diodes [6]. In standard fibers the pump waveguide can be achieved with a low index fluorinated polymer cladding. The supported NA of the pump region is defined by the refractive index difference between silica and the polymer cladding. Typically this translates to a maximum supported NA of ~ 0.48 . In high-power systems there is a risk of degradation of the polymer. This degradation is caused by the elevated temperature of the fiber, and can ultimately lead to failure of

the laser[7–9]. If a lower NA can be tolerated the pump cladding can also be achieved by a low index ring of fluorinated silica. A maximum NA of 0.3 can be achieved with this approach. A triple clad fiber can also be realized with a fluorinated silica cladding that is surrounded by a low index polymer cladding. The silica cladding guides the low NA light thereby reducing the amount of light reaching the polymer.

Optical fibers can also have a microstructured cross section. These fibers are called microstructured optical fibers (MOFs) or photonic crystal fibers (PCFs), and they would typically contain air-holes that run along the fiber length. The work on these fibers was pioneered by Russel and co-workers, who demonstrated guidance in a solid core PCF in 1996 [10, 11]. Guiding in a PCF with a solid core and a surrounding cladding with air-holes, that effectively lower the refractive index of the cladding, can be explained as modified TIR [12]. With the unique cladding design of the PCF, large SM core fibers can be fabricated [13]. The PCF design can also be used to fabricate double-clad fibers, with a MM pump core defined by a ring of air-holes [14, 15]. With this so called air-cladding, the silica bridge width between the air-holes define the NA [16]. Typically, these fibers are designed to support an NA of ~ 0.6 . The increase in NA compared to polymer clad fibers allows for reducing the pump core size, which increases the pump absorption per unit length. This allows for shortening the length of the active fiber. Another advantage of the air-clad is that the pump light is not in contact with the polymer coating, thereby minimizing the risk of fiber degradation at high pump powers [17–19].

Fused, all-fiber, pump combiners and pump/signal combiners for double-clad fibers are key components for building monolithic fiber lasers and amplifier systems. The pump combiner is designed to combine the output from one or more fiber coupled MM pump diodes into the pump core of a double-clad fiber. The pump/signal combiners are designed to do the same, but in addition to combining the pump diodes, they also combine the output from a SM fiber into the signal core of the double-clad fiber. Monolithic combiners for polymer clad double-clad active fibers have been described in a number of publications [20–35], and are today commercially available components [36, 37]. Fused, all-fiber, combiners that are custom designed for the air-clad technology are more rare. These components and their use for realizing high-power fiber lasers and amplifiers are the topic of this thesis.

The work in this thesis builds on the pioneering work by Martin D. Maack (Formerly Martin D. Nielsen) for designing and fabricating MM pump com-

biners for PCFs. In [38–41] pump combiners for PCFs are demonstrated, thereby eliminating the last missing link for the construction of monolithic fiber lasers based on air-clad technology. While these air-clad combiners did feature a 0.6 NA delivery fiber they were without a signal feed-through required to build monolithic fiber amplifiers. In this Ph.D. project these feed-through combiners for PCFs were developed. The fabricated combiners were tested in laser and amplifier configurations, and also used for super-continuum generation in a highly nonlinear PCFs. The results of these tests are also described in this thesis.

Another component described in this thesis is a signal combiner, that combines the output from 7 SM fiber lasers into a single MM fiber. The component enables further scaling up the output power out of a single optical fiber, while avoiding the nonlinear effects that limit the power of SM fiber lasers. A description of a high-power test with a combined output power of 2.5 kW is included in this thesis.

Finally, the thesis holds a description of some additional components that are developed for the field of astrophotonics. One of these components is the MM to SM converter or photonic lantern. This work expands on the proof of concept component developed by Leon-Saval *et. al* [42]. Low-loss versions of the component are described and also components with MM delivery fibers. Finally, fused bundles of MM fibers or hexabundles are described. These are also for use within astrophotonics.

The outline of the thesis is as follows:

Chapter 2 gives an introduction to optical fibers. Both the standard optical fiber and the PCF are described. The basic properties of the fibers are described, and an introduction to the modeling tool used to simulate the fiber modes is given. The chapter ends with a description of fiber splicing and tapering, which are both relevant for the fabrication of fused combiners.

Chapter 3 describes the very basics of fiber lasers and amplifiers. The chapter also gives an introduction to fused fiber based combiners, and an overview of different combiner concepts. The MM pump diodes that are used to pump the fibers are also briefly described. The chapter ends with a description of some of the limiting factors for reaching high power levels with fiber lasers.

Chapter 4 describes the MM pump combiners developed for the PCF technology, and the application of these combiners for fabricating all-fiber, monolithic continuous wave (CW) fiber lasers. The chapter ends with a description

of supercontinuum generation using a monolithic air-clad fiber laser.

Chapter 5 describes the signal combiners, for combining the output from multiple SM fiber lasers into a single MM fiber. A high power test of the combiner is also included in the chapter.

Chapter 6 describes the pump/signal combiners developed for the PCF technology. The chapter begins with a description of a mode field diameter (MFD) preserving taper element, which is the enabling part in the combiner. Then the fabrication of the combiner and the optical properties of the component are described. A full pulse amplification system is also described where the combiner is used for pump and signal coupling into the active fiber. The chapter ends with a description of supercontinuum generation using the fabricated pulsed fiber laser.

Chapter 7 describes the two components developed for the field of astrophotonics. First the fused fiber bundle or hexabundle is described and then the MM to SM converter or photonic lantern.

Chapter 8 holds the conclusion of this thesis.

Chapter 2

Optical fibers

This chapter gives an introduction to the basic properties of the step-index fiber and the photonic crystal fiber (PCF). Maxwell's equations will be presented, and an introduction to the modeling tool used to calculate modes in optical fibers will be given. The basic properties of fiber splicing and tapering of both single-mode (SM) and multi-mode (MM) fibers are also described.

2.1 Step-index fibers

The step-index fiber is the most common type of optical fiber, and is commonly referred to as a standard fiber. The fiber consists of a cylindrical core surrounded by a cladding with a lower refractive index than the core. Figure 2.1(a) shows an illustration of the step-index fiber, and (b) shows the refractive index profile. A simple way of explaining the guiding mechanism of the fiber, is that the high refractive index core of the fiber guides light due to total internal reflection (TIR). This principle is illustrated in Fig. 2.1(c). A light ray in the core of the fiber with an angle of incidence below the critical angle θ_c is guided in the core. The critical angle can be found from Snell's law as follows [43]

$$n_1 \sin \phi_i = n_2 \sin \phi_r |_{\phi_r=90^\circ} \Rightarrow \phi_c = \sin^{-1} \frac{n_2}{n_1}. \quad (2.1)$$

From Eq. 2.1 the acceptance angle θ_a can be calculated. Light rays incident on the fiber in a smaller angle than the acceptance angle are guided in the core of the fiber. This acceptance angle is normally expressed in terms of

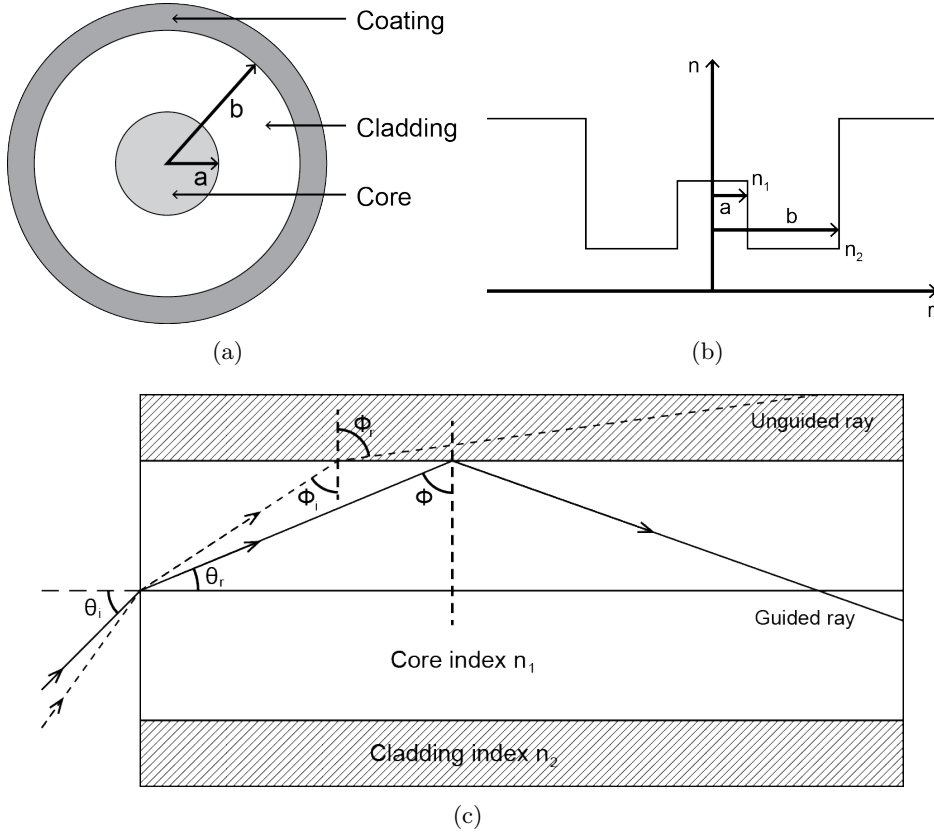


Figure 2.1: (a) Cross section and (b) refractive index profile of the step-index fiber. (c) Illustration of total internal reflection in a step index fiber.

the numerical aperture (NA) of the fiber. The NA is defined as follows [43]

$$NA = \sin \theta_a = n_1 \sin \theta_r = \sqrt{n_1^2 - n_2^2}. \quad (2.2)$$

2.1.1 Fiber optical modes

A fiber optical mode is a spatial distribution of energy that propagates unchanged through the waveguide. The ray description of the guiding mechanism, is only valid if the fiber core radius is much larger than the wavelength and the refractive index difference between core and cladding is large, i.e. for highly MM fibers.

The parameter that determines the number of guided modes in a step-index fiber is the V-parameter.

$$V = \frac{2\pi}{\lambda} a \sqrt{n_{co}^2 - n_{cl}^2}, \quad (2.3)$$

where λ is the free space optical wavelength, a is the radius of the waveguide core, and n_{co} and n_{cl} are the refractive index of the core and cladding, respectively. For a V-parameter below 2.405 the fiber only supports a single optical mode. For a V-parameter above this value the fiber supports more modes [43]. An approximate expression for the total number of modes M supported by a step-index fiber, is calculated from the V-parameter [44, 45]

$$M \approx \frac{V^2}{4}. \quad (2.4)$$

In the equation M is the total number of modes in only one polarization orientation. By multiplying with a factor of two, the total number of modes in both polarization states can be found.

The fundamental mode of the optical fiber can be approximated by a Gaussian distribution. With this approximation, an analytical expression

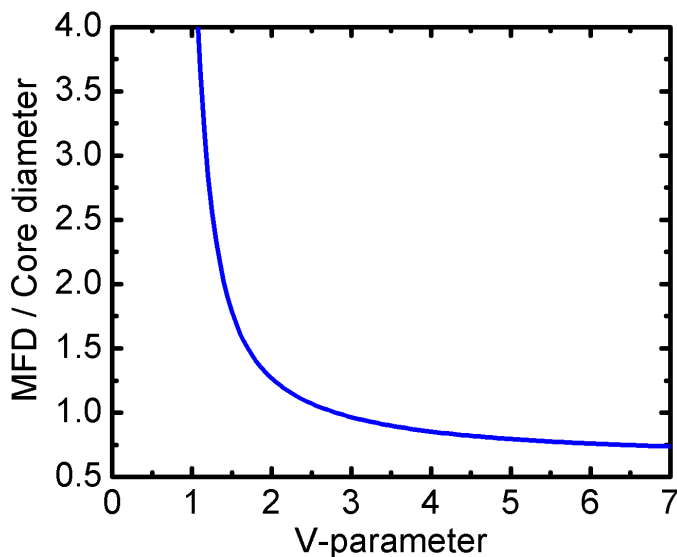


Figure 2.2: Normalized MFD as a function of V-parameter for the fundamental mode in a step-index fiber.

for the spot size or MFD can be found normalized to the core diameter d of the fiber [46]

$$MFD/d \approx 0.65 + 1.619V^{-3/2} + 2.879V^{-6}. \quad (2.5)$$

The MFD is defined as the diameter where the optical power in the mode has decreased by a factor of $1/e^2$ (13.5%) compared to its maximum value. Figure 2.2 shows a plot of the MFD as a function of V-parameter. For a SM fiber with a V-parameter close to a value of two the mode will be mostly confined to the core of the fiber. When the V-parameter approaches a value of one, the mode will expand out of the core and extend far into the cladding of the fiber.

2.1.2 Double-clad fibers

A standard step-index fiber would normally be surrounded by a high-index polymer coating. This polymer both protects the fiber, but also strips out any light that is not guided in the core of the fiber. These fibers are called single-clad fibers. If the fiber has a second low-index cladding the fiber is a double-clad fiber. Figure 2.3(a) shows an illustration of the double-clad step-index fiber, and (b) shows the refractive index profile. The second cladding can be made of a low index fluorinated polymer. The maximum NA supported by such a cladding is typically ~ 0.48 . The second cladding can also be realized by a low index ring of fluorinated silica. The maximum NA supported in this case is typically below 0.3 [9].

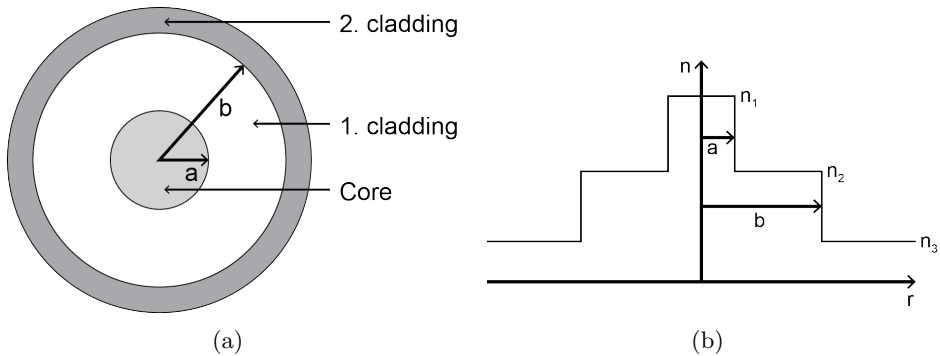


Figure 2.3: (a) Cross section and (b) refractive index profile of the standard double-clad step-index fiber.

2.2 Photonic crystal fibers

A solid core PCF consists of an arrangement of air-holes running along the length of the fiber. These air-holes are arranged in a background material, which is typically silica. The core of the fiber is formed by one or more missing air-holes in the center of the fiber [10, 11]. Figure 2.4(a) shows an illustration of a PCF. The air-hole pitch is given by Λ and the diameter of the holes is d . In this fiber the core is formed by a single missing air-hole. The holes in the solid core PCF effectively lower the refractive index of the fiber cladding, thereby creating a refractive index step between core and cladding. A simple way of explaining the guiding mechanism is by modified TIR [12]. Figure 2.4(b) shows a scanning electron microscope (SEM) image of the end facet of a solid core PCF. The fiber in the image is fabricated by NKT Photonics [47].

Due to the wavelength dependence of the effective refractive index of the air-hole cladding, fibers with a d/Λ smaller than ~ 0.42 are single-mode at all optical wavelengths. In practice, this is still true if $d/\Lambda < 0.45$. Since the first higher order core mode is weakly guided and therefore subject to high bend and propagation losses. For a $d/\Lambda > 0.45$ the fiber can still be single-mode but it will have a cut-off wavelength below which the fiber is multi-mode [11, 48–50].

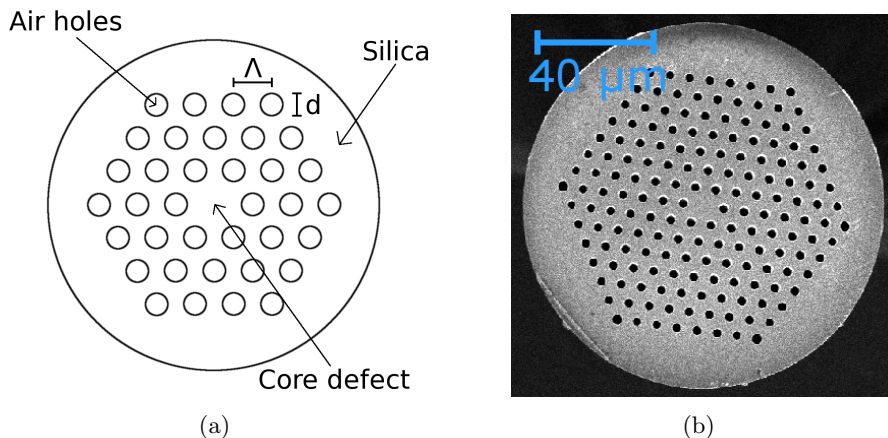


Figure 2.4: (a) Illustration and (b) SEM image of solid core PCF.

2.2.1 Air-clad photonic crystal fibers

Double-clad fibers can be fabricated with the PCF technology by creating a ring of closely spaced air-holes [14, 15]. Figure 2.5 shows images of two different air-clad PCFs. The fiber in (a) also has a PCF signal core defined by the small holes inside the air-clad. The core in this case is made by removing 19 holes in the center of the fiber. The fiber in (b) has a standard step-index core. Both fibers are made to be polarization maintaining (PM) by placing boron doped stress rods on either side of the core.

The silica bridge width between the air-clad holes define the NA of the air-clad [16]. Figure 2.6 shows a plot of the air-clad NA as a function of bridge width (Δ) over wavelength (λ). The inset in the figure shows the definition of the bridge width. Due to the large refractive index difference between silica and air, a much higher NA can be achieved with an air-clad than with a fluorinated polymer cladding. Air-clad fibers with NA approaching 0.9 have been demonstrated [16]. In order to reach such a high NA, very thin silica bridges are required and cleaving of these very high NA fibers is therefore challenging. In order to maintain a good cleavability, the air-clad PCFs are typically designed to support an NA of ~ 0.6 [18].

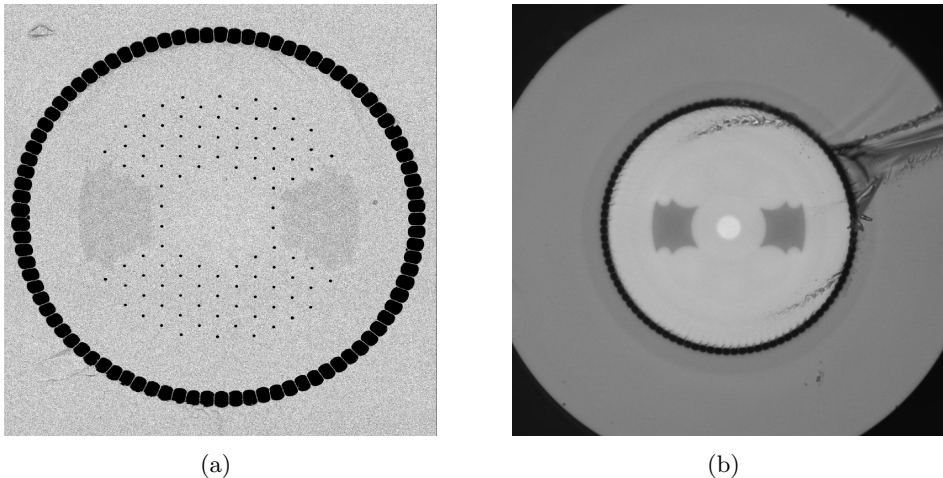


Figure 2.5: (a) SEM image of air-clad fiber with a PM PCF single-mode core. (b) Microscope cross sectional image of air-clad fiber with a PM step-index core.

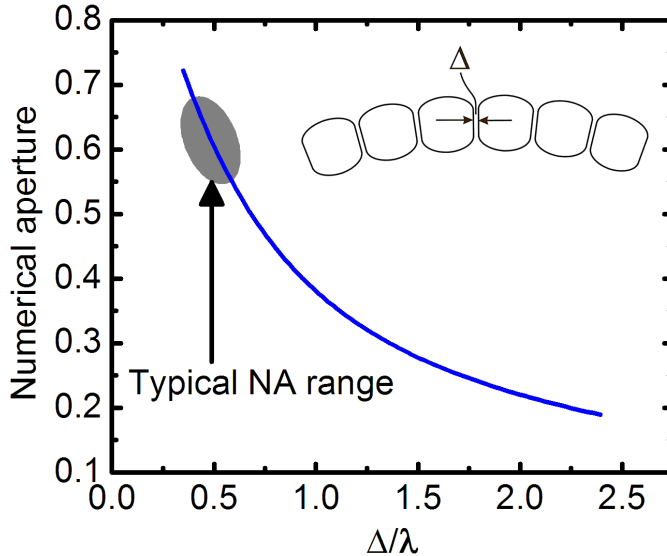


Figure 2.6: NA as a function of bridge width Δ . The NA is typically chosen to be in the range 0.55-0.65.

2.3 Modeling of optical fibers

The explanation of the guidance properties in optical fibers due to internal reflections is a very simplified explanation. A complete description of the propagation of light through the fiber is described by Maxwell's equations. Maxwell's equations in a linear, isotropic, source free, dielectric medium can be written as [43]

$$\nabla \times \mathbf{E} = -\frac{\delta \mathbf{B}}{\delta t} \quad (2.6)$$

$$\nabla \times \mathbf{H} = \frac{\delta \mathbf{D}}{\delta t} \quad (2.7)$$

$$\nabla \cdot \mathbf{D} = 0 \quad (2.8)$$

$$\nabla \cdot \mathbf{B} = 0 \quad (2.9)$$

In the equations \mathbf{E} is the electric field, \mathbf{H} is the magnetic field, and \mathbf{D} and \mathbf{B} are the electric and magnetic flux densities, respectively. For nonmagnetic materials the relation between the field and the flux densities is described

by the equations

$$\mathbf{D} = \epsilon_0 \epsilon_{\mathbf{r}} \mathbf{E} \quad (2.10)$$

$$\mathbf{B} = \mu_0 \mathbf{H}, \quad (2.11)$$

where μ_0 is the free space magnetic permeability, ϵ_0 is the free space dielectric permittivity, and $\epsilon_{\mathbf{r}}$ is a tensor describing the relative dielectric constant.

In order to have a single equation to describe the propagation of light, the magnetic field is split into a spatial and a time-varying part

$$\mathbf{H}(\mathbf{r}, t) = \mathbf{H}(\mathbf{r}) e^{i\omega t}, \quad (2.12)$$

where ω is the angular frequency of the light. Combining the above equations, a wave equation describing the magnetic field in a dielectric material can be found

$$\nabla \times \frac{1}{\epsilon_{\mathbf{r}}} \nabla \times \mathbf{H}(\mathbf{r}) = \frac{\omega^2}{c^2} \mathbf{H}(\mathbf{r}), \quad (2.13)$$

where $c = \frac{1}{\sqrt{\epsilon_0 \mu_0}}$ is the speed of light in vacuum. Solutions to equation (2.13) are the optical modes of the fiber.

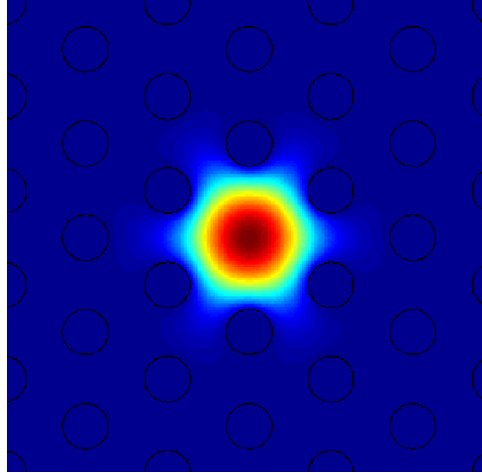


Figure 2.7: Simulated transverse mode profile of the LP_{01} like core mode at $\lambda = 1 \mu\text{m}$. The diameter of the holes is $d = 3.45 \mu\text{m}$ and the pitch is $\Lambda = 7.15 \mu\text{m}$. The image shows the dominant x-component of the electric field.

A number of simulation tools to solve the wave equation exist. In this thesis the MIT Photonic Bands software, that uses the plane-wave expansion method to solve the wave equation is used [51]. Figure 2.7 shows an example of an optical mode found with the software. The image shows the fundamental LP_{01} mode at a wavelength of $1 \mu\text{m}$ in a solid core PCF. The diameter of the holes is $3.45 \mu\text{m}$, the pitch is $\Lambda = 7.15 \mu\text{m}$ and the refractive index of fused silica at a wavelength of $1 \mu\text{m}$ is 1.45.

2.4 Fusion splicing of optical fibers

Fusion splicing of optical fibers is the process of welding two optical fibers together, thereby creating a permanent, high-strength and ideally low-loss joint between the two fibers [52]. Coupling of light from one optical fiber to another can also be achieved by free-space coupling, mechanical splicing or with optical fiber connectors. Fusion splicing is the preferred connectorization method if a stable low-loss joint with high mechanical strength and long-term reliability is preferred. The fusion splice creates a joint with a stable optical transmission that does not change with temperature or over time. Also, the amount of back-reflected light from the joint is low, the joints can withstand high temperatures and high power densities, and dust can not enter the optical beam path. For these reasons, fusion splicing is the superior approach for joining fibers for high-power applications.

A fused joint between two optical fibers is achieved by heating the two fiber tips to the softening point and melting them together. For silica fibers the softening temperature is $\sim 2000^\circ\text{C}$ [53]. The heat source used for fusion splicing can be an electric arc [54], a resistively heated metal or graphite filament [55], a flame [56], or a CO_2 laser [57]. Electric arc discharge heating is most commonly used in commercially available fusion splicers. A voltage is applied across two or three electrodes separated by an air gap. The resulting current flow heats the fibers. Flame heating can be achieved with a hydrogen flame. Laser heating can be achieved with a CO_2 laser, where the fibers are heated due to the strong absorption in silica at the $10.6 \mu\text{m}$ wavelength of the laser. Resistively heated metal or graphite filaments have the advantage that the temperature of the filament is controllable and can be tuned in a wide temperature range. This is a great advantage for splicing PCFs. These fibers need to be spliced at a low temperature, compared to a standard fiber with a similar diameter. This is to ensure that the air-holes do not collapse in the splice, which would result in a high splice loss. The glass processing stations

from Vytran (New Jersey, USA) use the resistive heating of a filament as the heat source [58, 59]. Therefore, these machines are suitable for splicing PCFs.

2.5 Tapering of optical fibers

Tapering of an optical fiber basically means to make the fiber thinner. This is done by heating the fiber to the softening point and stretching it. The heat sources that can be used for tapering of silica fibers are the same as can be used for splicing. For tapering PCFs the temperature of the fiber needs to be controlled in order to prevent a collapse of the air-holes. Therefore, the glass processing stations from Vytran are also suitable for tapering of PCFs.

2.5.1 Tapering of single-mode fibers

Tapering of a single-mode fiber has to be slowly varying. If the tapering is to abrupt optical power from the fundamental mode will couple to higher order modes (HOMs) of the fiber. This will usually result in a lossy taper. As long as the change in the fibers core radius (Δr) over the beat length (L_B) between the fundamental mode and the first HOM is small, the taper is slowly varying [60–63]. This is formulated as follows, where r is the fibers core radius

$$\frac{\Delta r}{r} \ll 1. \quad (2.14)$$

The local change in fiber core radius over the beat length can be written as $\Delta r = L_B \frac{dr}{dz}$, where $\frac{dr}{dz}$ is the local slope of the taper. The beat length between the core mode and a HOM can be expressed as

$$L_B = \frac{2\pi}{\beta_1 - \beta_2}, \quad (2.15)$$

where β_1 and β_2 are the propagation constants of the core and HOM, respectively. By inserting the expression for the local taper slope in Eq. 2.14 a criteria can be found that has to be fulfilled in order for the taper to have a low loss. This is called the adiabatic criteria.

$$\frac{dr}{dz} \leq \frac{r}{L_B} = \frac{r}{2\pi}(\beta_1 - \beta_2) \quad (2.16)$$

In the adiabatic criteria, β_2 refers to the propagation constants of the first HOM. This mode will have a propagation constant closest to the core mode, and give the largest value of for the beat length. This means that the strictest criteria is set by using this mode in the calculation.

For a linear taper profile, the taper slope (dr/dz) will be the same over the entire taper. The maximum beat length ($L_{B,max}$) and the total taper ratio (TR) will therefore define the length of the taper (L) in order to be adiabatic. The taper ratio is here defined as $TR = \frac{r_1}{r_2}$, where r_1 and r_2 is the fiber core radius in the untapered and tapered end, respectively. Eq. 2.16 can be reduced to (See appendix A.1)

$$L \geq (TR - 1)L_{B,max}. \quad (2.17)$$

For an adiabatic taper, light that is launched into the fundamental mode of an optical fiber will stay in this mode. Figure 2.8 shows the calculated MFD of the fundamental mode of a tapered step-index fiber in (a) and a PCF in (b). Both calculations are at a wavelength of 1064 nm, and are made with the MIT Photonics Band software. The step-index fiber has a constant NA of 0.14 and becomes MM at a core diameter above 5.7 μm . The PCF has a relative core diameter of $D/\Lambda=0.45$, which is constant over the taper. The MFD of the step-index fiber follows the core diameter, until the V-parameter approaches one. Here the mode expands rapidly. This agrees well with the analytical expression for the MFD of the step-index fiber shown in Fig. 2.2.

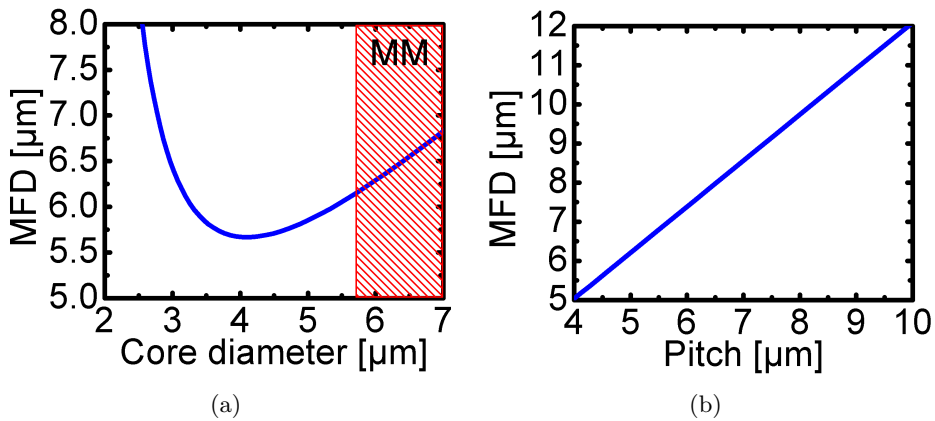


Figure 2.8: (a) MFD of a tapered step-index fiber. (b) MFD of a tapered PCF.

The MFD of the tapered PCF is proportional to the air hole pitch of the fiber [64]. The reason for this is that the effective index of the cladding is not constant, but increases as the fiber is tapered. Also, the fiber remains single-mode throughout the taper, since the D/Λ ratio is unchanged.

2.5.2 Tapering of multi-mode fibers

For MM fiber tapers usually lots of modes are excited in the fiber and not just one. Therefore the adiabatic criteria in Eq. 2.16 can not be used. Instead the change in the MM fibers core radius (Δr) over a half ray period (z_p) has to be small [60]. The half ray period is defined in Fig. 2.9. The result is an adiabatic criteria that is similar to the one for single-mode fiber tapers, but with the beat length replaced by the half ray period

$$\frac{dr}{dz} \leq \frac{r}{z_p}. \quad (2.18)$$

For a given NA a ray that passes through the axis of the optical fiber (meridional ray) will have the longest half ray period. For such a ray the half ray period is given by

$$z_p = \frac{2r}{\tan \theta_z}. \quad (2.19)$$

Inserting the expression for z_p into the adiabatic criteria, the equation becomes

$$\frac{dr}{dz} \leq \tan \theta_z / 2. \quad (2.20)$$

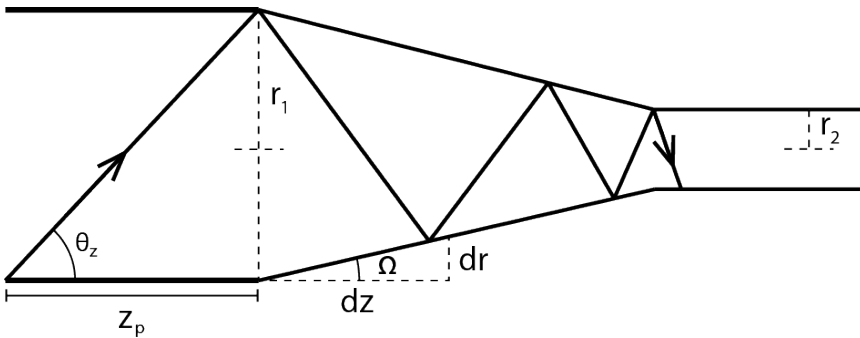


Figure 2.9: Tapering of a MM fiber.

The factor dr/dz can also be described as the local angle (Ω) as seen in Fig. 2.9. An adiabatic taper is therefore ensured if the ray angle is at least twice as big as the taper angle at any point along the taper ($2\Omega \leq \theta_z$).

For a linear taper profile, a minimum taper length for the MM fiber can be derived, that ensures fulfillment of the adiabatic criteria. Just as for the SM fiber taper. The minimum taper length is (See appendix A.2)

$$L \geq \frac{D_1 - D_2}{\tan \theta_z}. \quad (2.21)$$

The minimum taper length of a linearly tapered MM fiber will depend on the NA of the light launched into the fiber. For 0.22 NA launched light, and with a refractive index of the core of $n_{co} = 1.45$, the ray angle for a meridional ray is $\theta_z = \sin^{-1} \frac{NA}{n_{co}} = 8.7^\circ$. With this launch NA, and for a MM fiber tapered with a linear profile from a diameter of $D_1 = 400 \mu\text{m}$ down to $D_2 = 150 \mu\text{m}$, the minimum taper length will therefore be $L_{min} = 1.6 \text{ mm}$.

For tapering double-clad fibers the adiabatic criteria has to be fulfilled for both the signal and the pump core. For large mode area (LMA) signal cores, the adiabatic criteria for the signal core will usually be the most strict, and therefore be the one defining the minimum taper length.

For passive optical devices the brightness theorem states that the brightness or radiance is conserved [65]. The brightness L_R is defined as power flowing per area per solid angle ($W/m^2/sr$)

$$L_R = \frac{\Phi}{A\Omega}, \quad (2.22)$$

where Φ is the flux through a given area A , and Ω is the solid angle. Brightness originally refers to the brightness perceived by the human eye of a radiating object [66]. The term has however become standard in connection with lasers and will therefore be used in this thesis.

From the brightness theorem it follows that an adiabatically tapered MM fiber is brightness conserving. For a MM fiber $A = \pi r^2$, where r is the fiber core radius. The solid angle is $\Omega = 4\pi \sin^2 \frac{\theta}{2}$, where θ is the divergence half-angle. The flux is equal to the power P carried by the fiber. The brightness of the light in a MM fiber (L_{MM}) can therefore be written as

$$L_{MM} = \frac{P}{\pi r^2 \pi \sin^2 \theta}. \quad (2.23)$$

For an adiabatic and lossless taper the conservation of brightness means that a relation between the NA and the core diameter D at the input and output

end of a taper can be derived

$$D_{in} \sin(\theta_{in}) = D_{out} \sin(\theta_{out}) \Rightarrow D_{in} NA_{in} = D_{out} NA_{out}, \quad (2.24)$$

where D is the core diameter of the MM fiber and NA is the numerical aperture of the light. The equation shows that for an adiabatic brightness conserving MM fiber taper the core diameter multiplied by the NA of the light is constant.

2.6 Summary of chapter 2

In this chapter an introduction to the basic properties of the step-index fiber and the PCF are given. Maxwell's equations are briefly described, together with an introduction to the MIT Photonic bands modeling tool. Fiber splicing and tapering of both single-mode and MM fibers are also described.

Chapter 3

High power fiber lasers and amplifiers

One of the major application areas for high power fiber lasers is within material processing. Marking, cutting and welding of metals, ceramics and plastics, are just some of the applications where lasers have advantages over traditional methods. The advantages of using a laser are that the material processing is contact free. This means that there is no wear of the equipment, as there is with traditional milling machines. No chemicals are used, making the processing environmentally clean, and computer control of the laser beam makes the system easy to reconfigure. Traditionally, CO₂ and solid-state lasers have dominated this market, but fiber lasers are excellent candidates for replacing these. This is due to their low running cost, high beam quality, high efficiency, easy fiber based beam delivery and small footprint [67–69].

This chapter gives an introduction to high power fiber lasers and amplifiers. The basic concept of the double-clad active fiber and the advantages of the air-clad are described. An introduction to the fused combiner that can be used for coupling pump and signal light into the double-clad fiber is given. The pump diodes used for optically pumping the double-clad active fibers are also briefly described. The chapter ends with a description of the factors that limit the output power of the fiber laser and how these limiting factors can be overcome by combining of multiple fiber lasers.

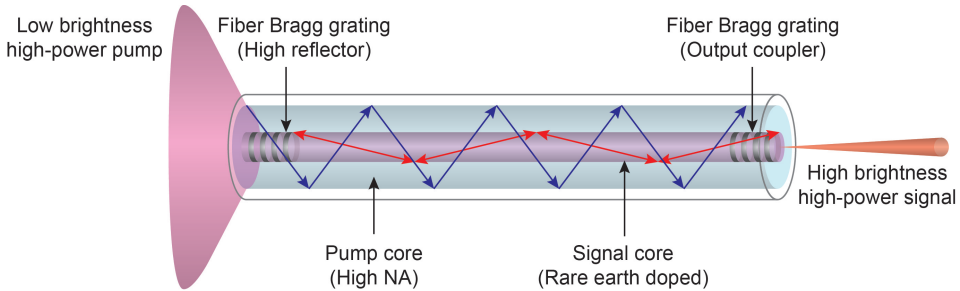


Figure 3.1: Illustration of double-clad fiber laser.

3.1 Double-clad active fibers

High power fiber lasers and amplifiers are basically brightness converters. Converting low brightness light from a multi-mode (MM) pump diode into a single-mode (SM) output [5, 6]. The conversion is done by doping the core of a double-clad fiber with a rare earth dopant and pumping this with MM light. Pump light will then be absorbed by the rare earth atoms, and light will be re-emitted at lower photon energies. Since the emission will happen through stimulated emission, the re-emitted light will be guided in the SM core of the fiber.

3.1.1 Double-clad fiber lasers

The basic concept of the double-clad fiber laser is illustrated in figure 3.1. Low brightness pump light from a diode laser is coupled into the pump core of the double-clad fiber. This ensures that pump light is guided through the fiber, such that it can be absorbed by the rare earth ions in the signal core. Absorption of a pump photon brings a rare earth ion into an excited state. The absorbed energy is then re-emitted as signal photons through stimulated emission, ensuring that the emitted light is confined to the signal core of the fiber. A laser resonator is made by inscribing fiber Bragg gratings in the core of the fiber, these reflect a certain wavelength which will become the dominant laser wavelength.

3.1.2 Double-clad fiber amplifiers

The basic concept of the double-clad fiber amplifier is illustrated in figure 3.2. The principle is similar to the double-clad fiber laser, except that no gratings

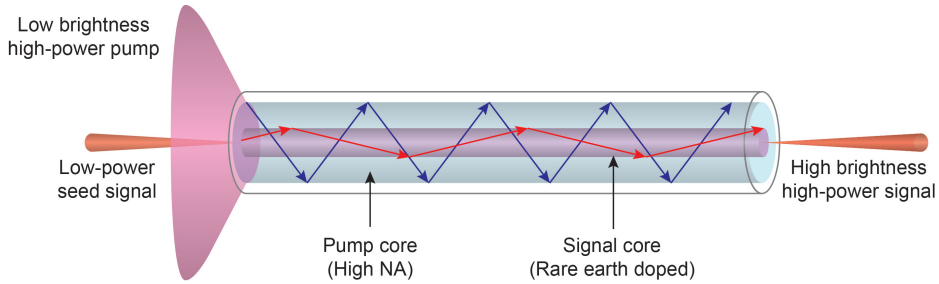


Figure 3.2: Illustration of double-clad fiber amplifier.

are needed. Instead a low power seed signal is coupled into the signal core of the fiber. Pump photons are absorbed by the rare earth ions, and the absorbed energy is re-emitted as signal photons through stimulated emission, thus amplifying the seed signal.

3.1.3 Air-clad fibers

As described in chapter 2 high numerical aperture (NA) double-clad fibers can either be fabricated with a low index fluorinated polymer surrounding the fiber or with an air-cladding. The advantage of having an air-clad in an active fiber is that a higher NA can be obtained compared to polymer based double-clad fibers. This allows for reducing the pump core size, which in turn increases the pump absorption per unit length. This allows for shortening the length of the active fiber. Another advantage of the air-clad is that the pump light is not in contact with the polymer coating, thereby minimizing the risk of fiber degradation at high pump powers [7–9, 17, 18].

3.2 Fused combiners for double-clad fibers

Pump and signal light can be coupled into the double-clad fiber using bulk optics. In order to make alignment free and robust systems, fused and all-fiber combiners are required. These combiners are designed to combine the output from one or more MM pump diodes into the pump core of a double-clad fiber. They can also include a signal feed-through, where the output from a SM fiber is coupled into the signal core of the double-clad fiber. Monolithic combiners for polymer clad fibers are described in a number of publications [20–35], and are today commercially available components [36, 37]. The highest pump absorption is achieved if the area of the pump core is

reduced. For this reason, most of the combiner approaches include a tapered section that increases the intensity of the pump.

Some of the approaches for realizing combiners for polymer clad fibers are illustrated in Fig. 3.3. The figures illustrate the following approaches.

(a) Side coupling. A MM pump fiber is fused directly onto the double-clad

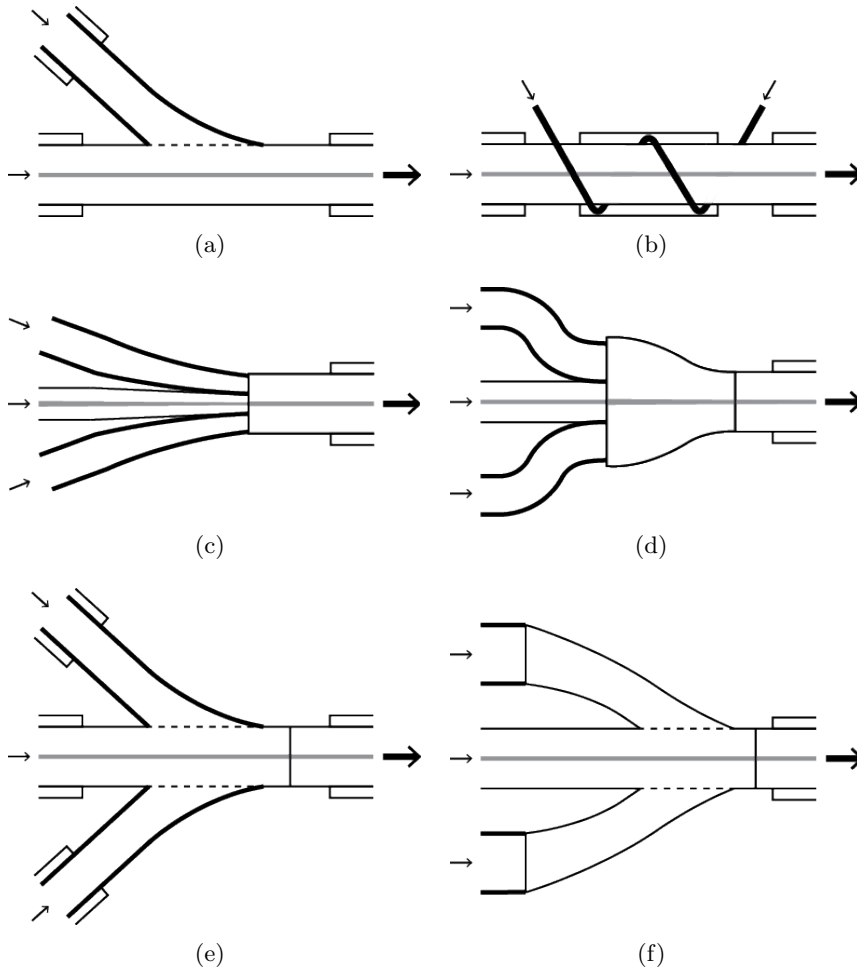


Figure 3.3: Approaches for realizing combiners for polymer clad fibers. (a) Side coupling, (b) distributed side coupling, (c) tapered fiber bundle, (d) fused fiber bundle with tapered bridging fiber, (e) MM fibers fused to signal fiber, and (f) MM fibers fused to signal fiber via collapsed capillary tube.

fiber. Light will then leak from the pump fiber and into the pump core of the polymer clad fiber [20–22].

- (b) Distributed side coupling. Similar to the side coupling described above, except that the MM fiber is fused to a long length of active fiber. This allows for pumping the active fiber from both sides [23, 24].
- (c) Tapered fiber bundle. A number of pump fibers are fused together, tapered down and spliced to the active fiber. Such a bundle could include a signal fiber in the center [25–29].
- (d) Fused fiber bundle with tapered bridging fiber. A fused fiber bundle is spliced to a bridging fiber. This bridging fiber is tapered and spliced to the active double-clad fiber [30].
- (e) MM fibers fused to signal fiber. A number of tapered MM fibers are fused onto a SM fiber and spliced to a double-clad fiber [31, 32].
- (f) MM fibers fused to signal fiber via collapsed capillary tube. A number of MM fibers are spliced to a silica capillary tube. This tube is then tapered, collapsed and fused to the SM fiber. The signal fiber with fused capillary tube is then spliced to a double-clad fiber [33–35].

Fused, all-fiber, combiners that are custom designed for the air-clad technology are more rare. A tapered fiber bundle approach was patented in 2004 [70]. Figure 3.4(a) shows an illustration of the approach. A number of fibers are fuse together, tapered down and spliced to the air-clad photonic crystal fiber (PCF). A signal fiber can be included in the center. To the best of the authors knowledge, at the time of writing, no experimental data has been published further exploring this approach.

A side-coupling approach for air-clad PCFs has also been demonstrated [71, 72]. The holes of the air-clad are collapsed and a MM fiber is fused to the side of the fiber in the collapsed region. See Fig. 3.4(b). A good coupling efficiency was achieved, but the concept was only demonstrated for low power.

The approach with the most potential is illustrated in Fig. 3.4(c). A number of fibers are fused together into a solid fiber bundle, that is spliced to a bridging fiber or taper element. This taper element has an air-cladding big enough to hold all the pump fibers. This bridging fiber is then tapered down and spliced to the air-clad PCF. The bridging fiber can also have a

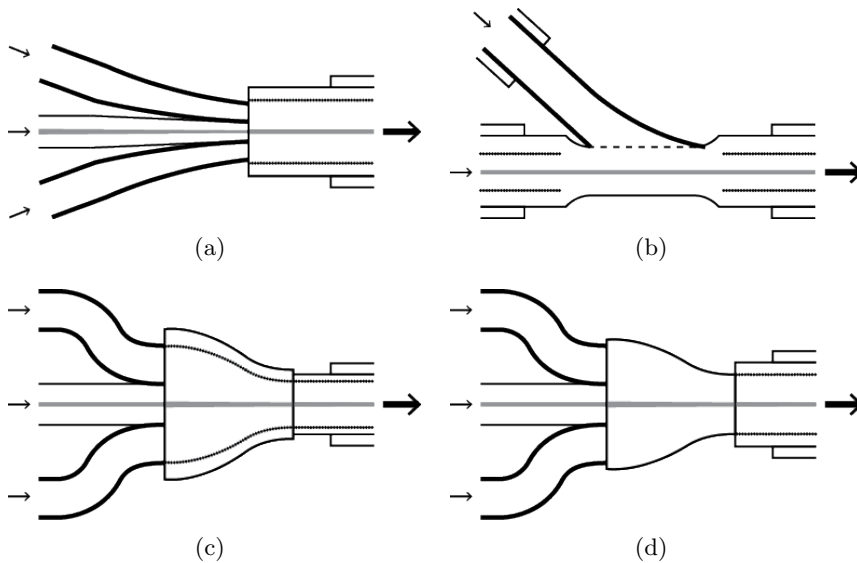


Figure 3.4: Approaches for realizing combiners for air-clad fibers. (a) Tapered fiber bundle, (b) side coupling, (c) fused fiber bundle with tapered bridging fiber and (d) fused fiber bundle with etched bridging fiber.

signal core that transfers signal light from a signal fiber into the signal core of the output fiber [38–41, 73, 74]. These pump and pump/signal combiners are described in further detail in chapter 4 and chapter 6, respectively.

Recently, a new promising approach was demonstrated illustrated in Fig. 3.4(d). A number of MM fibers are fused together with a signal fiber into a fiber bundle. This bundle is then spliced to a bridging fiber. This fiber is an uncoated silica fiber with a step-index core. The outer diameter of the bridging fiber is then reduced by a chemical wet etching process and spliced to the air-clad fiber [75]. Pump light is guided by the glass air interface, which means that the outer diameter of the bridging fiber in the tapered end should match the inner diameter of the air-clad of the PCF. The signal is guided in a signal core which is unaffected by the etched taper process. Therefore, this approach could potentially result in combiners with a low signal loss.

3.3 Fiber coupled laser diodes

The output power of fiber coupled single-emitter laser diodes has increased steadily over the years. Today, more than 100 W out of a 100 μm core MM fiber can be achieved [76–78]. Traditionally, micro-channel cooled bar stacks have been used for high power applications, but due to the high efficiency, long lifetime, reliability, and cost ($\$/\text{W}$) the single-emitter laser diodes are today gaining more and more interest. Today, combining of multiple single-emitter laser diodes is a common approach for fabricating industrial high-power fiber lasers [79–82].

3.4 Power limitations of fiber lasers and amplifiers

The main factors that limit the single-mode output power of fiber lasers and amplifiers are stimulated Raman scattering (SRS), stimulated Brillouin scattering (SBS), facet damage and self focusing [83].

SRS is the scattering of signal photons by the molecules in the optical fiber. Molecules are excited to higher vibrational states, resulting in scattered photons with lower frequency, since some of their energy is lost. The threshold for when SRS becomes significant is

$$P_{SRS} \approx \frac{16A_{eff}}{g_R L_{eff}}, \quad (3.1)$$

where $A_{eff} = \pi(MFD/2)^2$ is the effective area of the optical mode, L_{eff} is the effective length of the fiber and g_R is the Raman gain coefficient. For silica g_R is on the order of 10^{-13} m/W [84]. The effective length is

$$L_{eff} = \frac{1}{g}(e^{gL} - 1), \quad (3.2)$$

where L is the fiber length and g is the gain coefficient.

SBS occurs when a high intensity signal generates an acoustic wave in the fiber. This wave modulates the refractive index of the fiber and creates a grating that reflects the signal backwards. The threshold for when SBS becomes significant is

$$P_{SBS} \approx \frac{17A_{eff}}{g_B(\Delta\nu)L_{eff}}, \quad (3.3)$$

where $g_B(\Delta\nu)$ is the Brillouin gain coefficient, which depends on the spectral linewidth of the laser signal. For a spectrally broad signal, SRS will limit the output power rather than SBS.

Facet damage is a breakdown of the glass matrix, which occurs when the power density at the fiber facet becomes higher than a critical value. A high intensity electric field can result in the acceleration of free electrons. This transfers energy to the glass matrix causing melting or fracturing [85]. For bulk silica the damage threshold is $\sim 30 \text{ W}/\mu\text{m}^2$, this value is lower in optical fibers due to dopants and impurities. At the fiber facet the damage threshold is even lower. The damage threshold for the facet is $\sim 10 \text{ W}/\mu\text{m}^2$ [67, 86]. In order to avoid facet damage pure silica end-caps are normally attached to the output end of the fiber. In these end-caps the beam can expand, thus decreasing the power density at the facet to a value below the damage threshold.

Self focusing is a process where the signal beam in the optical fiber is focused inside the fiber. This results in a breakdown of the glass matrix, when the damage threshold is reached. The focusing occurs as a result of the high intensity in the center of the beam. This increases the refractive index of the center of the fiber due to the Kerr effect, and creates a lens that focuses the beam. Theoretical studies show that the threshold for self focusing is independent of core size and is reached at around 4.3 MW [87, 88].

3.5 High-power beam combining

The output power of single or few-mode fiber lasers has increased steadily over the years, such that it today extends well into the kW regime [82, 89–93]. Coherent or incoherent beam combining of fiber lasers enables further scaling of the output power. Coherent beam combining of single-frequency lasers requires control of the phase of each source. This is necessary to ensure constructive interference of the combined beam. Incoherent combining on the other hand does not require phase control. This results in a simpler system but also in a less spectrally pure combined beam [94]. Free space setups for incoherent spectral beam combining have shown great potential and combined powers of up to 2 kW have been reached with near diffraction limited beams [95, 96]. With an all-fiber fully fused beam combiner approach, bulk optical components are not necessary, thereby allowing for robust and stable laser systems. Recently, tapered fiber bundles of SM fibers have shown potential for realizing all-fiber components for incoherent beam

combining [97]. Another promising approach is by etching of the SM input fibers and then fusing them together in a low index tube [98]. With this approach a 4 kW combined laser output has been demonstrated [81]. In chapter 5 a combiner fabricated with a tapered fiber bundle approach is described in further detail.

3.6 Summary of chapter 3

In this chapter an introduction to the basic properties of fiber lasers and amplifiers is given. The fused combiners are introduced together with the pump diodes. The limiting factors for high power fiber lasers are described and the concept of beam combining is introduced.

Chapter 4

Pump combiners for air-clad fiber lasers

This chapter describes a monolithic, all fiber, tapered pump combiner for air-clad fibers. Such fused fiber based combiners for coupling pump light into active fibers are essential components for making robust high power fiber lasers [27]. The combiners are fabricated using the fused fiber bundle with tapered bridging fiber approach illustrated in Fig. 3.4(c) [38–41].

The chapter begins with a description of the fabrication of the pump combiners. Combiners with 7, 19, 37 and 61 pump ports are described. A 1x1 pump combiner is also briefly described.

The chapter also describes two applications of the pump combiners. The first is a high-power fiber laser and the second is to use such a laser for supercontinuum generation in a nonlinear photonic crystal fiber (PCF).

4.1 Pump combiner fabrication

Figure 4.1 shows an illustration of a fused pump combiner for the air-clad technology. The illustration shows a 7 port combiner, but the principle can be extended to include more pump fibers. The multi-mode (MM) pump fibers are fused together, to form a fused fiber bundle. This bundle is spliced to a bridging fiber or taper element, that has an air-clad to hold the pump light. The inner diameter of the air-clad should match the combined outer diameter of the cores of the MM fibers, i.e. all the fiber cores should be within the air-clad of the taper element. The bridging fiber is tapered and spliced to an air-clad delivery fiber. The air-clad of the taper element in

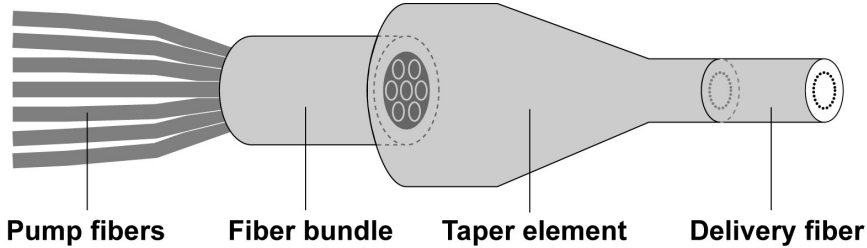


Figure 4.1: Illustration of fused 7x1 pump combiner.

the tapered end should match that of the delivery fiber. This ensures that the taper element couples the pump light from the pump fibers of the fiber bundle into the pump-guide of the delivery fiber.

A tapered section is included in the combiner in order to reduce the pump guide area. This reduction increases pump absorption in the active fiber, which means that shorter active fibers can be used. Shorter fibers results in higher thresholds for undesirable nonlinear effects. For an adiabatic brightness conserving MM fiber taper the product of core diameter and numerical aperture (NA) of the light is constant (see Eq. 2.24). This means that the maximum taper ratio that can be achieved is decided by the NA of the pump diodes and the NA of the delivery and active fiber. With 0.22 NA pump diodes and with the air-clad of the delivery and active fiber supporting an NA of 0.6, the maximum taper ratio (TR) is

$$TR = \frac{D_{in}}{D_{out}} = \frac{NA_{out}}{NA_{in}} = 2.7. \quad (4.1)$$

For a higher taper ratio the output NA will exceed the accepted NA of the delivery and active fibers, resulting in a loss of pump light.

Figure 4.2(a) shows a cross sectional image of an air-clad taper fiber. The fiber is tapered from a core diameter of $400 \mu\text{m}$ down to $150 \mu\text{m}$, using a filament based GPX glass processing station from Vytran [58, 59]. The filament power is controlled in order to prevent a collapse of the air-clad holes. An image of the taper is shown in Fig. 4.2(b). Figure 4.2(c-d) show the measured NA in the untapered and tapered end of the fiber. The NA in the untapered end is 0.22, matching that of the pump diode used in the measurement. In the tapered end the NA of the light is 0.6. This NA increase agrees well with Eq. 2.24 and indicates that the taper is brightness conserving.

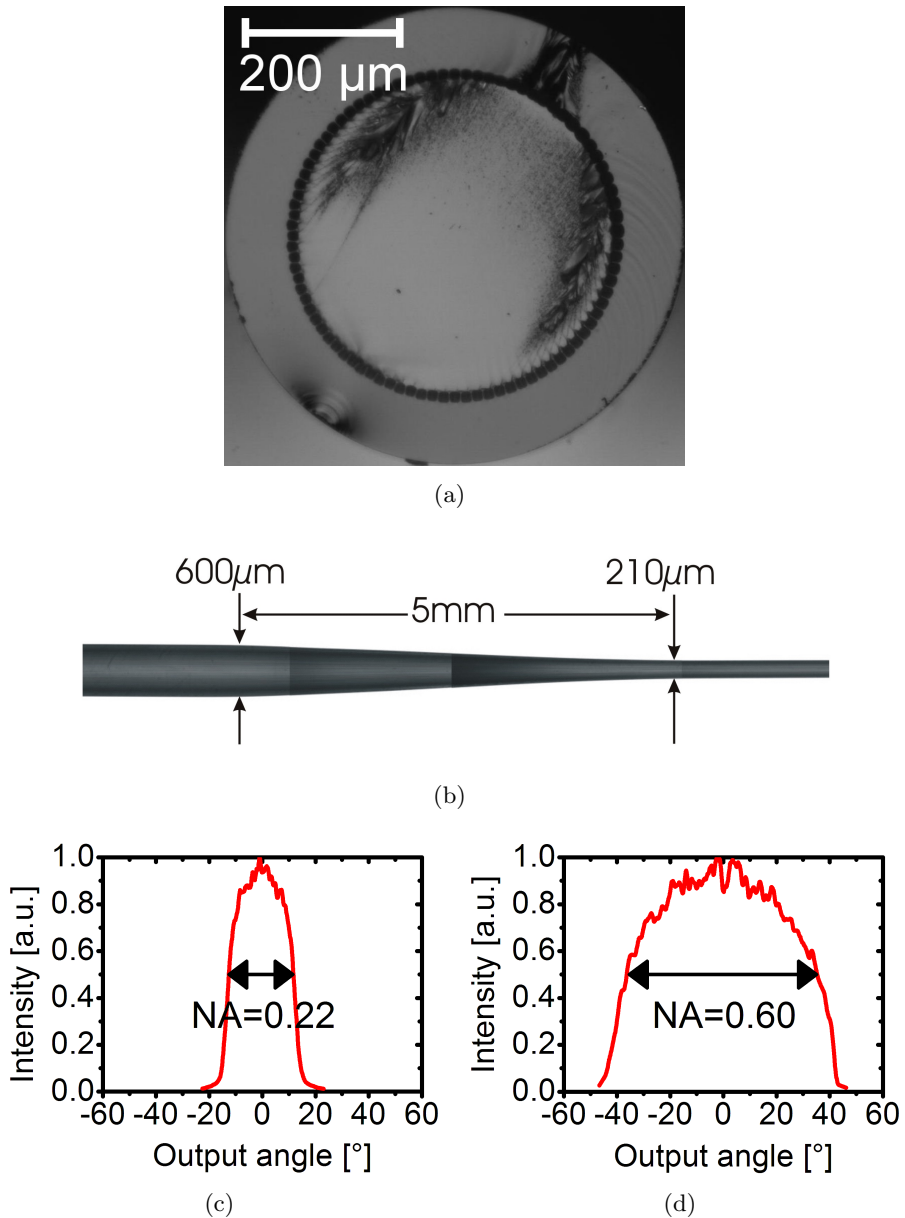


Figure 4.2: (a) Microscope cross sectional image of an air-clad taper fiber. (b) 5 mm long air-clad pump taper. The fiber is tapered from a core diameter of $400 \mu\text{m}$ to $150 \mu\text{m}$. (c-d) Measured NA of the light in the untapered end (b) and in the tapered end (c).

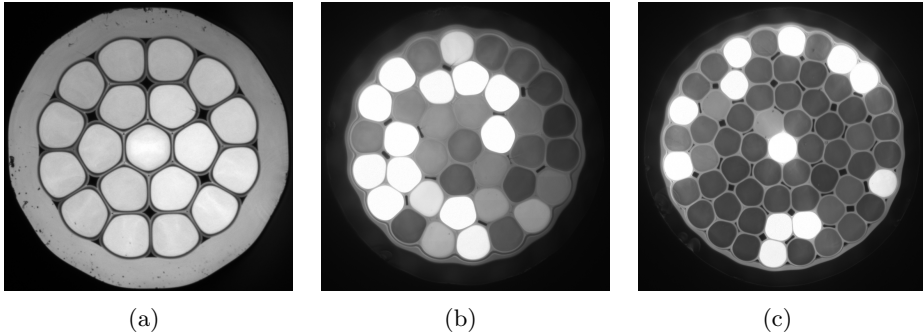


Figure 4.3: Fused bundles of $105\ \mu\text{m}$ core MM fibers From left to right the images show 19, 37 and 61 fiber bundles.

As described in chapter 3, single emitter laser diodes are attractive for making high power fiber lasers. The output is typically delivered in a $105\ \mu\text{m}$ core fiber and in an NA of 0.15 or 0.22 [99, 100]. For this reason the pump fibers of the fabricated combiners are 0.22 NA fibers with a core and cladding diameter of $105\ \mu\text{m}$ and $125\ \mu\text{m}$, respectively. With these pump fibers 7, 19, 37 and 61 port combiners have been realized [18, 19, 38]. Images of the fiber bundles used in these combiners are shown in Fig. 4.3.

4.2 Air-clad fiber laser

With the above described combiner approach a monolithic 350 W laser has been fabricated. Figure 4.4(a) shows an illustration of the laser setup. The laser consists of a master oscillator and a power amplifier. The master oscillator is defined by two fiber Bragg gratings (FBGs), written in the photosensitive step-index core of the ytterbium-doped air-clad fiber. The first FBG is a high reflector (HR) with a reflectivity of $>98\%$ and a bandwidth of 800 pm. The second FBG is an output coupler (OC) with a reflectivity of $\sim 30\%$ and a bandwidth of 600 pm. The OC is written 7 m into the active fiber, and the total length of active fiber is 25 m. The fiber laser is designed for pumping at a wavelength of 915 nm. Since both FBGs are written in the signal core of the active fiber, this means that the high NA pump light is not reflected by the gratings. In the power amplifier section the signal is therefore further amplified. The laser output is delivered in a passive step-index single-mode fiber, that is spliced to the active fiber. The mode field diam-

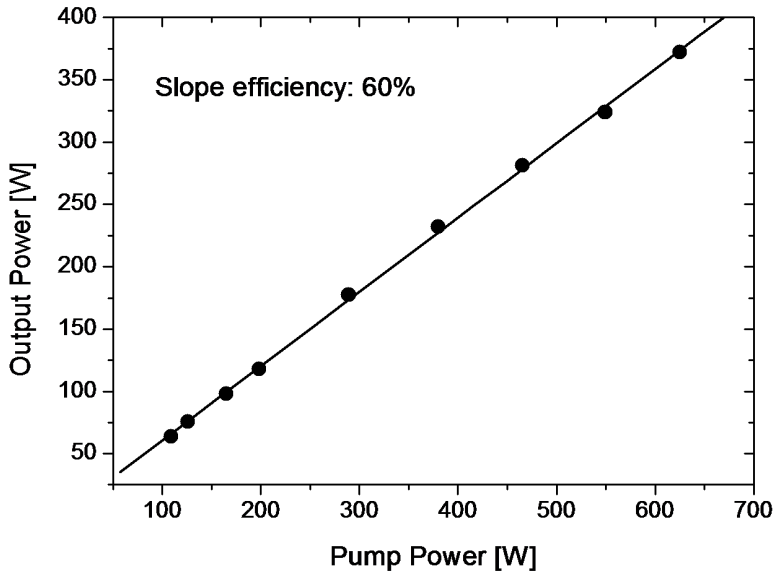
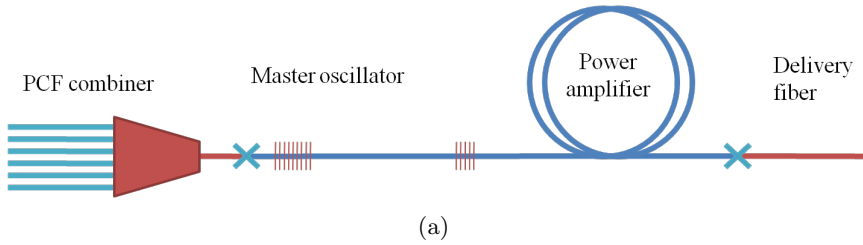


Figure 4.4: (a) Schematic illustration of the 350 W monolithic MOPA fiber laser configuration. The fiber laser is pumped with an air-clad combiner spliced to the active fiber. The combiner can either be a 1x1 or 61x1 combiner. The laser output is delivered through a passive step-index single-mode fiber.

eter (MFD) of both the active fiber and the signal delivery fiber is $15 \mu\text{m}$. The inner diameter of the air-clad is $250 \mu\text{m}$, and the pump absorption at a wavelength of 915 nm is 0.5 dB/m .

An output power of 350 W is reached with either a 61x1 pump combiner or a 1x1 combiner. The 61x1 combiner is fabricated as described in the previous section. It has an air-clad delivery fiber of $245 \mu\text{m}$ and supports 61 single emitter diodes with an NA of 0.15 and an output power of 10 W delivered in $105 \mu\text{m}$ core fibers. The average pump power loss for a single

pump port is typically <0.2 dB. The 1x1 combiner is a simple air-clad taper, that couples the output from an 800 W fiber coupled pump module operating at 915 nm into the active fiber. The pump power is delivered in a 400 μm MM fiber and in an NA of 0.22. The pump laser has several diode laser stacks that are multiplexed and coupled into the delivery fiber using bulk optics. The laser is fabricated by Laserline [101]. The 1x1 combiner is fabricated similarly to the 61x1 combiner, except that the fused bundle is replaced by the 400 μm core delivery fiber of the pump laser. The pump power loss in this combiner is <0.2 dB. Figure 4.4(b) shows the optical to optical efficiency of the air-clad fiber laser, when pumped by the Laserline pump module. A maximum signal power of just above 350 W is achieved with a slope efficiency of 60%. The M^2 value of the signal is measured to be <1.1 . This indicates a strictly single-mode (SM) output from the laser.

4.3 Gain switched air-clad fiber laser for supercontinuum generation

Supercontinuum generation is extreme spectral broadening of a laser pulse. This can be achieved in a highly nonlinear PCF. Supercontinuum generation has been explored by a number of groups in the past decade, and supercontinuum generated light spanning the entire transmission window of silica based fibers has been demonstrated [102–104].

Typically, pulsed laser sources are used for pumping the nonlinear PCF. This is due to the high peak power that can be achieved with these sources. A high peak power results in a broad spectrum. An alternative approach is to use a high-power continuous wave (CW) fiber laser. With such a laser both a higher average power and a higher spectral power density of the supercontinuum generated light can be achieved. A drawback of the system is that the reduced peak power, results in less spectral broadening in the nonlinear PCF.

A method to greatly improve the spectral broadening of the generated supercontinuum, is by a fast on/off modulation of the fiber laser [105, 106]. This is done by a fast on/off modulation of the fiber lasers pump diodes. When the pump diodes of the fiber laser are turned on the laser sends out a few powerful laser pulses before it goes CW. These spikes are known as relaxation oscillations. With a fast on/off modulation of the pump diodes in the 100 kHz range, the first and most powerful spike can be isolated. A pulse train of high peak power pulses is then generated, with a repetition

rate equal to the modulation frequency applied to the pump diodes. This method of turning a CW laser into a pulsed source is referred to as gain-switching [107, 108].

With a gain switched fiber laser spliced to a highly nonlinear PCF a completely monolithic supercontinuum source can be created. The result is a more simple supercontinuum system, compared to the more common approach with a low power Q-switched laser, that is amplified in a number of amplifier stages.

4.3.1 Gain switched air-clad fiber laser

The air-clad fiber laser that is used for gain switching is described in section 4.2 of this chapter. In order to be able to do a fast on/off modulation of single-emitter laser diodes the 61x1 combiner is used in stead of the 1x1 combiner. 10 fiber-coupled 915 nm laser diodes with a maximum rated output power of 10 W are used to pump the fiber laser. A high-power laser diode driver controlled by a pulse generator is used to drive the laser diodes. The pulse generator controls the repetition rate and duty-cycle of the current that drives the laser diodes. With 10 diodes pumping the fiber laser, a maximum CW average output power of 64 W can be achieved.

Figure 4.5(a) shows the behavior of the fiber laser after instantaneous

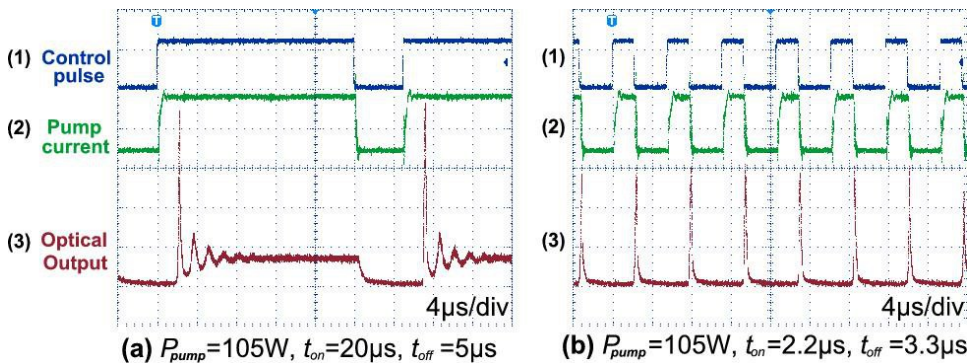


Figure 4.5: Oscilloscope traces of the transient behavior of the fiber laser. (a) shows the relaxation oscillation regime, and (b) shows the gain-switching regime. The blue line shows the control pulse, which is the output from the pulse generator. The green line shows the pump current, which is the output of the high power laser diode driver. The red line shows the optical output of the fiber laser measured with a fast photodiode.

turn-on of the pump. The figure shows three oscilloscope traces. The output from the pulse generator (blue line), the output of the high power laser diode driver (green line), and the optical output of the fiber laser measured with a fast photodiode (red line). The spikes or pulses that are seen before the laser goes into CW operation are the relaxation oscillations.

With a shorter width of the pump pulses only the first spike will appear, and the fiber laser will be running in gain-switched operation. Figure 4.5(b) shows this single pulse operation regime. A maximum peak power of 700 W can be achieved, with a pulse duration of 200 ns, a repetition rate of 210 kHz, an average power of 29 W and a pulse energy of 150 μJ .

4.3.2 Supercontinuum generation with air-clad fiber laser

In order to generate a supercontinuum, the delivery fiber of the laser is spliced to 100 m of nonlinear PCF (SC-5.0-1040 from NKT Photonics A/S). This splice is made by the use of an intermediate fiber, that reduces the MFD from 15 μm to 4 μm in order to match the MFD of the nonlinear PCF. The total splice loss between the delivery fiber and the nonlinear PCF is 0.7 dB.

Supercontinuum generation in a nonlinear PCF pumped with pico or nanosecond pulses is initiated by modulation instabilities. This creates solitons in the anomalous dispersion region and dispersive waves in the normal dispersion region below the pump wavelength. The solitons redshift due to Raman scattering and trap the dispersive waves through four-wave mixing causing them to blueshift. The long wavelength edge of the spectrum is defined by silica absorption at infrared wavelengths, and the short wavelength edge is defined by group velocity matching to the long wavelength edge [103, 109, 110].

Figure 4.6 shows the supercontinuum generated spectra, with the laser in CW and in gain-switched operation. Both spectra are obtained with an average laser output power of 29 W. For the gain-switched operation, the peak power of the pulses is 700 W and the pulse duration is 200 ns. The supercontinuum spectra is much narrower with the laser in CW operation. This is due to the much lower peak power compared to gain-switched operation, which means that the modulation instability is less efficient. The high-energy solitons that can redshift to the loss edge are simply not formed. For the laser in CW operation the spectrum spans from 950 nm to 1650 nm, when the edges are defined as the -10 dBm/nm power level. The total average output power is 17 W. For the laser in gain-switched operation, the spectrum spans from 500 nm to 2250 nm, when the -10 dBm/nm power limit

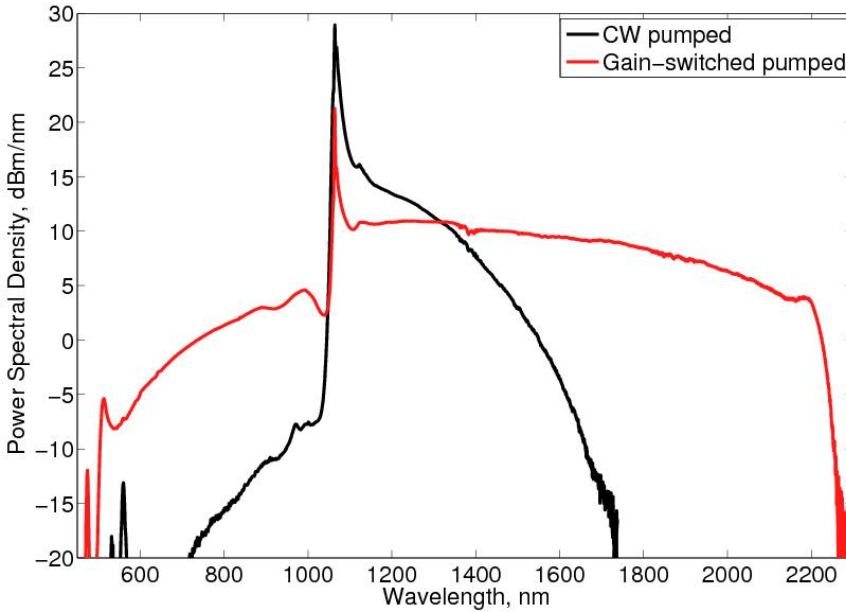


Figure 4.6: Supercontinuum generation in the nonlinear PCF pumped by the air-clad fiber laser. The spectrum is shown with the laser in CW operation and in gain-switched operation. Both spectra are obtained with an average laser output power of 29 W. In gain-switched operation the peak power of the pulses is 700 W and the pulse duration is 200 ns.

is used. At infrared wavelengths the edge of the spectrum is determined by absorption in the silica based fiber. The total average output power is 12 W, which is lower than for the CW case. This is due to the broader spectrum, which means that some light is lost at the infrared-loss edge of the nonlinear PCF.

The demonstrated supercontinuum spectrum with the fiber laser in gain-switched operation is broader than what has been reported with 100 W and even 400 W CW fiber lasers [111, 112]. Furthermore, the setup used to generate the supercontinuum is much simpler than the typical ps-pumped supercontinuum sources.

4.4 Summary of chapter 4

In this chapter monolithic, all-fiber, tapered pump combiners for air-clad fibers are described. The combiners are fabricated using the fused fiber bundle with tapered bridging fiber approach. A 350 W fiber laser is described, which is made possible by the use of a 61x1 or 1x1 pump combiner. The chapter ends with a description of supercontinuum generation with the air-clad fiber laser. Broad spectra are demonstrated, with the fiber laser in gain-switched operation. In this operation the total average output power is 17 W, and a spectrum that spans from 500 nm to 2250 nm, when the -10 dBm/nm power limit is used.

Chapter 5

Signal combiners for beam combining of fiber lasers

This chapter describes an all-fiber 7x1 signal combiner for incoherent laser beam combining. This is a potential key component for reaching several kW of stable laser output power. The combiner couples the output from 7 single-mode (SM) fiber lasers into a single multi-mode (MM) fiber. The input signal fibers have a core diameter of $17\ \mu\text{m}$ and the output MM fiber has a core diameter of $100\ \mu\text{m}$. In a tapered section light gradually leaks out of the SM fibers and is captured by a surrounding fluorine-doped cladding. The combiner is tested up to 2.5 kW of combined output power.

5.1 Signal combiner fabrication

The combiners are fabricated using filament based GPX glass processing stations from Vytran [58]. These stations are used for fusing of bundles, tapering and splicing. Figure 5.1 shows an illustration of the combiner. The signal fibers are step-index single-clad fibers with a core diameter of $17\ \mu\text{m}$ and an outer diameter of $125\ \mu\text{m}$. A bundle of 7 of these fibers is inserted into a fluorine-doped glass capillary tube. This fiber filled capillary tube is fused and tapered down into a solid glass element. The tapered element will act as a MM waveguide with a core that consists of the fused SM fibers and a cladding formed by the low-index capillary tube. Figure 5.1(b)-(c) shows images of the fused and tapered bundle cross-section along the length of the taper. The tapered fiber bundle is spliced to a MM fiber with a core diameter of $100\ \mu\text{m}$, an outer diameter of $660\ \mu\text{m}$ and a numerical

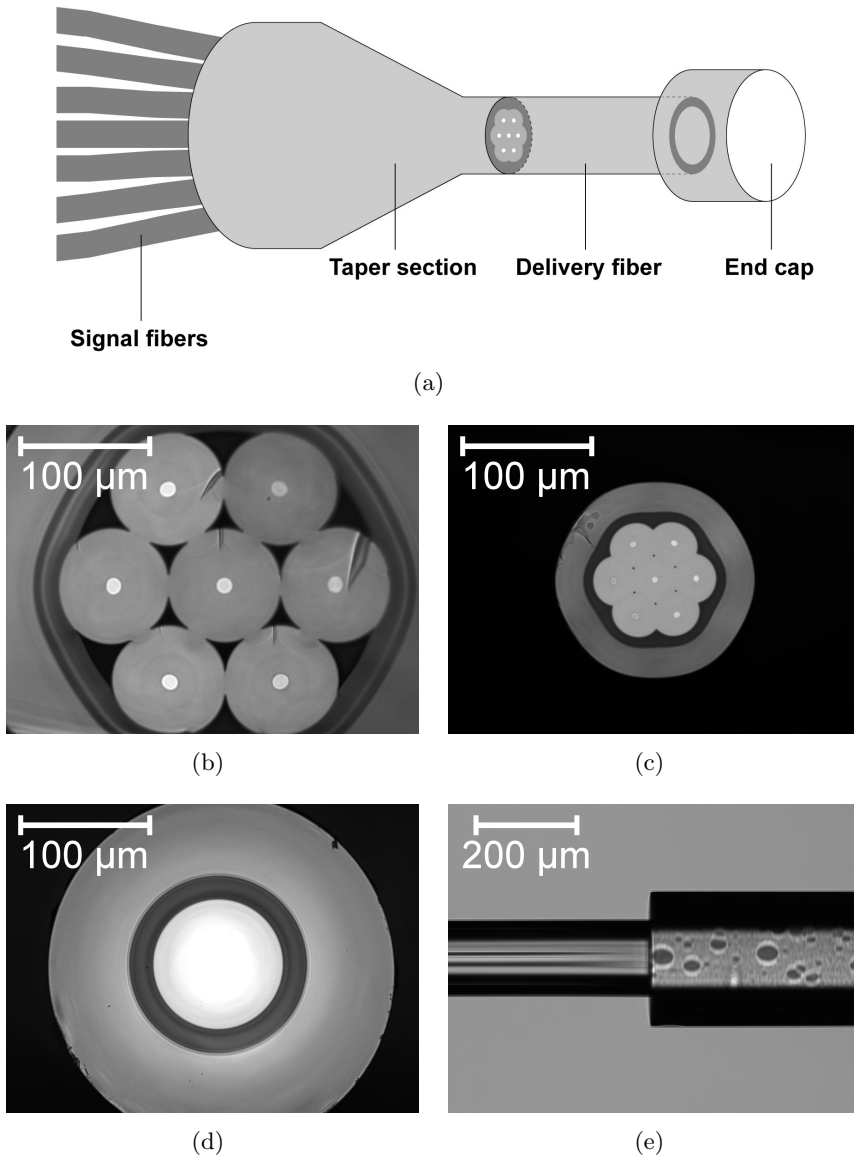


Figure 5.1: (a) Schematic illustration of the signal combiner. (b)-(c) Images of the taper cross-section along the length of the taper. The diameter of the 7 fibers is $255\ \mu\text{m}$ and $95\ \mu\text{m}$, respectively. (d) Image of the multi-mode fiber facet. In the image the fiber is etched to better match the outer diameter of the fused bundle. The diameter of the core is $100\ \mu\text{m}$. (e) Image of the tapered fiber bundle (right) spliced to the etched MM fiber.

aperture (NA) of 0.22. In order to increase the mechanical strength of the splice, the outer diameter of the MM fiber is reduced by a chemical wet etching process. Figure 5.1(d) shows a cross-sectional image of the etched MM fiber. Figure 5.1(e) shows an image of the splice.

5.2 High-power connector

To avoid back-reflections into the signal combiner, the MM fiber is fitted with a high-power connector from Optoskand [113]. This connector consists of an aluminum holder, in which the MM fiber is fixed. It also holds a 20 mm long fused silica end-cap which is spliced to the MM fiber. The exit surface of the end-cap is anti-reflection coated, which reduces the overall losses in the connector. The connector is designed for withstanding very high levels of back-reflection from the work piece, as might be the case in material processing. It is specified to handle 5 kW of average power and has a loss of less than 3%. Figure 5.2(a) shows an illustration of the connector.

To achieve a high performance with low losses it is crucial to make a strong optical bond between the fiber and the end-cap. Figure 5.2(b) shows the defect-free optical bond between a 100 μm -core fiber (outer diameter 660 μm) and a fused silica end-cap seen through the 20 mm long end-cap. Both the core of the MM fiber and the endcap are pure silica. This means

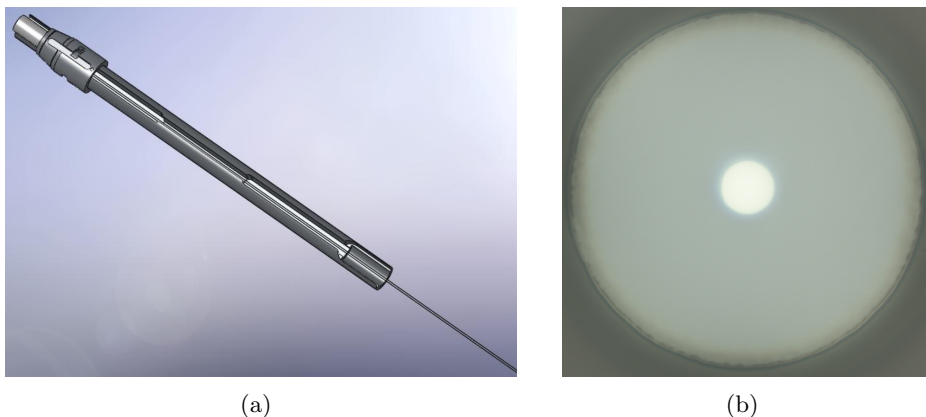


Figure 5.2: (a) Open QB pig-tail connector from Optoskand. (b) Optical bond between 100 μm -core fiber and fused silica end-cap seen through the end-cap. White light is guided in the core of the MM fiber.

that there is no refractive index step in the optical bond minimizing losses and back-reflections.

5.3 Optical testing of the signal combiner

The combiner is first characterized at low power. The transmission loss of the combiner, the optical far-field and the M^2 value when combining 7 signals are measured. All measurements are made with a fiber laser delivering an output power of ~ 1 W at a wavelength of 1060 nm. For measuring the transmission loss, the fiber laser is in turn spliced to each of the signal ports of the combiner. The loss for each of the ports is measured and shown in Table 5.1. All of the ports have approximately the same low loss with an average value of 4.6%.

By launching light into all of the 7 input ports of the combiner the combined optical far-field out of the MM fiber can be measured. This measurement is also made at low power with a combined output power of ~ 1 W and at a wavelength of 1060 nm. The measured NA filling corresponds to 95% of the light having an NA lower than 0.06. Using a Spiricon laser beam profiler the beam quality is investigated and the value for M^2 was found to be 6.8.

Port number	Signal loss [%]
1	3.8
2	4.6
3	5.4
4	4.9
5	4.5
6	4.9
7	4.4
Average	4.6

Table 5.1: Measured signal loss in the combiner for each of the 7 input ports.

5.4 High-power fiber lasers

For high power testing of the combiner, three kW continuous wave (CW) fiber lasers manufactured by Rofin-Sinar Laser GmbH are used [114]. The lasers have a passive output fiber with a core diameter of $20\ \mu\text{m}$ and give a single-mode output with a beam parameter product (BPP) of $<0.4\ \text{mm} \times \text{mrad}$. The wavelength of operation is 1070 nm or 1080 nm. The kW class fiber lasers are based on an all-fiber oscillator. The optical to optical efficiency is about 80% depending on the pump wavelength. An electrical to optical efficiency of up to 38% can be achieved.

5.5 High-power beam combining

The three kW fiber lasers are spliced onto three randomly chosen ports of the signal combiner. These ports have the numbers 4, 6 and 7, and turned out to be the center port and two of the side ports spaced by one fiber. The splice between the delivery fiber of the fiber laser and the input fiber of the combiner is done with a Fujikura large diameter fiber splicer. The splice loss is $\sim 4\%$. The power out of the three fiber lasers is simultaneously increased, such that the power into each of the input ports is approximately the same. The combined output power as a function of total input power is

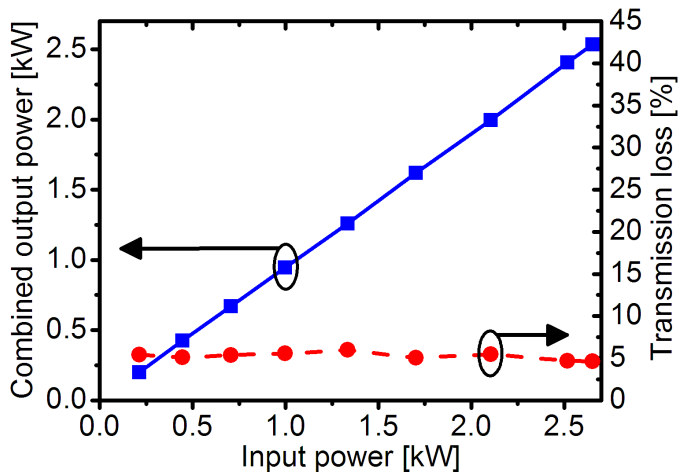


Figure 5.3: Combined output power as a function of total input power (solid line). Transmission loss of the signal light in the combiner (dashed line).

shown as the solid line in Fig. 5.3. In the figure, the transmission loss of the signal light is shown as the dashed line. A linear behavior of the combiner is observed with no roll off at high powers and with an average signal loss of 5.3%. The highest achieved output power is 2.54 kW. At this power level the combiner dissipates 129 W of the signal, but only a minor increase in device temperature to 38°C is observed. This means that most of the light is successfully stripped off optically rather than being absorbed.

The beam quality is investigated with a Primes Focus monitor [115]. This is done at a combined output power of 600 W. A beam parameter product of 2.22 mm x mrad corresponding to an M^2 value of 6.5 is measured. These measurements are in excellent agreement with the values measured at low power. The power distribution in the near-field of the MM fiber is shown in Fig. 5.4. From the figure it is clear that the distribution is not uniform. A large peak in the intensity is seen in the left side of the figure. By launching light into all of the ports of the combiner instead of only three, a more uniform distribution can be obtained. It is also believed that the distribution

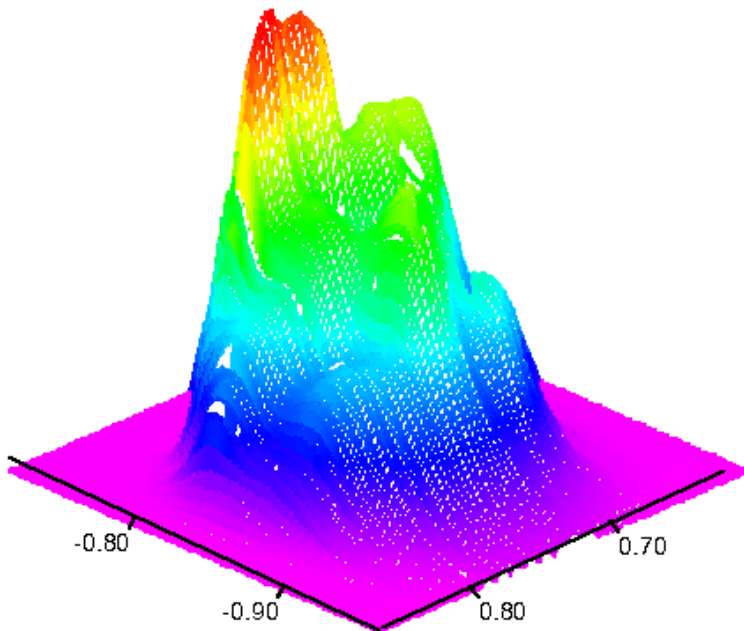


Figure 5.4: Power distribution in the near-field of the MM fiber at a combined output power of 600 W.

can be made more uniform by increasing the taper ratio of the fiber bundle. A larger taper ratio will result in smaller high-index inclusions in the tapered end of the fiber bundle. This means that the light will be less confined to these inclusions and more smeared out over the entire MM core.

5.6 Summary of chapter 5

This chapter describes an all-fiber 7x1 signal combiner for incoherent laser beam combining. The 7 input fibers are step-index single-clad fibers with a core diameter of 17 μm . The output fiber is a MM fiber with a core diameter of 100 μm . A maximum combined CW output power of 2.5 kW is demonstrated with an M^2 value of 6.5. The signal loss in the combiner is $\sim 5\%$, which is effectively stripped away such that it does not damage any of the fiber coatings. The combined near-field showed peaks with very high intensity. It is believed that a more uniform near-field can be achieved by increasing the taper ratio of the fiber bundle, and also by using all the 7 ports of the combiner instead of only three.

Chapter 6

Pump/signal combiners for air-clad fiber amplifiers

This chapter describes a monolithic, all fiber, tapered 7+1x1 pump/signal combiner for air-clad fibers. Such fused fiber based combiners for coupling pump and signal light into active fibers are essential components for making fiber lasers and amplifiers [27]. The combiners are fabricated similarly to the combiners for photonic crystal fibers (PCFs) described in chapter 4. They have a fused fiber bundle that is spliced to a bridging fiber or taper element. The bridging fiber is tapered and spliced to a passive delivery fiber. The difference is that the combiners described in this chapter also have a signal feed-through, so that they can be used for pulse amplification.

The chapter begins with a description of the concept that makes the signal feed-through possible. This is a dual-core microstructured fiber concept that preserves the mode field diameter (MFD) in fiber tapers. A 6 μm MFD and a 15 μm polarization maintaining feed-through are described.

The fabrication of the combiner is then described. The combiner is designed for Yb-doped active fibers, which means a signal wavelength of 1064 nm and a pump wavelength of either 915 nm or 976 nm. The combiner is designed for pumping with 0.15 numerical aperture (NA) pump diodes, with the pump light delivered in 105 μm core fibers. It has a 15 μm MFD single-mode (SM) and polarization maintaining (PM) signal feed-through.

The chapter also describes two applications of the combiner. The first is pulse amplification and the second is using the amplifier for supercontinuum generation in a nonlinear PCF. For the pulse amplification, the combiner is operated in a backward pumped configuration. Supercontinuum generation

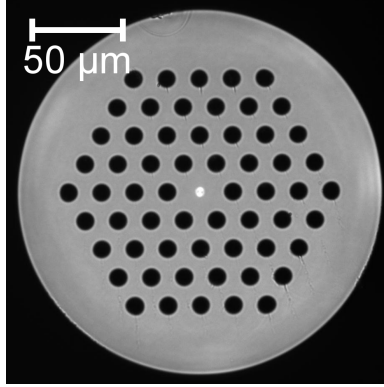
has been explored by a number of groups in the past decade, as described in chapter 4. This chapter shows that the fabricated combiner is useful for making a monolithic, all-spliced system for generating a broad high-power supercontinuum.

6.1 Mode field diameter preserving fiber tapers

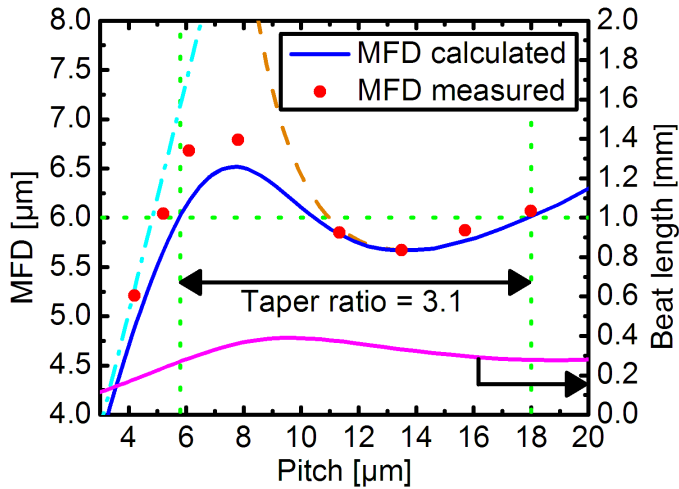
In order to have a signal feed-through in a tapered fiber there is a need to control the MFD of the signal light through the tapered section. This control can be achieved with dual-core fibers. These fibers can be realized with a pedestal design that consists of a step-index core with a highly doped region in the center [116, 117]. In the untapered fiber, light is guided in a central step-index core and in the tapered fiber it is guided in a second step-index pedestal core. In the tapered region light is coupled adiabatically between the two cores. An alternative approach is a concentric dual-core structure with a step-index core and a microstructured cladding region. In the untapered section of the fiber light is guided in a Ge-doped core. When the fiber is tapered, the light couples adiabatically to the core defined by a triangular PCF structure of air-holes [118]. The advantage of this approach is that a large taper ratio can be achieved with only two cores, and where the light is guided in a SM waveguide throughout the tapered section. This minimizes the risk of light scattering to higher order modes (HOMs). Furthermore, since the MFD in a large mode area PCF is proportional to the air-hole pitch of the fiber [64], the dual core PCF approach offers a larger degree of tailoring the MFD in the down tapered region. A dual-core PCF was first demonstrated by Eggleton *et al.* [119]. In this work a low NA Ge-doped center of a PCF, enabled the writing of Bragg and long period gratings in the fiber.

6.1.1 Air-hole based 6 μm MFD feed-through

The structure of the fabricated dual-core fiber is shown in Fig. 6.1(a). In the center of the fiber the step-index core can be seen and around this core the triangular structure of air-holes. Except for the doped center, the material of the fiber is pure Silica. The step-index core is Ge-doped, has a diameter of 5.4 μm and a NA of 0.14. This results in a fiber with a MFD of 6.1 μm at a wavelength of 1064 nm and a HOM cut-off wavelength of 990 nm. The air-hole pitch is 18 μm , and the light in the core mode of the untapered fiber is unaffected by the presence of the holes. This is due to a



(a)



(b)

Figure 6.1: (a) Microscope cross sectional image of air-hole based $6\ \mu\text{m}$ MFD feed-through taper fiber. (b) MFD as a function of air-hole pitch for the $6\ \mu\text{m}$ MFD feed-through taper fiber. The full line shows the simulated MFD and the dots show the measured MFD at different positions along the taper. The vertical dotted lines indicate the pitch of the taper fiber in the tapered and untapered end where a $6\ \mu\text{m}$ MFD is maintained. The dashed line indicates the MFD for a pure step-index fiber and the dash-dotted line indicates the MFD for a pure PCF. The purple line shows the beat length between the core mode and the first cladding mode.

small overlap between the core mode and the air-hole structure, and because the effective index of a large pitch microstructured cladding approaches the index of Silica. The diameter of the holes relative to the pitch is 0.48. The taper fiber is designed to maintain a 6 μm MFD for a taper ratio of 3.1. Figure 6.1(b) shows a calculation of the MFD in the fiber as a function of air-hole pitch (solid blue line). The calculation is made using a full vectorial mode solver based on the plane-wave expansion method [51]. When the fiber is tapered the MFD initially decreases slightly and then increases. This follows the normal behavior of a step-index core. As the guiding of the step-index core becomes weaker, the air-holes approach the center of the fiber and gradually take over the guiding of the light. This decreases the MFD once again. For reference Fig. 6.1(b) shows the MFD as a function of pitch in a pure step-index fiber without the presence of air-holes (dashed line), and in a pure PCF without the presence of the step-index core (dash dotted line).

To ensure a low taper loss the adiabatic criterion defined in Eq. 2.16 has to be fulfilled. Since the tapering is made with a simple linear taper profile, Eq. 2.17 can be used to define the length of the taper (L) in order to be adiabatic. The purple full line in Fig. 6.1(b) shows the beat length between the core mode and the first HOM. The beat length has a maximum value of $L_{B,max} = 0.39$ mm. With a taper ratio of 3.1 the minimum taper length to ensure an adiabatic linear taper is

$$L \geq (TR - 1)L_{B,max} = \underline{0.82 \text{ mm}}. \quad (6.1)$$

The fiber is tapered using a filament based GPX glass processing station from Vytran [58, 59]. This is done by careful control of the filament power in order to prevent a collapse of the air-holes. A long taper length of 3 mm is chosen in order to be sure that the taper is adiabatic and has low loss. In Fig. 6.1(b) the experimentally measured MFD of the fiber is shown at different positions along a taper (red dots). The measurements were made using a 1064 nm light source and an infrared camera, and are in good agreement with the simulations. In Fig. 6.2 two of the measured near-fields of the taper fiber are shown. In Fig. 6.2(a) the near-field of the untapered fiber is shown, where the fiber pitch is 18 μm . A circular mode is observed and the MFD is measured to 6.1 μm . In Fig. 6.2(b) the near-field of the fiber tapered to a pitch of 5.2 μm is shown. A hexagonal mode, characteristic for the PCF, is observed and the MFD is measured to 6.0 μm . Hence, a MFD close to 6 μm is maintained when tapering the fiber by a factor of 3.1.

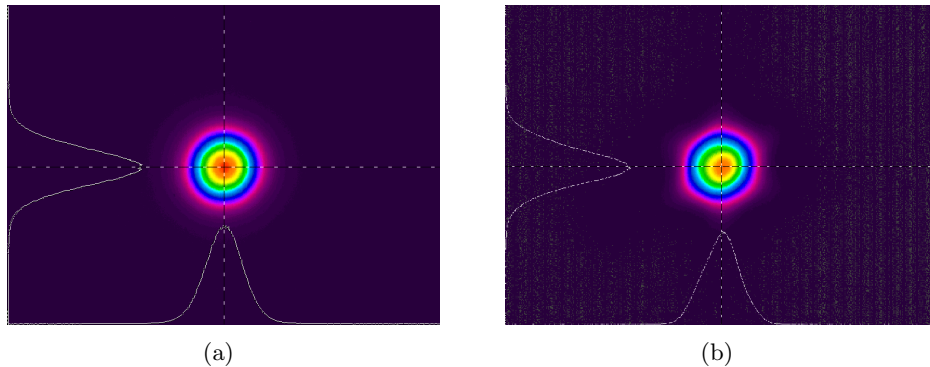


Figure 6.2: Experimentally obtained near-field images of $6 \mu\text{m}$ MFD feed-through taper fiber. (a) shows the untapered fiber. (b) shows the fiber tapereded by a factor of 3.5.

An important parameter when making combiners is the loss in the taper. In order to evaluate this loss, a Corning HI1060 fiber is spliced to both the tapered and the untapered end of the taper fiber. The HI1060 fiber has a MFD of $6.2 \mu\text{m}$ at a wavelength of 1060 nm , matching the MFD in both ends of the taper fiber. The combined loss in the two splices and the taper are measured to be 0.55 dB at a wavelength of 1064 nm . The loss in the two splices is estimated to $\sim 0.1 \text{ dB}$ for the HI1060 fiber to the untapered fiber, and $\sim 0.2 \text{ dB}$ for the HI1060 fiber to the tapered fiber. The higher splice loss to the tapered fiber is due to the need to preserve the air-holes with a cold splice and due to the slight reduction in the overlap between the modes caused by the hexagonal mode shape of the PCF. The taper loss is therefore $\sim 0.25 \text{ dB}$, which indicates that an adiabatic transition between the two cores in the tapering is achieved.

6.1.2 Air-hole based $15 \mu\text{m}$ MFD feed-through

For high-power double-clad fiber lasers and amplifiers, a PM signal feed-through and a larger MFD than $6 \mu\text{m}$ are generally required. A $15 \mu\text{m}$ MFD taper fiber is therefore investigated with a similar design as the $6 \mu\text{m}$ taper fiber. On either side of the core an air-hole is replaced with a Boron doped stress rod in order to ensure PM operation. Fig. 6.3(a) shows a microscope image of the taper fiber. The step-index core diameter is $13.3 \mu\text{m}$ and the HOM cut-off wavelength is $\sim 980 \text{ nm}$. The air-hole structure has a pitch of

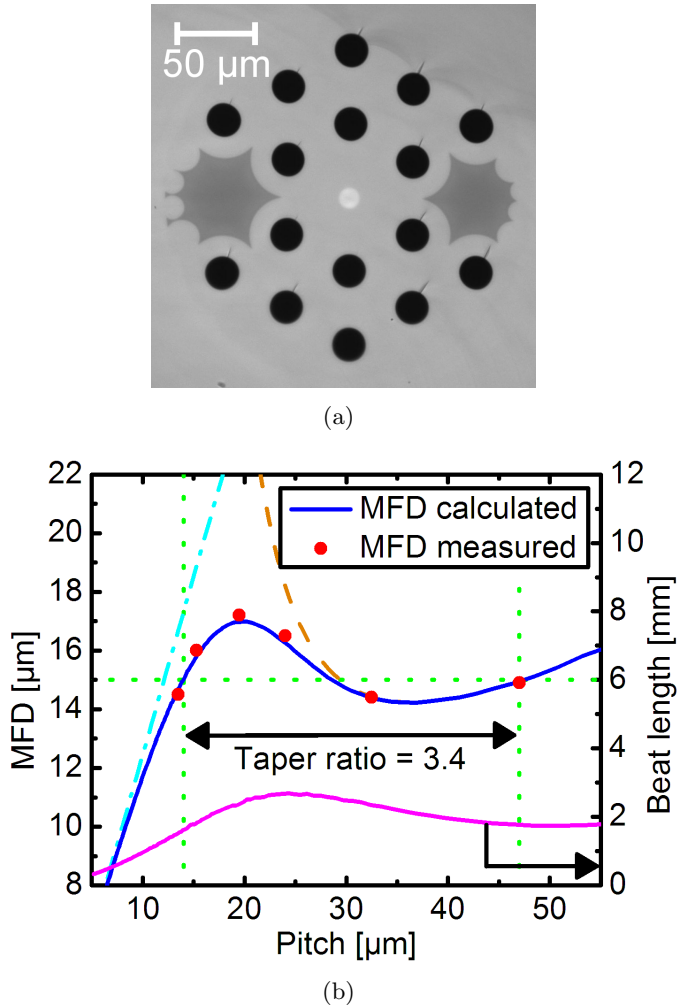


Figure 6.3: (a) Microscope cross sectional image of air-hole based 15 μm MFD feed-through PM taper fiber. (b) MFD as a function of air-hole pitch for the 15 μm MFD feed-through fiber. The full line shows the simulated MFD and the dots show the measured MFD at different positions along the taper. The vertical dotted lines indicate the pitch of the taper fiber in the tapered and untapered end where a 15 μm MFD is maintained. The dashed line indicates the MFD for a pure step-index fiber and the dash-dotted line indicates the MFD for a pure PCF. The purple line shows the beat length between the core mode and the first cladding mode.

47 μm and an air-hole diameter divided by pitch of 0.45.

Simulations are made to examine the evolution of the MFD through the taper. For the simulations, a perfect structure without stress elements is used. The results are shown in Fig. 6.3(b). The solid blue line indicates the MFD of the fiber, the dashed line shows the MFD of a pure step-index core fiber, and the dash dotted line shows the MFD of a pure PCF. The full purple line in Fig. 6.3(b) shows the beat length between the core mode and the first HOM. The beat length has a maximum value of $L_{B,max} = 2.69$ mm. For a taper ratio of 3.4, a MFD close to 15 μm will be maintained through the taper. From Eq. 2 the minimum taper length to ensure an adiabatic linear taper is $L = 6.46$ mm. In order to ensure that the taper is adiabatic a longer taper length of 15 mm is chosen. In the untapered fiber the MFD is 14.9 μm at a wavelength of 1064 nm. When the fiber is tapered down to a pitch of 13.5 μm , the air-hole structure facilitates guiding, resulting in a hexagonal mode with a MFD of 14.5 μm . Fig. 6.3(b) shows the measured MFD of the fiber at different positions along the taper (red dots). The measured MFD is in good agreement with the simulations.

In order to measure the loss in the taper a 15 μm MFD SM PM fiber is spliced to the untapered end of the taper fiber and to the down tapered end. The combined loss in the two splices and the taper is measured to be 0.70 dB at a wavelength of 1064 nm. Assuming the same splice loss as for the 6 μm fiber investigation, the loss in the taper is ~ 0.30 dB. This is comparable to what was achieved for the 6 μm taper fiber, again indicating a smooth adiabatic transition in the taper.

For making PM combiners it is important that light does not couple between the two polarization states of the taper fiber. The polarization cross talk is therefore measured with a polarized light source. It is found that through the combined setup of two splices and the taper, the cross talk between the two polarization states is below -18 dB. This fulfills the requirements for typical PM combiners.

6.1.3 F-doped rod based 15 μm MFD feed-through

When combining the air-hole based MFD preserving dual-core fiber concept with an air-clad in one fiber, there will be two sets of holes to control when the fiber is tapered. For this reason a dual-core fiber, where the air-holes are replaced with F-doped rods is investigated. Fig. 6.4(a) shows a microscope image of the taper fiber. In the center, the step-index core is seen and around this core the triangular structure of F-doped inclusions. On either side of

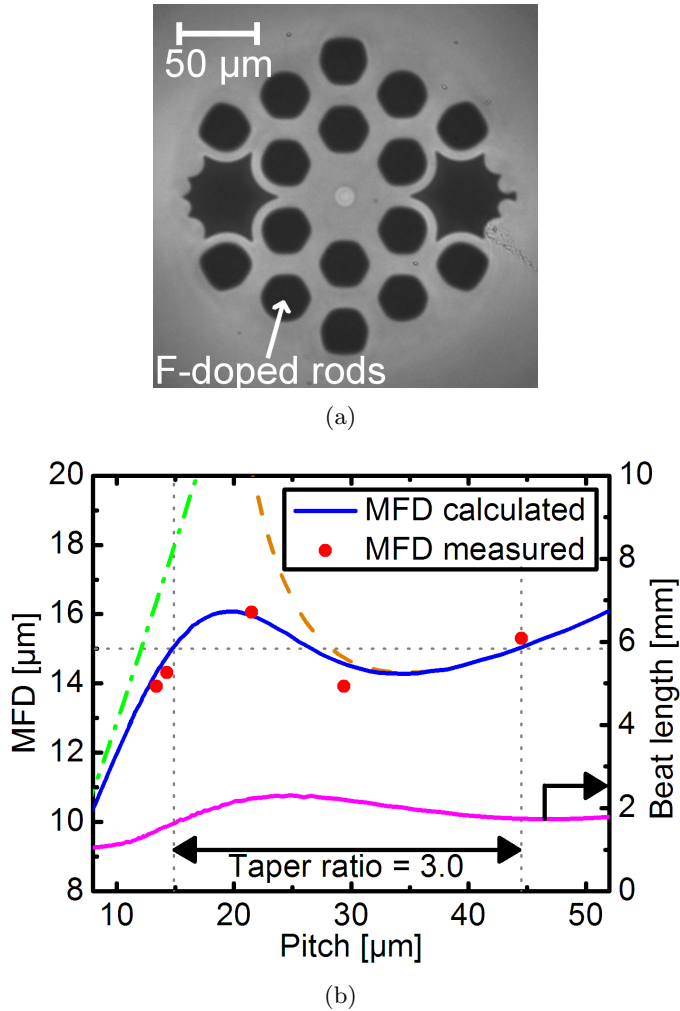


Figure 6.4: (a) Microscope cross sectional image of F-doped rod based 15 μm MFD feed-through PM taper fiber. (b) MFD as a function of taper element pitch. The full blue line shows the simulated MFD and the red dots show the measured MFD at different positions in the taper. The dotted grey lines indicate the pitch of the taper element where a 15 μm MFD is maintained. The dashed orange line indicates the MFD for a fiber with no F-doped rods and the dash-dotted green line indicates the MFD for a fiber with no step-index core. The purple line shows the beat length between the core mode and the first cladding mode.

the core an F-doped rod is replaced with a boron doped stress applying rod in order to facilitate PM operation. The background material of the fiber is pure silica. The step-index core has a diameter of $13.3 \mu\text{m}$ and an NA of 0.06. The F-doped rod pitch is $44.5 \mu\text{m}$, the diameter to pitch ratio is 0.6 and the refractive index is 7% lower than silica. Figure 6.4(b) shows a calculation of the MFD in the fiber as a function of the structural scale quantified by the F-doped rod pitch (solid blue line). The calculation is made using a full vectorial mode solver based on the plane-wave expansion method [51]. In the untapered fiber (pitch= $44.5 \mu\text{m}$) light in the step-index core mode is unaffected by the presence of the F-doped rods. As is the case for the air-hole based MFD preserving dual-core fibers. When the fiber is tapered the MFD initially decreases and then increases. As the guiding of the step-index core becomes weaker, the F-doped rods approach the center of the fiber and light gradually couples to the core defined by these rods. This decreases the MFD once again. As a result the taper fiber can be tapered by a factor of 3 while preserving a MFD of $15 \mu\text{m}$. For reference, Fig. 6.4(b) shows the MFD as a function of pitch in a pure step-index fiber without the presence of F-doped rods (dashed line), and in a pure PCF without the presence of the step-index core (dash dotted line).

The fiber is tapered with a simple linear taper profile and Eq. 2.17 is once again used to define the length of the taper (L) in order to be adiabatic. The purple full line in Fig. 6.4(b) shows the beat length between the core mode and the first HOM. The beat length has a maximum value of $L_{B,max} = 2.3 \text{ mm}$. With a taper ratio of 3 the minimum taper length to ensure an adiabatic linear taper is

$$L \geq (TR - 1)L_{B,max} = \underline{4.6 \text{ mm}}. \quad (6.2)$$

A long taper length of 15 mm is chosen in order to be sure that the taper is adiabatic and has low loss. In Fig. 6.4(b) the experimentally measured MFD of the fiber is shown at different positions along the taper (red dots). The measurements are made using a 1064 nm light source and an infrared camera, and are in good agreement with the simulations. Hence, a MFD of $15 \mu\text{m}$ is maintained when tapering the fiber by a factor of 3.

6.2 Pump/signal combiner fabrication

Figure 6.5 shows an illustration of the combiner and images of the three main parts of the component. A cross sectional image of the passive double-clad

delivery fiber is shown in Fig. 6.5(b). The air-cladding of the fiber is seen as the ring of closely spaced holes surrounding the fiber core. The fiber has a SM and PM signal core with a $15\ \mu\text{m}$ MFD and a pump cladding diameter of $133\ \mu\text{m}$. A microscope cross sectional image of the fused fiber bundle is shown in Fig. 6.5(d). The signal fiber in the center is surrounded by the 7 pump fibers. The pump fibers are 0.22 NA fibers with a core and cladding diameter of $105\ \mu\text{m}$ and $125\ \mu\text{m}$, respectively. The signal fiber is a passive step-index SM and PM fiber with a higher order mode cutoff wavelength of $\sim 980\ \text{nm}$, a MFD of $15\ \mu\text{m}$, and a cladding diameter of $160\ \mu\text{m}$. A cross sectional image of the taper element is shown in Fig. 6.5(c). The function of the taper element is to couple pump light from the pump fibers of the fiber bundle into the pump-guide of the double-clad fiber, and via a taper to reduce the pump guide area. This reduction increases pump absorption

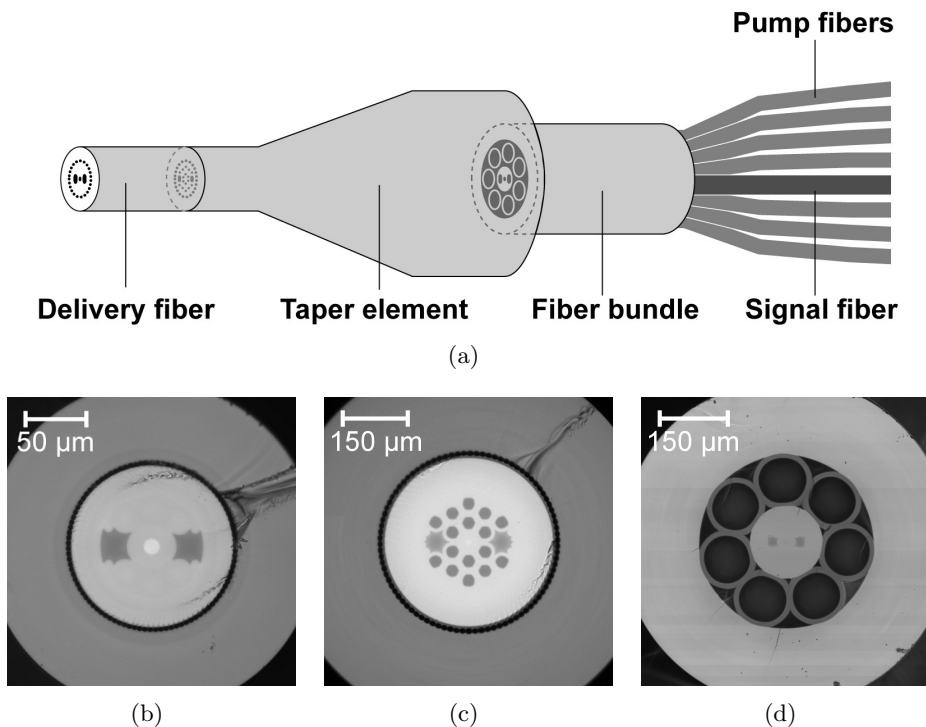


Figure 6.5: (a) Illustration of fused 7+1x1 pump/signal combiner. (b)-(d) Microscope cross sectional images of (b) delivery fiber, (c) taper element and (d) fiber bundle.

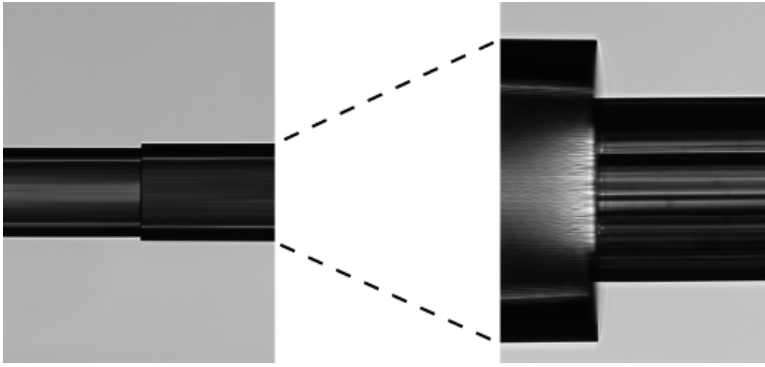


Figure 6.6: Images of the two splices in the combiner. Left side shows the splice between the passive delivery fiber and the tapered end of the taper element. Right side shows the splice between the taper element and the fused fiber bundle. The dashed line illustrates the tapering of the taper element.

in the active fiber. At the same time the taper element couples the signal light from the SM core of the double-clad fiber into the signal fiber of the fiber bundle (when operated in a backward pumped configuration).

The taper element has an air-cladding with an inner diameter of $400\ \mu\text{m}$ in the untapered end. When the taper element is spliced to the fiber bundle, this means that all the pump fibers are within the air-clad of the taper element. In the tapered end the diameter of the air-clad is $133\ \mu\text{m}$, which matches the diameter of the delivery fiber. The relation between pump core diameter and NA of the pump light in a tapered multi-mode (MM) fiber is given in Eq. 2.24. From this equation it is calculated that with the delivery fiber supporting a maximum NA of 0.6, and with a taper element tapered by a factor of 3, pump light with an $\text{NA} < 0.20$ will be supported by the combiner.

The center of the taper element is an F-rod based dual-core structure, similar to the one described in section 6.1.3. The minimum taper length of the taper element required to ensure a low loss for both pump and signal is defined by the low NA signal light and not by the high NA pump light. Therefore, the same 15 mm long linear taper profile as described in section 6.1.3 is used. The taper fiber is tapered using a filament based GPX glass processing station from Vytran [58]. This is done by control of the filament power in order to prevent a collapse of the air-clad holes.

The fused fiber bundle and the splices are also made using the GPX glass

processing station. The two splices of the combiner are shown in Fig. 6.6. The splice between the delivery fiber and the tapered end of the taper element is shown in the left side of the image, and the splice between the untapered end of the taper element and the fused bundle is shown on the right. The dashed line indicates the tapering of the taper element. Low temperature splices are made, in order to prevent a collapse of the air-clad holes. A slight collapse is seen in the bundle splice. This can be tolerated since the NA of the pump light is low in this end. The stress elements are aligned in the same plane throughout the combiner in order to facilitate PM operation of the component.

Characterization of the combiner is made for both pump ports and signal port. Pump transmission loss through the component is measured with a commercially available 915 nm 0.15 NA single-emitter laser diode. The diode is in turn spliced to each of the 7 ports and the transmission loss is measured. The average pump power loss is 0.13 dB, and the maximum pump power loss for a single port is 0.16 dB. Signal transmission loss is measured with a polarized light source at 1060 nm. The source is spliced to the signal fiber of the fused fiber bundle and the PER of the output light and the loss through the combiner is measured. The signal loss is 0.52 dB and the polarization extinction ratio (PER) is 20 dB.

6.3 Pulse amplification with active air-clad fiber

The combiner is tested in a pulse amplification system, using a commercially available Yb-doped double-clad PCF with a step-index 16 μm MFD PM signal core and a 135 μm air-clad (DC-135/15-PM-Yb from NKT Photonics A/S). Figure 6.7 shows an illustration of the setup. The active fiber is spliced to a pulsed fiber laser source, that seeds the active fiber with 6.5 ps pulses at a repetition rate of 80 MHz and an average power of 100 mW. The output fiber from the seed laser is a PM980 fiber with a MFD of 7 μm . The splice from PM980 to active fiber is made by a thermally expanded core (TEC) splice process. With this TEC splice a loss of ~ 0.5 dB for the signal is achieved. The active fiber is 6.2 m long and is spliced to the passive double-clad delivery fiber of the 7+1x1 combiner at the output end. The splice loss for the signal between the combiner and active fiber is ~ 0.3 dB. The fiber is pumped by four 10 W, 0.15 NA laser diodes emitting at a wavelength of 915 nm. Figure 6.8(a) shows the measured slope efficiency of the amplifier. The conversion efficiency of launched pump power into signal power is 53%.

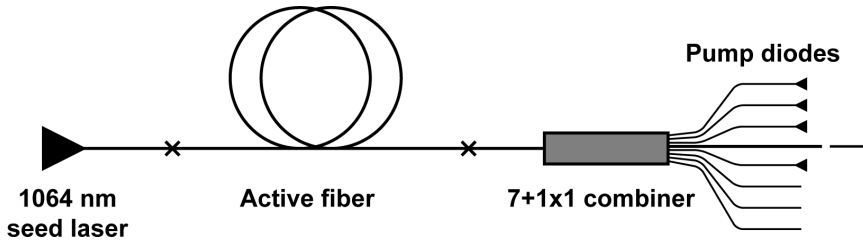


Figure 6.7: Illustration of pulse amplification setup.

After amplification the pulse width increases to 10 ps. The peak power of the pulses is shown in Fig. 6.8(a) on the right axis. A maximum average power of 17 W and a peak power of 21.3 kW is achieved. The signal to Raman noise level at this maximum power is 19 dB.

A SM signal out of the amplifier is obtained. This is due to the combiner and signal fiber which are strictly SM, with the latter having a higher order mode cutoff at ~ 980 nm. The M^2 value of the signal is measured to be < 1.1 . This value is measured from a low power level and up to 17 W.

In order to test the stability of the amplifier system, the setup is left running for 550 hours at a constant diode current. Figure 6.8(b) shows the results. Both the signal power (blue line) and the PER (red line) are recorded during the test. The vertical dotted green lines indicate a temporary stop in the test. The signal power drops from a starting power of 16.2 W down to a power of 15.3 W after 550 hours of operation. This translates to a decrease in signal power of 5.6%, and is related to photodarkening in the active fiber [120, 121]. Spikes in the PER of the amplified signal are observed when the amplifier is turned on. These are attributed to the relaxation of the thermal power meter used in the measurement. If these spikes are not taken into account, the PER is above 18 dB for the duration of the test.

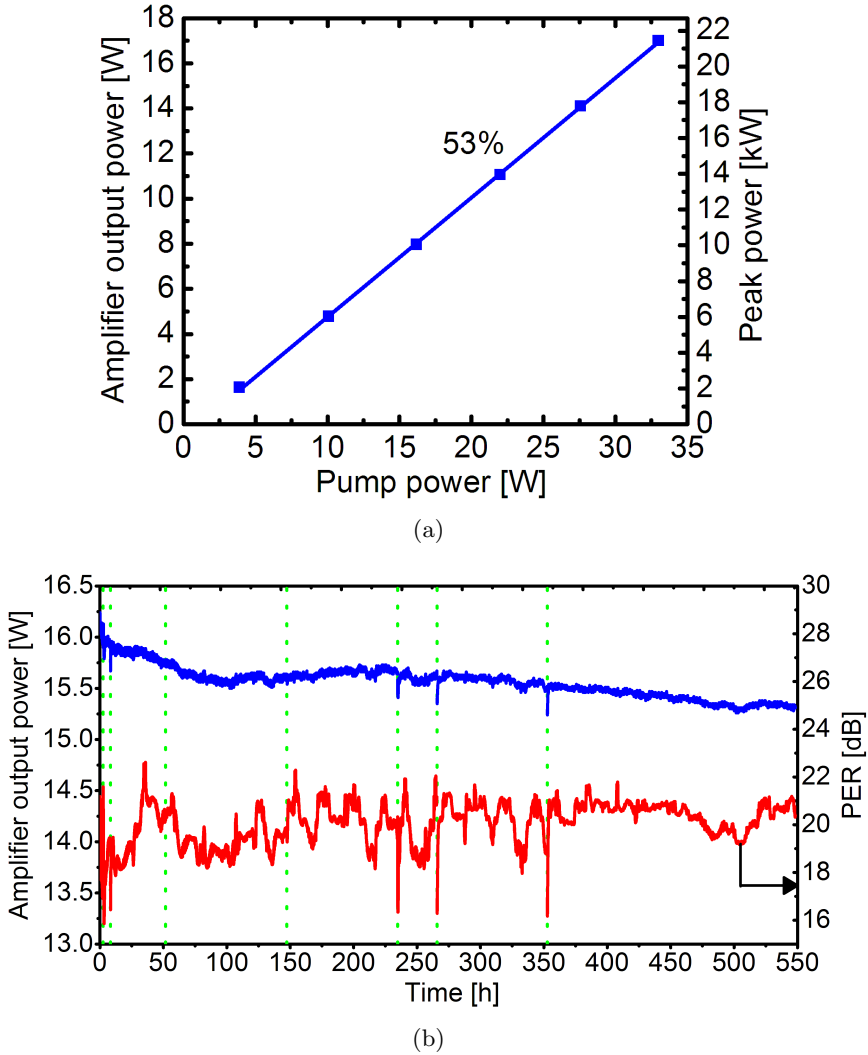
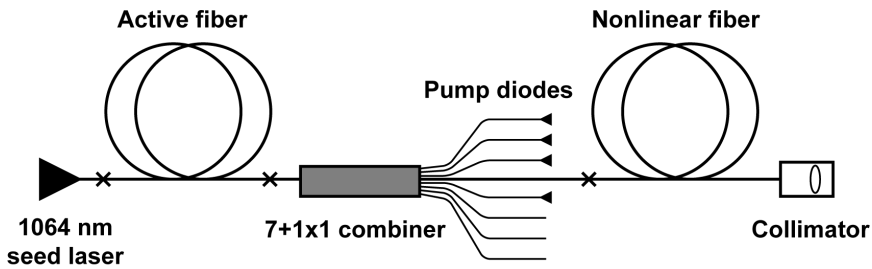


Figure 6.8: (a) Slope efficiency and peak power of the amplifier system. (b) Result of the 550 hour test of the amplifier system, with the pump diodes driven in constant current mode. The blue line shows the signal output power. The red line shows the PER of the signal output. Vertical dotted green lines indicate a temporary stop in the test.

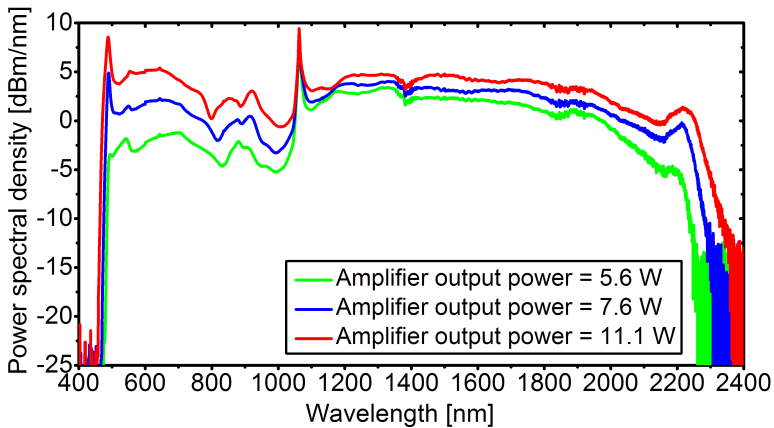
6.4 Supercontinuum generation with fiber amplifier

The amplifier described in section 6.3 is used as a pump source for generating a supercontinuum in a commercially available nonlinear PCF. A new length of active fiber is used in the amplifier in order to start with a pristine Yb-doped fiber. Figure 6.9(a) shows the setup used to generate the supercontinuum. The SM output fiber from the 7+1x1 combiner is spliced to 10 m of nonlinear fiber. The splice loss is 0.7 dB. The output of the nonlinear fiber is fitted with an achromatic collimator.

Figure 6.9(b) shows the build up of the supercontinuum generated spec-

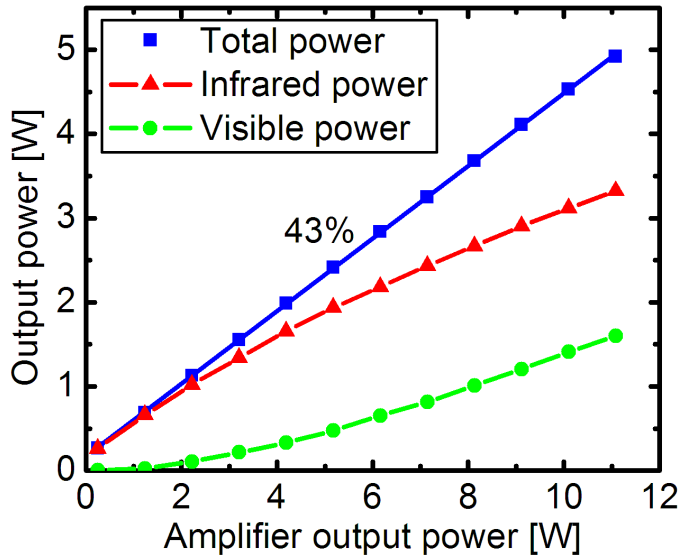


(a)

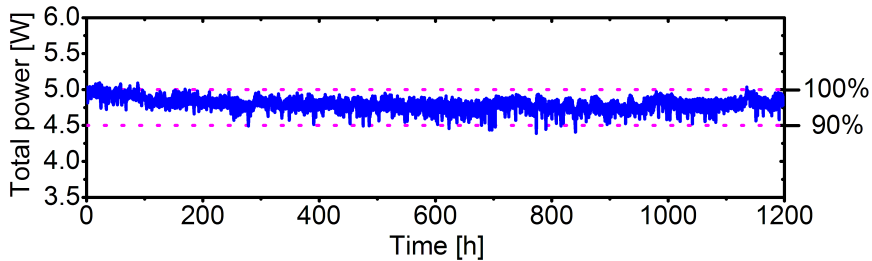


(b)

Figure 6.9: (a) Illustration of supercontinuum setup. (b) Supercontinuum generated spectra.



(a)



(b)

Figure 6.10: (a) Spectral power content of the supercontinuum generated light. The infrared power is the power above a wavelength of 850 nm and the visible power is the power below this wavelength. (b) Result of the 1200 hour test of the supercontinuum system, with the pump diodes of the amplifier module driven in constant current mode. The dotted purple lines indicate the power drop in percent. 100% equals the starting power of 5.0 W.

tra, as the power into the nonlinear fiber is increased. The green line is the measured spectra for an average amplifier output power of 5.6 W and the red line is for an average power of 11.1 W. The broadest spectrum spans from 470 nm and up to 2250 nm, when the edges are defined where the power drops below 0 dBm/nm. Figure 6.10(a) shows the total power in the spectrum, the power in the infrared part of the spectrum at wavelengths >850 nm and the power in the visible part of the spectrum (<850 nm). The total visible power is measured by inserting a reflection filter in the collimated beam which reflects wavelengths <850 nm. The IR power is found by subtracting the visible power from the total power. At an amplifier output power of 11.1 W, the total, infrared and visible power are 4.9 W, 3.3 W and 1.6 W, respectively.

The stability of the system is tested by letting it run for 1200 hours. The amplifier is running at a constant diode current and with an initial amplifier output power of 11.1 W. Figure 6.10(b) shows the results. A decrease in the supercontinuum generated power of 5% is observed, which again is related to photodarkening in the active fiber.

6.5 Summary of chapter 6

In this chapter a method for preserving the MFD in fiber tapers is described. The concept is experimentally verified with a 6 μm MFD feed-through and a 15 μm MFD PM feed-through. The 15 μm feed-through is demonstrated with both air-holes and F-doped rods as the second cladding. Low loss in the tapers is demonstrated and also low polarization cross talk in the 15 μm feed-through fibers.

Also, a monolithic pump/signal combiner with 15 μm MFD PM SM signal feed-through designed for air-clad PCFs that utilizes the MFD preserving concept is described. The combiner has an average pump and signal transmission loss of 0.13 dB and 0.52 dB, respectively. The PER of the signal is >18 dB. The combiner is used in a backward pumped configuration and features a system with a strictly SM signal output with an M^2 value <1.1 . A maximum average signal power of 17 W is reached when the system is seeded by 10 ps pulses with a repetition rate of 80 MHz. The slope efficiency of the system is 53%. A 550 hour test of the amplification system indicates a drop in power of 5.6%. The PER is >18 dB during the entire test. With the amplifier system, a supercontinuum is generated with a total power of 5 W that spans from 470 nm and up to 2250 nm.

Chapter 7

Combiners for astrophotonics

A large part of astronomical surveys is to measure the spectra of on-sky objects, such as galaxies, stars, or gas clouds. For these measurements, optical fibers can be used for guiding the light from the focal plane of the telescope to the optical spectrograph. For collecting a large amount of light, large core multi-mode (MM) fibers are preferred [122, 123]. Traditionally, the spectrograph has been mounted directly on the telescope, which means that the spectrograph moves with the telescope. This sets limitations to the size and weight of the spectrograph, and thereby also the spectral resolution. Alternatively, a complicated beam path needs to be created with a number of mirrors and lenses that guide the light to a spectrograph decoupled from the telescope. Decoupled spectrographs are preferred for two reasons. The size limitations are not as strict as telescope mounted spectrographs and they can be placed in a separate temperature controlled room. The result is a significant increase in the resolution of the spectrograph. With optical fibers light is easily routed to a decoupled spectrograph.

Figure 7.1(a) shows an illustration of a lens coupled spectrograph. A slit is placed in front of the object. The light is then collimated by a lens, dispersed by a prism and focused onto the detector by another lens. With a fiber link between the telescope and the spectrograph, simultaneous spectroscopic measurements of a number of objects can be made with only one spectrograph. This is done by utilizing the fact that the telescope images all objects within the field of view onto the focal plane. Therefore, a large number of fibers can be used, where each fiber is placed in front of a different stellar object. The other end of the fibers are aligned in a row and placed in front of the spectrograph. The core of the fibers make up for the

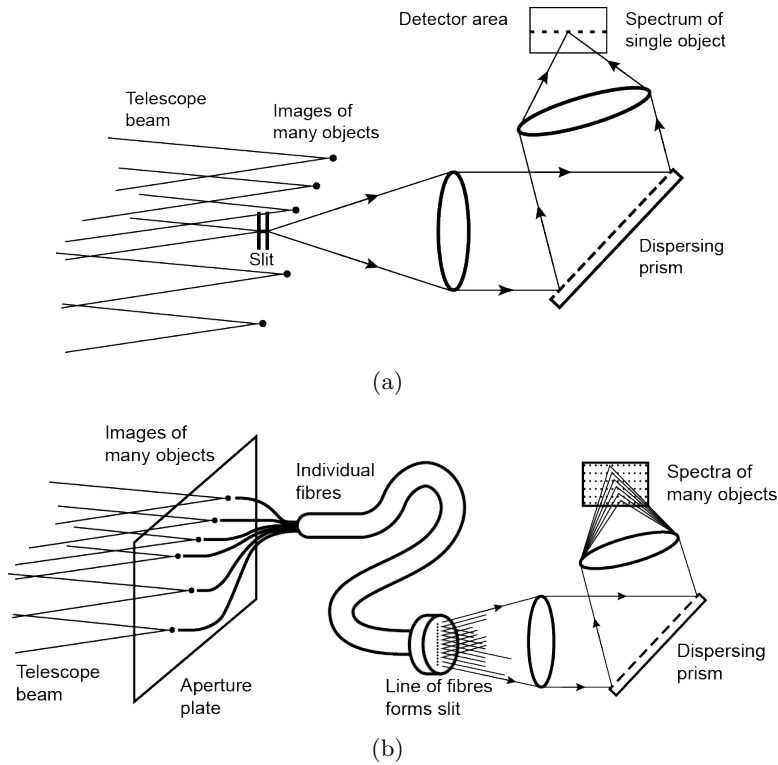


Figure 7.1: Illustrations of conventional (a) and fiber based (b) telescope, used for measuring spectra of astronomical objects.

slit and a spectrum of each of the fibers is recorded on the detector. An illustration of a fiber fed spectrograph is shown in Fig. 7.1(b). The ability to observe multiple objects at the same time gives a huge advantage in terms of maximizing the measurement capacity of the telescope.

This chapter describes two components developed for the field of astrophotonics. The first is a fused bundle of MM fibers or "hexabundle", and the second is a MM to single-mode (SM) optical fiber splitter or "photonic lantern".

The hexabundle is developed for measuring spectra of extended objects such as galaxies or gas clouds. The fiber bundle is placed in the focal point of a telescope and in the other end the individual fibers are aligned in a row in front of the spectrograph. With these hexabundles a more detailed observation can be made of large astronomical objects.

The photonic lanterns are developed for transforming MM starlight into an ensemble of SM fibers. This enables filtering of the light using advanced fiber Bragg gratings (FBGs) in the SM fibers. The chapter describes 7, 19 and 61 port low-loss devices.

7.1 Hexabundles

For extended objects such as galaxies or gas clouds, the material composition and internal motions, can vary across the object. Individual fibers can not be positioned close together in the telescope focal plane, making these variations difficult to observe. The solution is to closely pack a number of MM fibers together in a fiber bundle. These bundles of MM fibers for astronomy application are called hexabundles [124–127].

Figure 7.2 shows an illustration of two hexabundles placed in the telescope focal plane. On the backside of the hexabundles, the individual fibers fan out and are aligned in front of the spectrograph. In Fig. 7.3(a) an illustration of the hexabundle is shown. A bundle of MM fibers are inserted in a silica capillary tube and fused together using a GPX glass processing station from Vytran. The fibers have a pure silica core and a fluorinated silica cladding. A clean end-facet is important in order to have a good coupling into the fibers of the hexabundle. This is achieved by polishing the hexabundle.

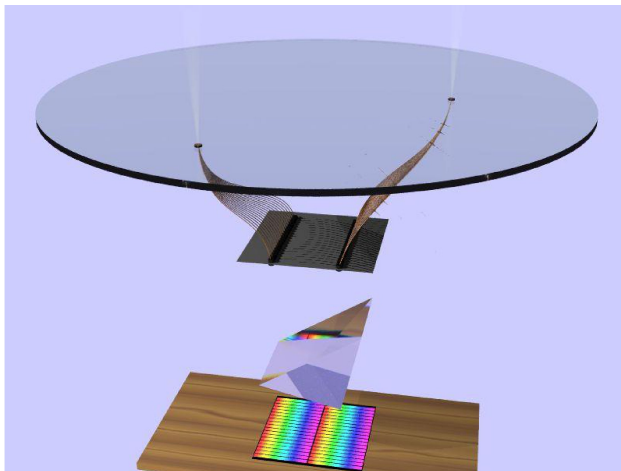


Figure 7.2: Illustration of two hexabundles placed in the telescope focal plane.

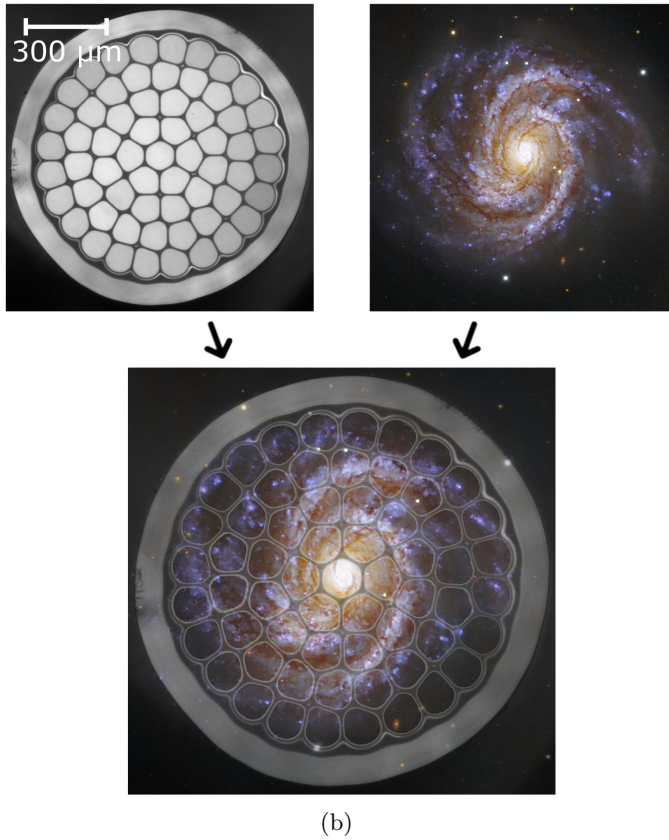
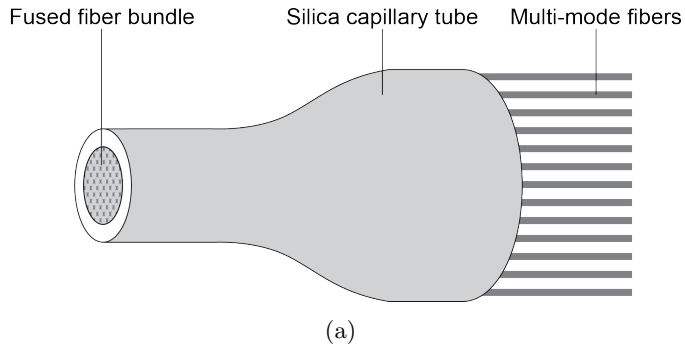


Figure 7.3: Illustration of a hexabundle (a) and of the hexabundle concept (b).

The hexabundle concept is illustrated in Fig. 7.3(b). The top left image shows the front side of a 61 port hexabundle, and the top right image shows a spiral galaxy. When the galaxy is focused onto the hexabundle, different parts of the galaxy are launched into different MM fibers of the hexabundle (bottom image). By measuring the spectrum out of each MM fiber, the spectral information of the different parts of the object are obtained.

7.1.1 7 port hexabundles

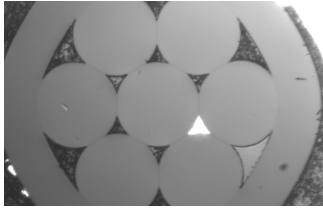
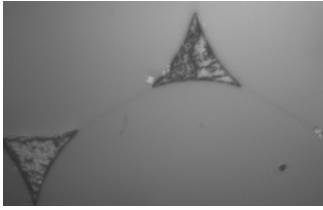
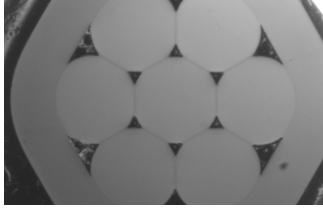
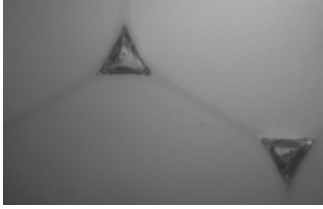
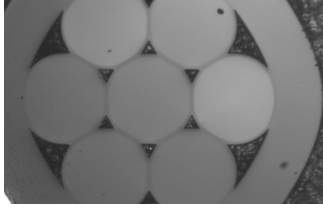

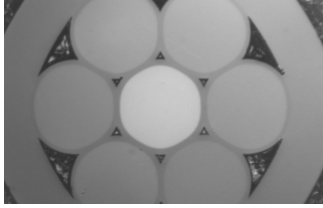

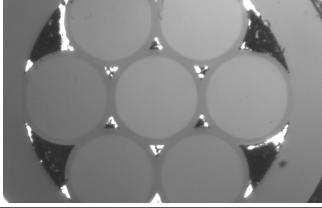
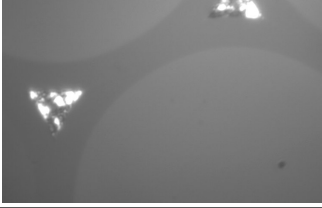
The hexabundles are fabricated with 0.22 numerical aperture (NA) MM fibers with a core and cladding diameter of $105\ \mu\text{m}$ and $125\ \mu\text{m}$, respectively. The fused surface of the hexabundle will consist of fiber core, fiber cladding and air-voids between the fibers. Light from the astronomical object that is not focused on a fiber core is not guided to the spectrograph. Therefore, there is a need to increase the collection area of the hexabundle. This can be achieved by reducing the MM fiber cladding thickness by chemical wet etching or by fully fusing the fibers together. For astronomy applications it is important that the transmission loss of the hexabundles is low. The objects that are studied are often very faint, so the loss of photons should be minimized. It is also important that the NA launched into the hexabundle is not scattered to a higher NA. The spectrograph is build to match the NA of the telescope, and a scattering to higher NA would therefore result in a loss of photons. Furthermore, it is important that the light that is coupled into a core does not couple into a neighboring core, i.e. the cross talk between cores should be low.

7.1.2 Cladding etch of 7 port hexabundles

A study is made of the performance of the hexabundles, when the cladding is reduced by etching. In the study, 7 fibers are used. A series of 5 hexabundles are prepared, with the MM fibers etched to different cladding thicknesses from $1\text{-}8\ \mu\text{m}$. Table 7.1 shows the end-facets of the fabricated hexabundles. The left column shows the cladding thickness of the MM fibers. The right column shows the minimum distance between two cores, i.e. the thickness of the F-doped layer between two cores.

In order to measure the transmission loss, cross talk and NA up-conversion of the individual ports of the hexabundle, the devices are tested in a reverse configuration. This is due to the close packaging of the fibers in the hexabundle, which makes it difficult to verify if light is only launched

Table 7.1: Microscope images of lightly fused hexabundles with the fibers etched to different cladding thicknesses. The left column shows the cladding thickness, and the right column shows the minimum core-to-core barrier thickness.

Etch [μm]	High magnification	Low magnification	C-C [μm]
1			1.7
2			2.9
4			5.5
6			8.1
8			11.5

into a single port. In turn a light source is spliced to each of the individual MM fibers. The transmission and the backscattered power in the neighboring port is measured. This is illustrated in Fig.7.4(a). The injected power is P_0 , the transmitted power is P_T and the reflected signal power in a neighboring fiber is P_X . Denoting the cross-talk fraction by X and the Fresnell reflection by R the cross-talk term can be expressed by the following:

$$P_X = 2P_0\alpha^2RX. \quad (7.1)$$

$$X = 10 \cdot \log \left(\frac{P_X}{2R\alpha^2P_0} \right), \quad \alpha = \frac{P_T}{P_0(1-R)}. \quad (7.2)$$

Figure 7.4(b) shows the transmission and cross talk as a function of core-to-core barrier thickness. The measurement is made with a 0.12 NA light source at a wavelength of $1.53 \mu\text{m}$. The figure shows that a thinner cladding guides weaker. As the cladding thickness decreases, more and more light leaks into neighboring ports. This results in transmission losses and cross-talk.

NA up-conversion for each of the 5 devices is also investigated. Figure 7.5(a) shows the far-field out of the hexabundles, when the light source is spliced to one of the outer input ports. For reference, the far-field of the

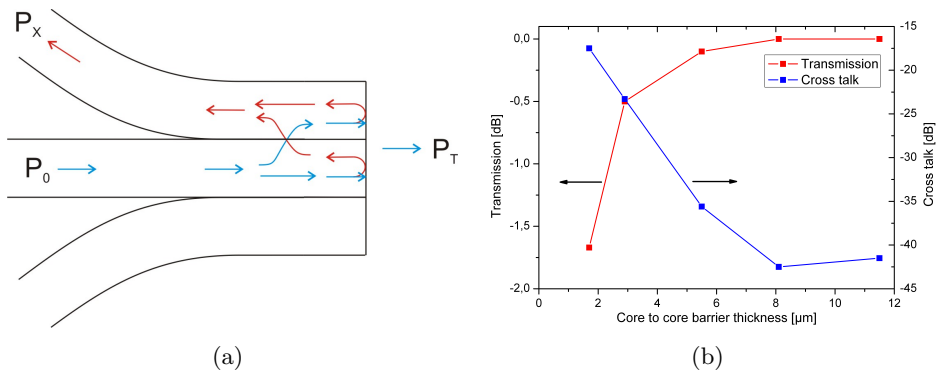


Figure 7.4: (a) Illustration of cross-talk. P_0 is the inserted power, P_T is the transmitted signal and P_X is the reflected signal in the neighboring fiber. (b) Transmission and cross talk as a function of core-to-core barrier thickness. at a wavelength of $1.53 \mu\text{m}$.

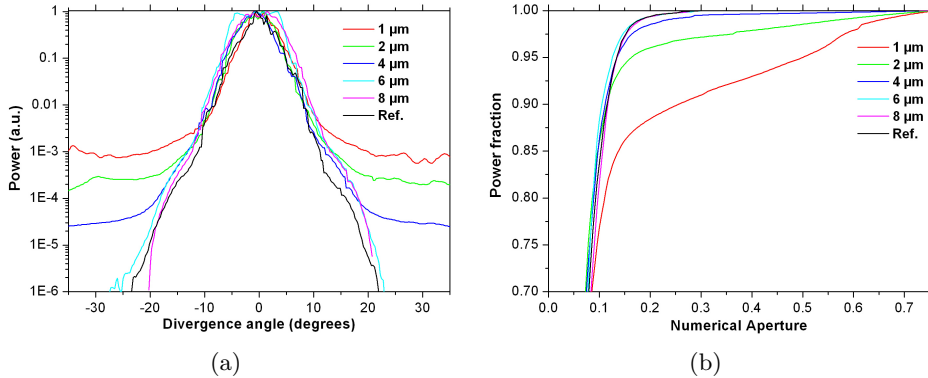


Figure 7.5: (a) Plot of far-field power as a function of divergence angle at a wavelength of $1.53 \mu\text{m}$. (b) Integrated power as a function of the NA.

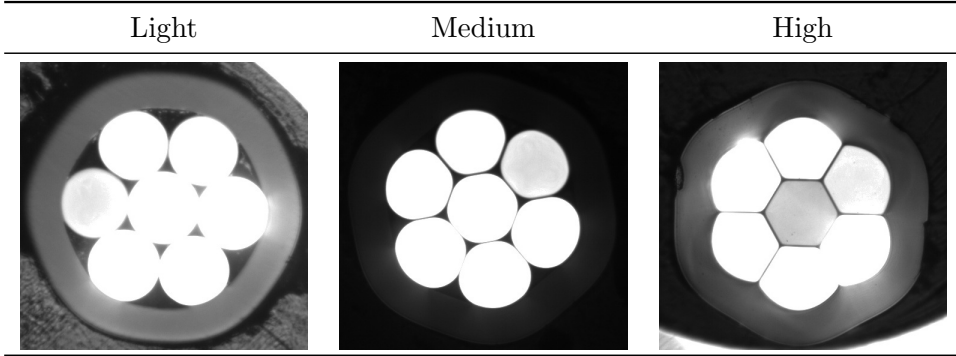
light source is shown (black line). Figure 7.5(b) shows a plot of the integrated power as a function of the divergence angle or NA. Such a plot is often referred to as "Power in the bucket", and shows the fraction of power that is within a given NA. The figures show that for a decreasing cladding thickness an increasing amount of light is scattered to very high divergence angles. If the 95% level is used for determining the NA, the two devices with the thinnest cladding thickness have significantly increased NAs. The NA of the remaining devices is very close to the input.

The data suggests that the losses, cross talk and NA up-conversion are coupled to each other. The reason is that the light that is lost out of the waveguides, as the cladding decreases, reaches the rough, etched surface of the fibers. This scattering results in both NA up-conversion and coupling to neighboring fibers.

7.1.3 Degree of fusing of the 7 port hexabundles

A similar investigation is made for the degree of fusing. Table 7.2 shows the end-facet of three different hexabundles. From left to right, the degree of fusing is light, medium and high. For lightly fused hexabundles the fibers maintain their circular shape. As the degree of fusing is increased the fibers become more and more deformed. It turns out that the deformation of the fibers, although it is done very slowly, causes a slight NA up-conversion. For astronomy applications, the lightly fused bundles are therefore preferred.

Table 7.2: Microscope images of lightly fused hexabundles with the fibers etched to different cladding thicknesses.



7.1.4 61 port hexabundle

With more fibers in the hexabundle a better resolution of the object is achieved. Therefore, a 61 port hexabundle is explored. These devices are fabricated by using what is learned from the 7 port hexabundles, i.e. they are lightly fused and etched to a cladding thickness of $6 \mu\text{m}$. Figure 7.6 shows a microscope image of the end-facet of the 61 port hexabundle. The devices have a transmission loss $<0.1 \text{ dB}$, very little cross talk and no NA up-scattering. The devices are currently being tested on the 3.9 m Anglo-Australian Telescope in Australia [127].



Figure 7.6: Lightly fused 61 port hexabundle.

7.2 Photonic lanterns

In the near infrared part of the spectrum from 1000 nm to 1800 nm, high altitude hydroxyl in the Earth's atmosphere radiates hundreds of extremely bright, ultranarrow emission lines that completely dominate the spectral background. In recent years FBGs have been demonstrated that can reflect the unwanted signal while allowing the desired signal to enter the spectrograph [128, 129]. These FBGs only work in SM fibers, so in order to make use of these gratings, a device that efficiently couples light from a large-core MM fiber to an ensemble of SM fibers is needed. Such a device is called a photonic lantern. A sketch of an optical system with two photonic lanterns coupled back-to-back and gratings in the SM fiber ports is shown in Fig. 7.7. The input photonic lantern splits light from a MM fiber core to an ensemble of SM fibers. Gratings in the SM fibers filter out unwanted emission lines and the output photonic lantern combines the light back into a MM fiber core.

Another promising instrument enabled by the photonic lantern is the photonic integrated multi-mode microspectrograph (PIMMS) [130, 131]. In this case the photonic lantern delivers a SM input for an arrayed waveguide grating that disperses the light. This concept potentially enables fabrication of compact and cheap spectrographs.

The principle of the photonic lantern was first demonstrated in 2005 by Leon-Saval *et al.* [42]. In this work, a special ferrule with air voids to obtain a transition from 19 SM fibers to a MM fiber was used. The MM fiber was defined by a silica core surrounded by air and suspended by thin silica bridges. Hereafter, low-loss photonic lanterns with 7, 19 and 61 SM ports have been demonstrated by the use of an F-doped layer in stead of a photonic crystal fiber (PCF) cladding [132–134].

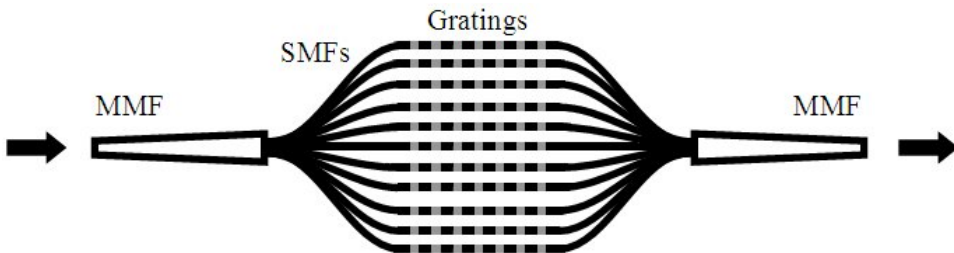


Figure 7.7: Schematic illustration of an optical system with two photonic lanterns in a back-to-back configuration and FBGs in each of the SM fiber ports.

Recently, two new approaches have been demonstrated that enable the fabrication of compact photonic lanterns. The first is by surrounding a multi-core fiber with a low refractive index tube, fusing the two together and tapering them down to form a MM fiber [135]. The advantage of this approach is that the FBGs can be inscribed simultaneously in the multi-core fiber, as opposed to inscribing gratings in a large number of individual SM fibers. The second approach is by direct inscription of the photonic lanterns in integrated waveguides with ultrafast lasers [136, 137].

This chapter describes the 7, 19 and 61 port photonic lanterns based on the F-doped cladding approach.

7.2.1 Photonic lantern fabrication

Figure 7.8 shows an illustration of a photonic lantern. A number of SM fibers are inserted into a low refractive index capillary tube. The fiber filled capillary tube is fused into a solid glass element and tapered to a MM waveguide. The core of the waveguide consists of the tapered SM fibers and the cladding is formed by the surrounding low-index capillary tube. A fabrication technique much similar to what is used for making 1x7 fused couplers [138].

Due to the gradual change from MM waveguide to SM fiber ensemble, a low-loss coupling of light from MM to SM and from SM to MM can be achieved. A low-loss coupling from the MM fiber into the SM fiber ensemble may only be achieved if the number of degrees of freedom in the SM fiber

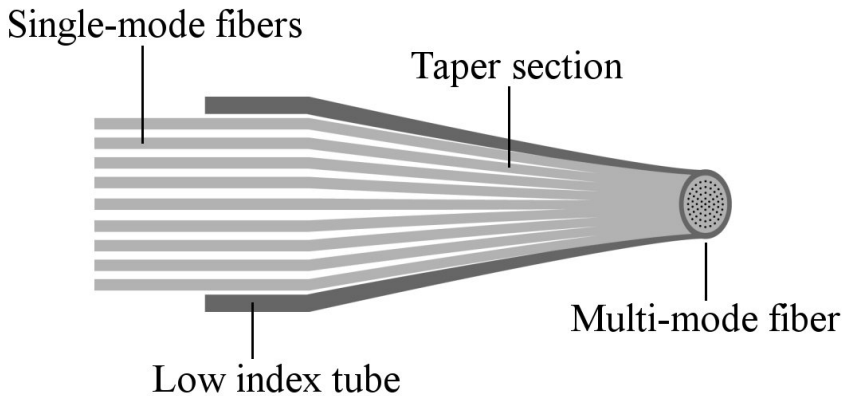


Figure 7.8: Schematic illustration of the photonic lantern.

ensemble is equal to or higher than in the MM waveguide [139]. Therefore, efficient coupling or transformation of modes from the MM waveguide to the SM fiber ensemble is possible, when the number of excited modes in the MM waveguide is less than or equal to the number of SM ports. The principle is illustrated for a two port photonic lantern in Fig. 7.9. In the top part of the figure the two SM waveguides are decoupled and light will propagate in the fundamental mode. In the middle part of the figure the structure is tapered and the diameter of the cores will decrease. The fundamental mode spreads out and coupling occurs between the two neighboring cores. This coupling results in two supermodes. In the bottom part of the figure the structure is tapered to a MM waveguide, where the original SM cores are no longer important for the guiding. In stead the two supermodes have evolved into the two lowest order modes of the MM waveguide. Coupling through the structure can occur both ways, as long as only the two lowest order modes are excited in the MM waveguide.

In order to excite the correct number of modes in the MM tip of the photonic lanterns, light needs to be coupled into the device with the correct NA. For a step-index fiber, the number of modes M in one polarization orientation is given by Eq. 2.4. Inserting the definition of the V parameter in this equation, an approximate expression for the NA of the first M number

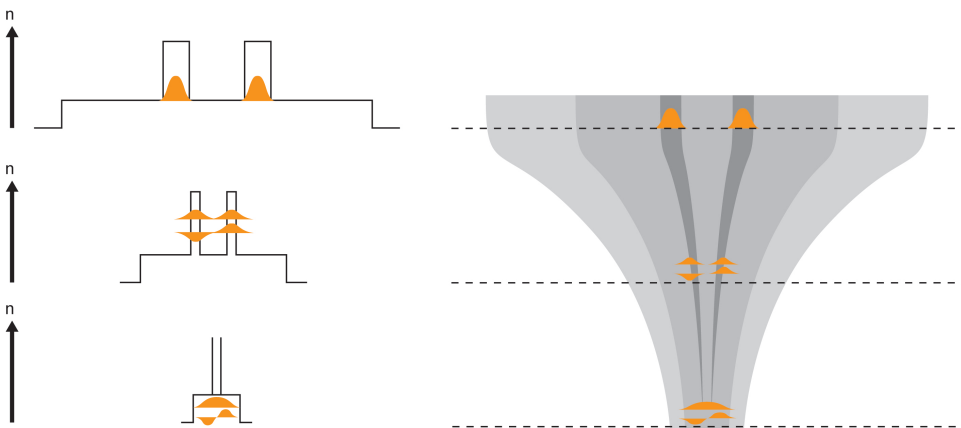


Figure 7.9: Schematic illustration of the mode coupling in the photonic lantern. The top shows the decoupled individual waveguides. The bottom shows the MM waveguide.

of modes is found

$$NA \approx \frac{\lambda\sqrt{M}}{\pi a}, \quad (7.3)$$

where λ is the free space optical wavelength and a is the core radius of the waveguide. Equation 7.3 can both be used to determine the optimum launch conditions into the MM tip of the photonic lanterns, and to check if the fiber bundle is tapered adiabatically. This is done by launching light into the SM fibers of a photonic lantern with X SM ports and measuring the NA of the light out of the MM tip. If the tapering is adiabatic, only the X lowest order modes are excited and the NA should therefore agree with Eq. 7.3.

7.2.2 7 port photonic lantern

A feasibility study of a 7 port photonic lantern is carried out. The device is fabricated with OFS Clearlite fibers [140]. The fibers have an outer diameter of $80 \mu\text{m}$, a mode field diameter (MFD) of $7.5 \mu\text{m}$, and a higher order mode (HOM) cut-off wavelength of $\sim 1500 \text{ nm}$. A bundle of 7 fibers is inserted into a low-index glass capillary tube. The fiber filled capillary tube is fused and tapered down by a factor of 4 into a solid glass element. Figure 7.10 shows microscope pictures of the bundle cross section at different positions along the taper. The tapering of the fiber bundle is done over a length of

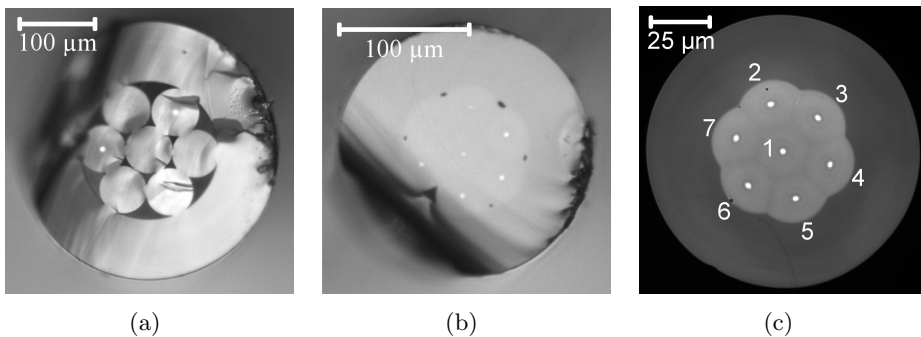


Figure 7.10: Microscope cross sectional images of the 7 port photonic lantern at different positions along the taper. Image (a) is obtained 5 mm into the taper, (b) is obtained 20 mm into the taper, and (c) shows the end-facet of the photonic lantern. The original SM fibers are identified in the MM fiber and marked as seen in (c).

40 mm. By adjusting the filament power during the taper, the point at which the fiber bundle fully collapses is controlled. In Fig. 7.10(a) the fibers are lightly stitched together and in Fig. 7.10(c) the fibers are completely fused together to form the core of the MM fiber. Since the HOM cut-off wavelength is ~ 1500 nm, the V parameter at this wavelength will be ~ 2.4 . This means that for a taper ratio of 4, the V parameter of the tapered SM fibers at a wavelength of 1500 nm is less than 1. Therefore, the MFD will be much larger than the diameter of the fiber core and light will leak from the SM cores into the MM fiber [46].

Mode simulation of the 7 port photonic lantern

A simulation of the mode evolution in the fabricated 7 port photonic lantern is performed by Leon-Saval *et. al* [139, 141, 142]. Figure 7.11 shows the effective refractive index of the modes (n_{eff}) as a function of the outer diameter of the 7 port photonic lantern. Counting both polarizations the 14 core modes are degenerate at large diameters. At smaller diameters

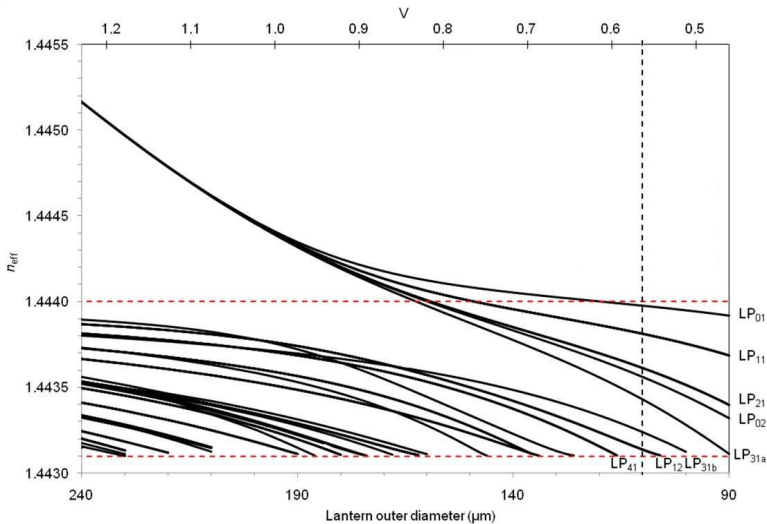
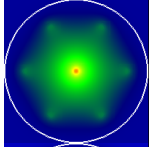
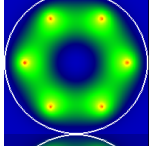
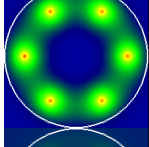
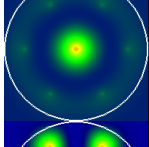
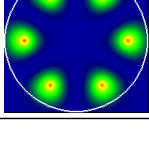
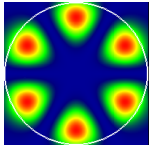
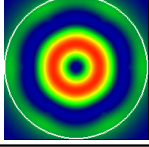


Figure 7.11: Evolution of the effective refractive index (n_{eff}) of the modes throughout the tapered transition of the 7 port photonic lantern. The red horizontal dashed lines indicate the core and cladding index of the final MM core. The vertical dashed line indicates the 110 μm outer diameter of the MM tip of the fabricated photonic lantern. [139].

Table 7.3: Details of the modes supported by the 110 μm outer diameter 7 port photonic lantern [139].

Scalar mode	Vector mode	Degeneracy	n_{eff}	Near field
LP ₀₁	HE ₁₁	2	1.44398	
LP ₁₁	HE ₂₁ TE ₀₁ TM ₀₁	4	1.44381	
LP ₂₁	EH ₁₁ HE ₃₁	4	1.44361	
LP ₀₂	HE ₁₂	2	1.44356	
LP _{31a} *	EH ₂₁	2	1.44343	
Originally cladding modes				
LP _{31b} *	HE ₄₁	2	1.44324	
LP ₁₂	HE ₂₂ TE ₀₂ TM ₀₂	4	1.44314	

*The LP₃₁ is four-fold degenerate for circularly symmetric structures. In this case the symmetry of the waveguide results in two distinct two-fold degenerate modes.

they become non-degenerate and fill the range of effective refractive index available in the MM waveguide. Figure 7.3 shows the details of the modes for an outer diameter of $110\ \mu\text{m}$, which is the diameter where the taper transition is stopped for the 7 port photonic lantern.

Modes in the MM section of the 7 port photonic lantern

In the tapered end the original SM cores no longer act as individual waveguides. Figure 7.12 shows near-field images of the MM waveguide at wavelengths from 1060 nm to 1600 nm. In the images light is coupled into the device through a single input port. At a wavelength of 1060 nm, the mode is confined to the cores of the original SM fibers. At longer wavelengths, the original cores no longer confine the mode, and the light is smeared out over the entire core of the MM waveguide. A tendency for the light to have the highest intensity around the original cores can still be observed.

The near-field images indicate that a set of super-modes are excited. Modes that are shown in Table 7.3. By gradually tuning the laser wavelength, while keeping the device mechanically fixed, the shape of the near-field undergoes gradual changes. This is because the effective index of the

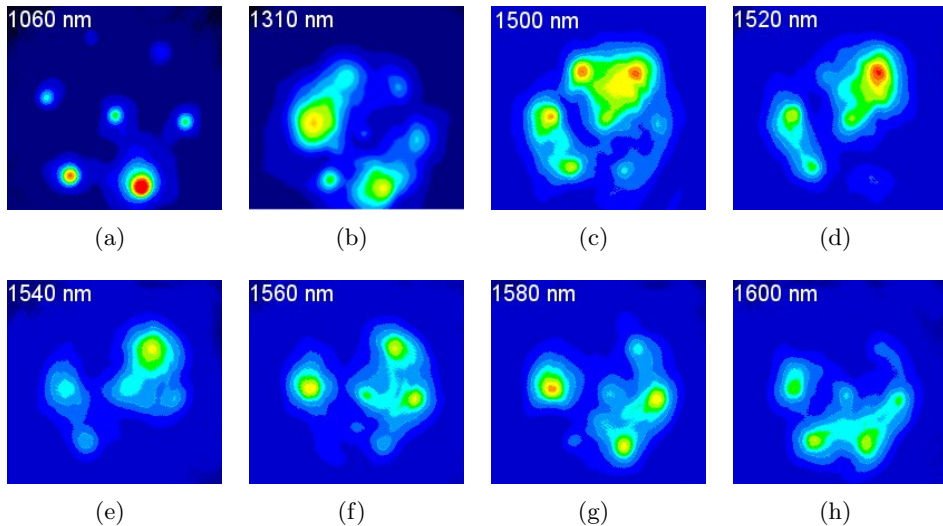


Figure 7.12: Near-field images of the MM waveguide at wavelengths from 1060 nm to 1600 nm.

different guided modes is wavelength dependent. A change in wavelength modifies the interference between the modes, thus altering the distribution of power in each mode.

SM to MM transmission efficiency of the 7 port photonic lantern

In order to characterize the transmission efficiency of the device, the loss is measured for light undergoing the transition from a SM fiber to the MM waveguide. The setup used for this measurement is shown in Fig. 7.13. 7 FC/PC connectorized SMF-28 patch cords, with a known loss, are spliced to each of the 7 input fibers. The transmission loss is measured by sending 1558 nm laser light into one SM fiber at the time and measuring the transmitted power out of the MM waveguide with an integrating sphere. In Fig. 7.10(c) the numbering of the ports is shown and Table 7.4 shows the losses of the device for each of the 7 ports. In the table, the coupling loss from the laser to the input port (typically 0.15 dB) and splice loss from SMF-28 to 80 μm fibers (0.1 dB) are not included. The average SM to MM loss of the device is 0.24 dB, corresponding to 95% transmission efficiency. The result shows that the fabricated device can indeed be used to combine light from the SM fibers into a MM fiber with a low transmission loss. A low transmission loss when going from SM to MM can be expected, since the degrees of freedom in the MM fiber are higher than in the SM fiber ensemble.

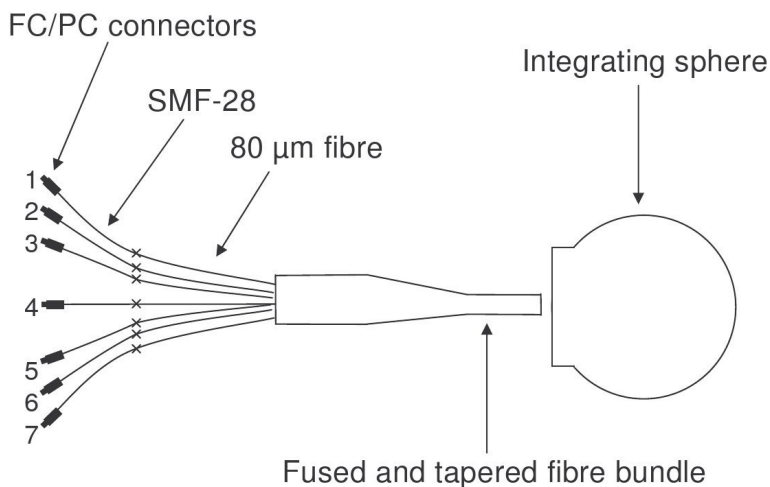


Figure 7.13: Illustration of setup used to measure SM to MM loss.

Input port number	SM to MM loss [dB]
1	0.19
2	0.29
3	0.36
4	0.24
5	0.13
6	0.18
7	0.28
Average	0.24

Table 7.4: Measured transmission loss from SM to MM.

MM to SM transmission efficiency of the 7 port photonic lantern

In real applications, astro-light will be coupled into the MM end of the photonic lantern. In order to achieve an efficient MM to SM coupling, it is critical to optimize the coupling optics to match both spot size and NA. This will ensure that light is coupled into the lowest order transverse modes and that the number of excited modes not exceeds the number of SM fibers. A method of ensuring a correct number of excited modes is by coupling two devices back-to-back, i.e. using the MM output from one photonic lantern to couple into the MM end of another. In this configuration, the input SM to MM device ensures that ~ 7 transverse modes are excited, which means that an optimal coupling into the photonic lantern is achieved. This is opposed to using a lens, where it will be difficult to verify the exact number of excited modes.

The setup for measuring the SM through MM to SM loss is shown in Fig. 7.14. Light is coupled between the two photonic lanterns by splicing the MM sections together. At the output, all 7 fibers are cleaved and mounted side-by-side using double adhesive tape. A 2 cm stripped length was left on all fibers and a drop of high-index liquid was applied to remove cladding light. Adding the high-index liquid changed the measured power less than 0.01 dB, showing that all light is in fact guided in the SM cores. An integrating sphere is used to measure the total power transmitted through the 7 output fibers. Light from a 1558 nm laser is coupled to one input port at the time, and the combined light out of the 7 SM ports of the device to the right is measured. The transmission losses are shown in Table 7.5. The

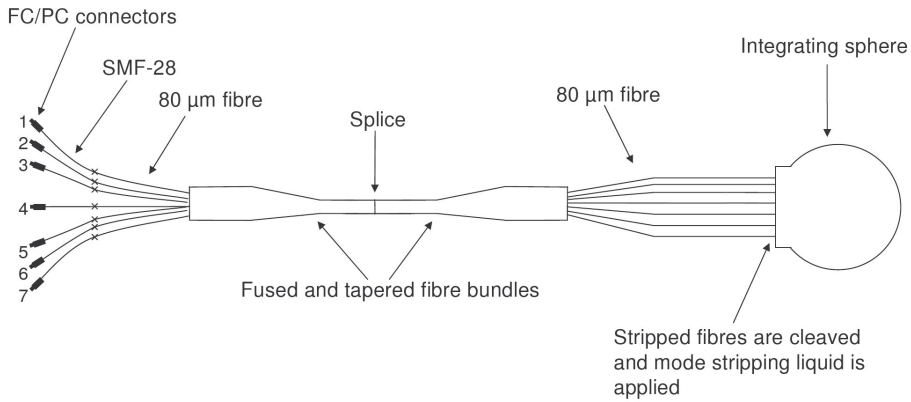


Figure 7.14: Illustration of setup for measuring the SM through MM to SM loss.

losses in the table include transmission losses through both devices as well as splice loss between the two MM sections. Coupling loss from the laser to the input port (typically 0.15 dB) and splice loss from the SMF-28 to 80 μm fiber (0.1 dB) are not included. The numbering of the input ports follows the numbering shown in Fig. 7.10(c).

Table 7.5 shows that the transmission loss through the two devices is low. The average loss for light undergoing the transition from SM waveguide to MM waveguide and back into SM waveguides is 0.56 dB. Of this loss, 0.24 dB originates from the SM to MM transition shown in Table 7.4. Therefore, the

Input port number	SM-MM-SM loss [dB]
1	0.91
2	0.52
3	0.52
4	0.69
5	0.24
6	0.52
7	0.49
Average	0.56

Table 7.5: Measured transmission loss from SM through MM to SM fibers.

average transmission loss from MM fiber to the SM fiber ensemble is only 0.32 dB, corresponding to a transmission of the photonic lantern of 93%. This shows that it is indeed possible to make a low loss transition from a MM fiber to a number of SM fibers.

7.2.3 61 port photonic lantern

A 7 port photonic lantern can only convert 7 modes from the MM fiber into the SM fiber ensemble. This means that only low NA light can be coupled into the device, making them difficult to use in practice. Therefore, a 61 port photonic lantern was investigated. This photonic lantern is fabricated with the more standard SMF-28 fibers manufactured by Corning, USA [143]. The diameter of the core, cladding and coating of the fiber is $8.2\ \mu\text{m}$, $125\ \mu\text{m}$ and $250\ \mu\text{m}$, respectively. The fibers are single-mode for wavelengths longer than $1260\ \text{nm}$.

The 61 port photonic lanterns are fabricated by inserting the fibers into a low refractive index glass capillary tube, and tapering by a factor of 10 over a length of 100 mm. The thin end acts as a MM waveguide with a core consisting of the 61 fused SM fibers and a cladding formed by the low refractive index glass capillary tube. By adjusting the filament power during the taper, the point at which the fiber bundle fully collapses is controlled. Figure 7.15 shows microscope pictures of the bundle cross section at different positions along the taper. In Fig. 7.15(a) the fibers are lightly stitched

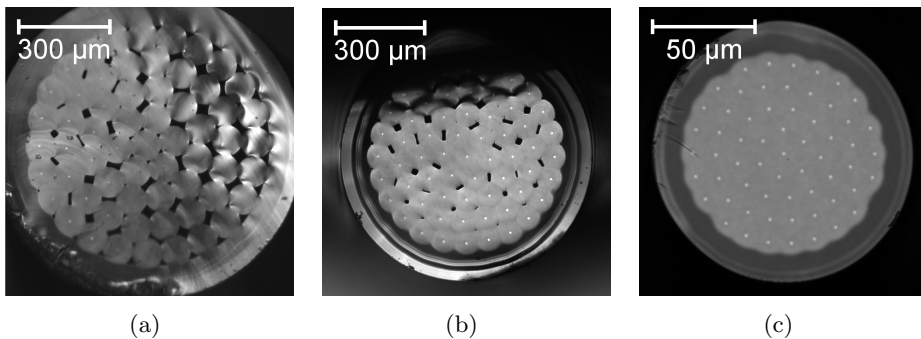


Figure 7.15: Microscope images of the cross section of the 61 port photonic lantern through the taper. From left to right the outer diameter of the low-index tube is $1025\ \mu\text{m}$, $840\ \mu\text{m}$, and $125\ \mu\text{m}$, respectively. The MM tip of the photonic lantern is seen in (c).

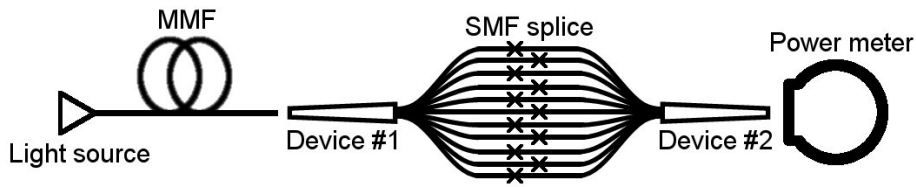
together and in Fig. 7.15(b) the interstitial holes between the fibers begin to close. Figure 7.15(c) shows the fully fused MM tip of the photonic lantern. The core diameter of the MM waveguide is $100\ \mu\text{m}$ and the outer diameter of the tip is $125\ \mu\text{m}$. Two photonic lanterns (#1 and #2) are fabricated, such that MM to SM to MM characterization can be performed.

The SM to MM transmission loss of the two photonic lanterns is measured for 10 randomly chosen SM fibers. Incoherent light from an amplified spontaneous emission (ASE) source centered at $1530\ \text{nm}$ and with a $10\ \text{dB}$ width of $40\ \text{nm}$ is coupled into the SM fiber under test and the transmitted power out of the MM end of the photonic lantern is measured with an integrating sphere. The average SM to MM transmission loss of the two photonic lanterns was measured to be $0.01\ \text{dB}$ for device #1 and $0.03\ \text{dB}$ for device #2.

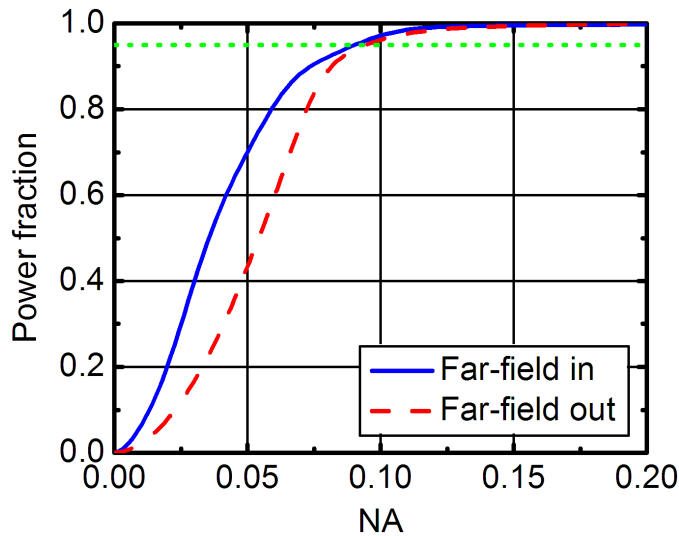
The far-field out of the MM end of the two devices is also measured. 10 measurements are made with light coupled into 10 randomly chosen SM ports one at the time. The average NA filling out of the MM end of the photonic lanterns corresponds to 95% of the light having an NA below 0.10 for device #1 and 0.11 for device #2. From Eq. 7.3 it is calculated that the 61 lowest order modes have an NA of ~ 0.076 . A core diameter of $100\ \mu\text{m}$ and a wavelength of $1.53\ \mu\text{m}$ is used in the calculation. The measured NA is slightly higher than the theoretical value, but close enough to confirm that only little scattering occurs to higher NAs.

To imitate the astronomy application, the two fabricated photonic lanterns are spliced back-to-back. The two sets of 61 SM fibers are spliced together in a random order as illustrated in Fig. 7.16(a). With this system the MM to SM to MM transmission loss is measured.

The coupling conditions, i.e. spot size and NA of the light coupled into device #1 needs to be carefully controlled, such that no more than 61 modes in the MM photonic lantern tip are excited. This achieved with a $95\ \mu\text{m}$ core MM launch fiber. The NA filling of the launch fiber is tailored by a fiber taper section inserted between the light source and the launch fiber. The measured integrated far-field out of the MM launch fiber is shown in Fig. 7.16(b) as the solid blue line. This NA filling corresponds to 95% of the light having an NA below 0.090, matching that of the photonic lanterns. Launching of light into the MM tip of device #1 is done by aligning with the MM launch fiber on an XYZ-stage. The transmitted power out of device #2 is measured using a power meter. The total MM-SM-MM transmission loss is measured to be $0.76\ \text{dB}$ corresponding to a transmission of 84%. The resulting integrated far-field measured at the output of device #2 is shown in Fig. 7.16(b) as the



(a)



(b)

Figure 7.16: (a) Schematic illustration of the setup used to characterize two photonic lanterns coupled back-to-back. (b) Measured integrated far-field coupled into device #1 (solid blue line) and resulting far-field out of device #2 (dashed red line).

dashed line. The NA filling corresponds to 95% of the light having an NA lower than 0.095, and is in agreement with the average NA measured over 10 randomly chosen SM ports within measurement uncertainty. Figure 7.16(b) shows that the shape of the integrated far-fields are not identical, which suggests that the power in each mode (modal power distribution) of the input and output are not the same. This is expected, since the SM fibers of the two devices are spliced together randomly.

7.2.4 19 port photonic lantern with multi-mode delivery fiber

A high port count of 61 SM fibers, means that 61 identical FBGs need to be written in each of the SM fibers. Due to the high cost of these gratings a compromise between high throughput and cost needs to be made. The compromise ended up being 19 port photonic lanterns. These photonic lanterns also feature a MM delivery fiber spliced to the tapered tip of the fiber bundle. Figure 7.17 shows an illustration of the fabricated photonic lantern.

The purpose of the delivery fiber is in one end to guide the star light from the focal plane of the telescope to the photonic lantern and in the other end to guide the light from the photonic lantern to the spectrograph. This allows for a more robust system, where the photonic lanterns can be packaged and isolated away from the optomechanical interfaces of the telescope and the spectrograph. Crucially, this allows the telescope delivery fibers to be optically interfaced to micro-optics placed at the telescope focal plane, and allows the spectrograph delivery fibers to be installed in close-contact in a V-groove array that forms the spectrograph slit.

The 19 port photonic lantern is also fabricated with SMF-28 fibers. For this device, the fiber bundle is tapered by a factor of 11 in diameter over a length of 60 mm. This results in a $50\ \mu\text{m}$ core MM waveguide. Figure 7.18(a) shows the tip of the fused tapered fiber bundle. The bundle tip is spliced

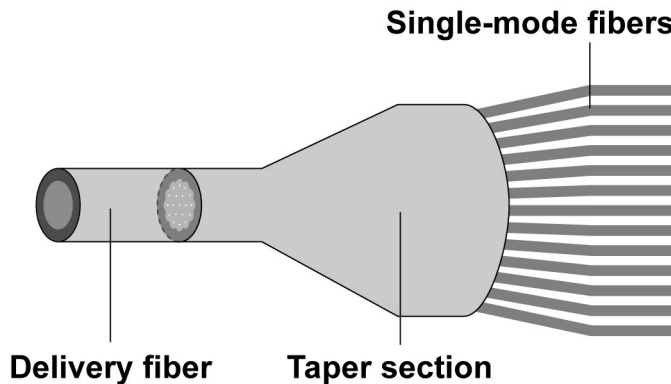


Figure 7.17: Schematic illustration of the photonic lantern. The right hand side shows the fused and tapered SM fiber bundle and the left hand side shows the MM fiber spliced to the tapered tip.

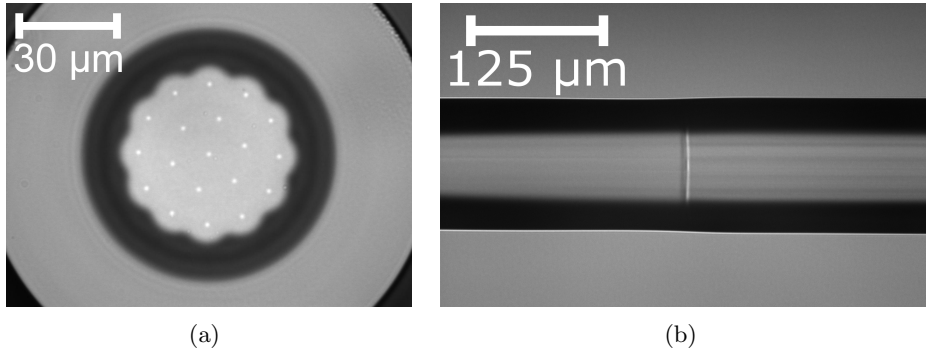


Figure 7.18: Microscope image of the cross section of the tapered MM tip of the photonic lantern. (b) Splice between the tapered MM tip of the photonic lantern (right side) and the $50\ \mu\text{m}$ core MM fiber.

to a step-index MM fiber with a core diameter of $50\ \mu\text{m}$ and an NA of 0.22 (Fiberguide Industries, USA [144]). A 5 m long length of MM fiber is used, ensuring that the fiber can reach the focal plane feed-optics of a telescope. Figure 7.18(b) shows an image of the splice.

At a wavelength of $1.53\ \mu\text{m}$ and for a core diameter of $50\ \mu\text{m}$, the 19 lowest order modes have an NA of ~ 0.085 . The core diameter and NA are chosen to sufficiently sample the seeing-limited telescope point-spread-function for the 4 m diameter Anglo-Australian Telescope [145].

MM to SM transmission efficiency of the 19 port photonic lantern

Three photonic lanterns were fabricated. Incoherent light from an ASE source centered at 1530 nm and with a 10 dB width of 40 nm is in turn spliced to each of the SM fiber ports of the photonic lanterns. The SM to MM transmission loss and the NA of the light out of the MM fiber is then measured for each port. The transmitted loss is measured with an integrating sphere and the NA is measured by scanning the far-field. Table 7.6 shows the average measured loss and NA, and the highest measured value for a single port in brackets.

Low loss from SM to MM is measured for all three fabricated devices. This is expected, since the degrees of freedom in the MM fiber are higher than in the SM fiber ensemble. The output NA matches well to the calculated NA of exciting the 19 lowest order modes.

Table 7.6: Average SM to MM transmission loss and average NA of the light out of the MM delivery fiber. The values in brackets show the highest measured value for a single port.

	Device #1	Device #2	Device #3
SM to MM loss [dB]	0.18 (0.36)	0.16 (0.27)	0.05 (0.07)
NA 95% power limit	0.097 (0.108)	0.107 (0.114)	0.095 (0.109)

MM to SM to MM transmission efficiency of the 19 port photonic lantern

Three devices are fabricated such that two devices #1 and #2 can be spliced back-to-back. Thereby, the MM to SM to MM transmission loss of a system with two photonic lanterns can be measured. Device #3 is used as an input source for coupling light into the two devices. For such a system to work it is important that the NA of the light is maintained through the 5 m long MM delivery fiber of Device #1. NA up-conversion is due to mode coupling to HOMs of the optical fiber, and is caused by scattering or translation variance of the fiber, i.e. micro bends, fiber imperfections or diameter fluctuations. Coupling to modes higher than the 19 lowest order modes will result in a loss in the photonic lantern.

In order to investigate that the MM fiber preserves NA, light from the 1530 nm ASE source delivered in an SMF-28 fiber is coupled into the MM fiber. The light coupled in has an NA of 0.106. Figure 7.19 shows the measured transmission loss and the NA out of the fiber at different coil diameter. The figure shows that the NA is well preserved down to a coil diameter of around 5 cm, where some of the high NA light is lost. Transmission loss increases around a coil diameter of 7 cm.

The MM to SM to MM transmission loss of the photonic lanterns is measured by splicing the 19 SM fibers of device #1 randomly to the 19 SM fibers of device #2. The loss is measured by launching light with a 1530 nm ASE source into the MM fiber of device #1 and measuring the power out of the MM fiber of device #2 with an integrating sphere. Figure 7.20(a) shows the measured loss at different launch NAs. The different launch NAs are obtained by NA filtering of the light source using step-index fibers with different mode field diameters (square points) and with the photonic lantern device #3 (circular points). From low to high the NA is obtained with the

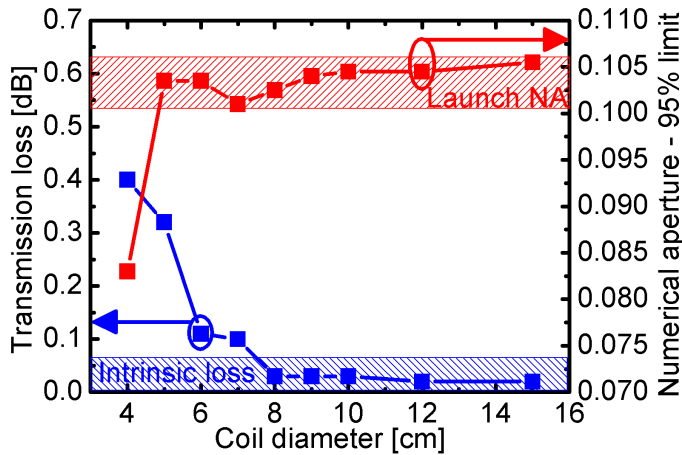
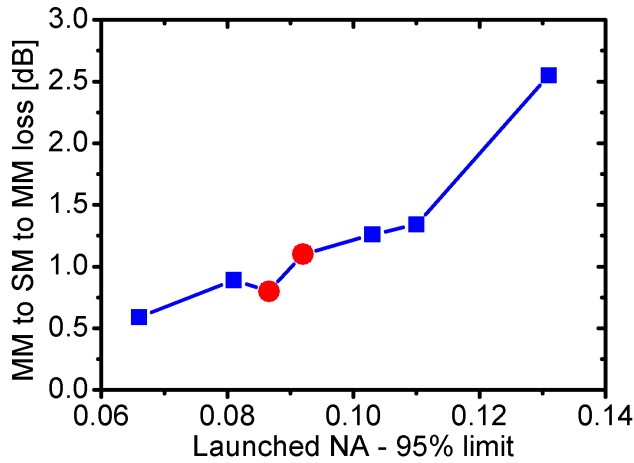


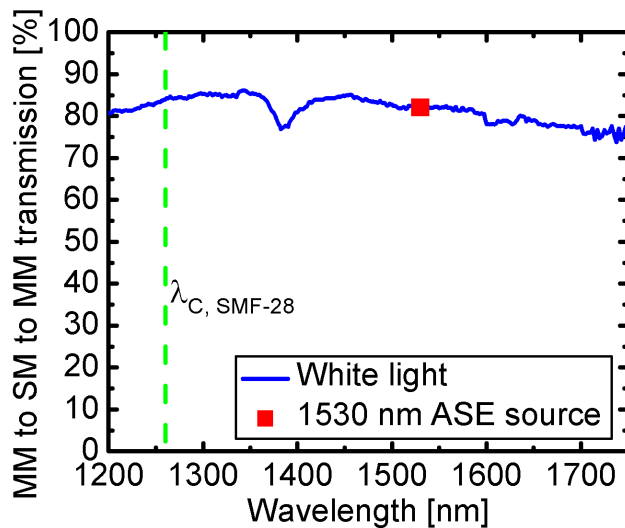
Figure 7.19: Transmission loss and NA dependence on the coiling diameter of the 5 m long $50\ \mu\text{m}$ core MM fiber.

following: $14\ \mu\text{m}$ core fiber, $10\ \mu\text{m}$ core fiber, low NA port of device #3 ($\text{NA}=0.087$), high NA port of device #3 ($\text{NA}=0.092$), SMF-28 fiber, HI1060 fiber and UHNA4 fiber. A loss below 1.1 dB is measured, when the launched NA is below 0.092.

The transmission loss of the two photonic lanterns in the back-to-back configuration is also characterized as a function of wavelength. This is done with the low NA port of device #3 as input and replacing the power meter with an optical spectrum analyzer and the ASE source with a white light source. Figure 7.20(b) shows the measured transmission (solid blue line). The transmission measurement made with the ASE source is indicated by the square and the cut-off wavelength for HOMs is indicated by the green dashed line. The transmission through the two devices is flat. A dip in transmission is observed at a wavelength of 1385 nm, which is attributed to the water absorption in the fibers.



(a)



(b)

Figure 7.20: (a) MM to SM to MM transmission loss through two photonic lanterns spliced back-to-back (Device #1 and #2) as a function of launched NA. The measurement is made with an ASE source centered at 1530 nm. (b) Spectral transmission through two photonic lanterns spliced back-to-back (solid blue line). The transmission measured with a 1530 nm ASE source is indicated by the red square. The dashed green line indicates the HOM cut-off wavelength of the SMF-28 fibers.

7.3 Summary of chapter 7

This chapter describes two fused optical components that have applications within astronomy. These components are a fused bundle of MM fibers or "hexabundle", and a MM to SM optical fiber splitter or "photonic lantern". The hexabundles are used for measuring the spectrum of extended objects such as galaxies or gas clouds, enabling a more detailed observation of these large astronomical objects. The photonic lanterns are developed for transforming MM starlight into an ensemble of SM fibers. This enables filtering of the light using advanced FBGs in the SM fibers. Both the 61 port hexabundles and the 19 port photonic lanterns are currently being tested on the 3.9 m Anglo-Australian Telescope in Australia.

Chapter 8

Conclusion

Since the first demonstration of a photonic crystal fiber (PCF) by Knight *et al.* in 1996, there has been a high interest in further developing the fiber and finding new application areas. Some of the promising types of PCF, that are currently receiving the most attention, are the nonlinear PCF and the rare-earth doped double-clad PCF. The nonlinear PCF is used for supercontinuum generation. These white light sources are today finding more and more applications within confocal microscopy, optical coherence tomography or as general light sources in the lab. The rare-earth doped double-clad PCFs are implemented as gain medium for high-power fiber lasers. Fiber lasers are interesting laser candidates for the material processing market, where they are finding more and more applications. Superior index control, large single-mode cores and pump cores without the need for low-index polymers, are some of the reasons why the PCF is interesting.

For the high-power fiber lasers based on the PCF technology to really become commercially successful, fully fused and monolithic fiber combiners are necessary. These enable the fabrication of laser systems, where free-space bulk optical coupling are not needed. Laser systems that make the PCF easy to use, are robust and have a stable operation. Such combiners for PCFs are described in this thesis.

Some of the applications of the combiners are also addressed in this thesis. These include the realization of high power fiber lasers. Both single-mode (SM) fiber lasers and the combining of these into a multi-mode (MM) format are realized. High power strictly SM fiber amplifier systems that rely on the fabricated pump/signal combiners are also described. Finally, two supercontinuum generation systems are described. In the first, the nonlinear

PCF is pumped by a gain-switched fiber laser. In the second, the pump is a low power pulsed seed laser that is amplified to high power in a PCF based amplifier.

The first combiners for the PCF technology described in this thesis, are monolithic, all-fiber, tapered pump combiners. The combiners consist of three main parts that are spliced together. These are a fused fiber bundle, a tapered bridging fiber and an air-clad delivery fiber. These combiners enable the fabrication of high-power fiber lasers. A 350 W fiber laser which is made possible by the use of a 61x1 or 1x1 pump combiner is described. Finally, supercontinuum generation with the air-clad fiber laser is described. A novel concept of gain-switching the fiber laser is demonstrated, that significantly broadens the supercontinuum generated spectra, compared to a pure continuous wave (CW) pumped system. In gain-switched operation a spectrum that spans from 500 nm to 2250 nm is achieved, when the -10 dBm/nm power limit is used. The total average output power of 17 W.

An all-fiber 7x1 signal combiner for incoherent laser beam combining is also described. The 7 input fibers are step-index single-clad fibers with a core diameter of 17 μm . The output fiber is a MM fiber with a core diameter of 100 μm . This signal combiner is not exclusively developed for the PCF technology. It can be used with any ytterbium-doped fiber laser, that can be coupled into the input fibers of the combiner with a low loss. In fact a demonstration is made with three standard double-clad fiber lasers from Rofin. With these lasers a maximum combined CW output power of 2.5 kW is reached. The M^2 value of the combined output is 6.5.

The main part of this Ph.D. project was to develop a monolithic pump/signal combiner for air-clad PCFs. Such a combiner with a 15 μm mode field diameter (MFD) polarization maintaining (PM) SM signal feed-through is described in this thesis. The enabling concept is a method for preserving the MFD in fiber tapers. The concept is described for 6 μm MFD feed-through and a 15 μm MFD PM feed-through. The 15 μm feed-through is demonstrated with both air-holes and F-doped rods as the second cladding. With this concept 12 μm feed-through and 15 μm feed-through combiners are developed. The 15 μm feed-through combiners are developed in two versions; one based on air-holes and one based on F-doped rods as the second cladding. The last of these are described in this thesis. They have an average pump and signal transmission loss of 0.13 dB and 0.52 dB, respectively. The polarization extinction ratio (PER) of the signal is >18 dB.

A fiber amplifier based on an active air-clad PCF is described. This

amplifier system is made possible by the developed pump/signal combiner. In the system, the combiner is used in a backward pumped configuration. The amplifier has a strictly SM signal output with an M^2 value <1.1 . A maximum average signal power of 17 W is reached when the system is seeded by 10 ps pulses, with a repetition rate of 80 MHz. The slope efficiency of the system is 53%.

Finally, supercontinuum generation with the air-clad fiber amplifier system is described. A supercontinuum with a total power of 5 W that spans from 470 nm and up to 2250 nm is generated. The spectrum is much broader than what is achieved with the gain-switched fiber laser. This is due to the higher peak-power of the amplifier system, which means that more visible light is generated. The supercontinuum generated by the gain-switched fiber laser does however have a higher average output power and a higher spectral power density at infrared wavelengths.

Although the focus of this Ph.D. thesis is on the fabrication of fused combiners for high-power fiber lasers and amplifiers, fused optical components with applications within astronomy are presented as well. These components are a fused bundle of MM fibers or hexabundle, and a MM to SM optical fiber splitter or photonic lantern. The hexabundles are used for measuring the spectrum of extended objects such as galaxies or gas clouds, enabling a more detailed observation of these large astronomical objects. The photonic lanterns are developed for transforming MM starlight into an ensemble of SM fibers. This enables filtering of the light using advanced fiber Bragg gratings (FBGs) in the SM fibers. Both of these devices are currently being tested on the 3.9 m Anglo-Australian Telescope in Australia.

Summing up, it is the hope of the author that the results obtained in this Ph.D. project can be used to further develop fused combiners for PCFs, and that these components will enable the fabrication of superior fiber laser and amplifier systems. It is also the hope that the work will give inspiration to research both at NKT Photonics and by external collaborators. Research that explores the integration of standard polymer-clad combiners with the PCF technology, different pump/signal combiner concepts for PCFs, and combiners with even larger MFD feed-through than what is presented in this thesis. All in all, so that the full power of the active PCFs can be unleashed.

Appendix A

Formula derivations

A.1 Minimum single-mode fiber taper length for a linear taper profile

For a linear taper profile, the taper slope (dr/dz) will be the same over the entire taper. The maximum beat length $L_{B,max}$ and the total taper ratio (TR) will therefore define the length of the taper (L) in order to be adiabatic. The taper ratio is here defined as $TR = \frac{r_1}{r_2}$, where r_1 and r_2 is the fiber core radius in the untapered and tapered end, respectively. Eq. 2.16 can be reduced to

$$\frac{dr}{dz} \leq \frac{r}{L_B} \tag{A.1}$$

↓

$$\frac{r_1 - r_2}{L} \leq \frac{r_2}{L_B} \tag{A.2}$$

↓

$$L \geq L_B \frac{r_1 - r_2}{r_2} \tag{A.3}$$

↓

$$\underline{L \geq (TR - 1)L_{B,max}} \tag{A.4}$$

In the right hand side of the above calculation, r is approximated by r_2 . This will give the largest value for the minimum taper length.

A.2 Minimum multi-mode fiber taper length for a linear taper profile

For a linear taper profile, the taper slope (dr/dz) will be the same over the entire taper. The fiber core radius in the untapered and tapered end are r_1 and r_2 , respectively. The corresponding fiber core diameter is D_1 and D_2 . Eq. 2.20 can be reduced to

$$\frac{dr}{dz} \leq \tan \theta_z / 2 \quad (\text{A.5})$$

↓

$$\frac{r_1 - r_2}{L} \leq \tan \theta_z / 2 \quad (\text{A.6})$$

↓

$$L \geq \frac{2(r_1 - r_2)}{\tan \theta_z} \quad (\text{A.7})$$

↓

$$L \geq \frac{D_1 - D_2}{\tan \theta_z} \quad (\text{A.8})$$

List of Acronyms

TIR	total internal reflection
PCF	photonic crystal fiber
MOF	microstructured optical fiber
MFD	mode field diameter
MM	multi-mode
SM	single-mode
BPP	beam parameter product
NA	numerical aperture
PM	polarization maintaining
PER	polarization extinction ratio
TEC	thermally expanded core
HOM	higher order mode
SBS	stimulated Brillouin scattering
SRS	stimulated Raman scattering
CW	continuous wave
SEM	scanning electron microscope
LMA	large mode area
MOPA	master oscillator power amplifier

FBG fiber Bragg grating

HR high reflector

OC output coupler

PIMMS photonic integrated multi-mode microspectrograph

ASE amplified spontaneous emission

Bibliography

- [1] D. Keck, R. Maurer, and P. Schultz, “On the ultimate lower limit of attenuation in glass optical waveguides,” *Appl. Phys. Lett.* **22**, 307–309 (1973).
- [2] J. Hecht, *City of Light: The Story of Fiber Optics* (Oxford University Press, 2004).
- [3] G. P. Agrawal, *Fiber-Optic Communication Systems* (John Wiley & Sons, Inc., New York, 2002).
- [4] J. Stone and C. Burrus, “Neodymiumdoped silica lasers in endpumped fiber geometry,” *Appl. Phys. Lett.* **23**, 388–389 (1973).
- [5] E. Snitzer, H. Po, F. Hakimi, R. Tumminelli, and B. C. McCollum, “Double clad, offset core Nd fiber laser,” in *Proceedings of Optical Fiber Sensors Conference*, PD5 (1988).
- [6] H. Po, E. Snitzer, R. Tumminelli, L. Zenteno, F. Hakimi, N. M. Cho, and T. Haw, “Double clad high brightness Nd fiber laser pumped by GaAlAs phased array,” in *Proceedings of Optical Fiber Communication Conference*, PD7 (1989).
- [7] J. LeGrange, E. Vogel, K. Quoi, D. J. DiGiovanni, A. Hale, R. Pedrazzani, and T. Strasser, “Optical reliability of cladding pump fiber for high power communication networks,” in *Proceedings of Military Communication Conference* **5335**, 690–693 (1999).
- [8] V. Bhagavatula, R. Bhat, G. E. Berkey, X. Chen, M. J. Dejneka, M. Gallagher, L. C. Hughes, K. W. Koch, J. Koh, M. J. Li, X. Liu, D. A. Nolan, M. H. Rasmussen, C. L. Tennent, N. Venkataraman, D. T. Walton, J. Wang, C. E. Zah, and L. A. Zenteno, “Progress in high power fiber lasers,” *Proc. SPIE* **5335**, 210–216 (2004).

- [9] K. Tankala, D. Guertin, J. Abramczyk, and N. Jacobson, "Reliability of low-index polymer coated double-clad fibers used in fiber lasers and amplifiers," *Optical Engineering* **50**, 111607 (2011).
- [10] J. C. Knight, T. A. Birks, P. S. J. Russell, and D. M. Atkin, "All-silica single-mode optical fiber with photonic crystal cladding," *Opt. Lett.* **21**, 1547–1549 (1996).
- [11] T. A. Birks, J. C. Knight, and P. S. J. Russell, "Endlessly single-mode photonic crystal fiber," *Opt. Lett.* **22**, 961–963 (1997).
- [12] P. Russell, "Photonic crystal fibers," *Science* **299**, 358–362 (2003).
- [13] M. D. Nielsen, J. R. Folkenberg, and N. Mortensen, "Singlemode photonic crystal fibre with effective area of $600 \mu\text{m}^2$ and low bending loss," *Electron. Lett.* **39**, 1802–1803 (2003).
- [14] D. J. DiGiovanni and R. S. Windeler, "Article comprising an air-clad optical fiber," U.S. Patent No. 5,907,652 (1999).
- [15] R. P. Espindola, R. S. Windeler, A. A. Abramov, B. J. Eggleton, T. A. Strasser, and D. J. DiGiovanni, "External refractive index insensitive air-clad long period fibre grating," *Electron. Lett.* **35**, 327–328 (1999).
- [16] W. J. Wadsworth, R. M. Percival, G. Bouwmans, J. C. Knight, T. A. Birks, T. D. Hedley, and P. S. J. Russell, "Very high numerical aperture fibers," *IEEE Photon. Technol. Lett.* **16**, 843–845 (2004).
- [17] J. Limpert, T. Schreiber, A. Liem, S. Nolte, H. Zellmer, T. Peschel, V. Guyenot, and A. Tünnermann, "Thermo-optical properties of air-clad photonic crystal fiber lasers in high power operation," *Opt. Express* **11**, 2982–2990 (2003).
- [18] K. P. Hansen, J. Broeng, K. Mattsson, M. D. Nielsen, T. Nikolajsen, P. M. W. Skovgaard, M. H. Sørensen, M. Denninger, C. Jakobsen, and H. R. Simonsen, "Airclad fiber laser technology," *Proc. SPIE* **6873**, 687307 (2008).
- [19] K. P. Hansen, C. B. Olausson, J. Broeng, D. Noordegraaf, M. D. Maack, T. T. Alkeskjold, M. Laurila, T. Nikolajsen, P. M. W. Skovgaard, M. H. Sørensen, M. Denninger, C. Jakobsen, and H. R. Simonsen, "Airclad fiber laser technology," *Opt. Engineering* **50**, 111609 (2011).

- [20] V. Gapontsev and I. Samartsev, "Coupling arrangement between a multi-mode light source and an optical fiber through an intermediate optical fiber length," U.S. Patent No., 5,999,673 (1999).
- [21] F. Hakimi and H. Hakimi, "A new side coupling method for double clad fiber amplifiers," in Proceedings of IEEE Conference on Lasers and Electro-Optics, paper CTuDP (2001).
- [22] Y. Sintov and P. Tikva, "Optical apparatus including pump guiding fiber and receiving fiber," U.S. Patent No., 7,277,612 (2007).
- [23] A. B. Grudinin, D. N. Payne, P. W. Turner, L. J. A. Nilsson, M. N. Zervas, M. Ibsen, and M. K. Durkin, "Multi-fibre arrangements for high power fibre lasers and amplifiers," U.S. Patent No., 6,826,335 (2004).
- [24] S. Norman, M. Zervas, A. Appleyard, P. Skull, D. Walker, P. Turner, and I. Crowe, "Power scaling of high power fiber lasers for micro-machining and materials processing applications," Proc. SPIE **6102**, 61021P (2006).
- [25] D. J. DiGiovanni and A. J. Stentz, "Tapered fiber bundles for coupling light into and out of cladding-pumped fiber devices," U.S. Patent No., 5,864,644 (1999).
- [26] A. Kosterin, V. Temyanko, M. Fallahi, and M. Mansuripur, "Tapered fiber bundles for combining high-power diode lasers," Appl. Opt. **43**, 3893–3900 (2004).
- [27] F. Gonthier, L. Martineau, N. Azami, M. Faucher, F. Séguin, D. Stryckman, and A. Villeneuve, "High-power all-fiber components: The missing link for high power fiber lasers," Proc. SPIE **5335**, 266–276 (2004).
- [28] F. Séguin, A. Wetter, L. Martineau, M. Faucher, C. Delisle, and S. Caplette, "Tapered fused bundle coupler package for reliable high optical power dissipation," Proc. SPIE **6102**, 61021N (2006).
- [29] A. Braglia, M. Olivero, A. Neri, and G. Perrone, "Fabrication of pump combiners for high power fiber lasers," Proc. SPIE **7914**, 79142V (2011).

- [30] M. Nakai, K. Shima, M. Saito, and T. Kitabayashi, "30W Q-SW fiber laser," Proc. SPIE **6453**, 645319 (2007).
- [31] F. Gonthier, L. Martineau, A. V. F. Seguin, M. Faucher, N. Azami, and M. Garneau, "Optical coupler comprising multimode fibers and method of making the same," U.S. Patent No., 7,046,875 (2006).
- [32] F. Gonthier, M. Garneau, and N. Vachon, "Multimode fiber outer cladding coupler for multi-clad fibers," U.S. Patent No., 7,933,479 (2011).
- [33] F. Gonthier, "Method and device for optically coupling optical fibres," U.S. Patent No., 7,539,377 (2009).
- [34] F. Gonthier, "Novel designs for pump and signal fiber combiners," Proc. SPIE **7580**, 758019 (2010).
- [35] A. Salokatve, "Means of coupling light into optical fibers and methods of manufacturing a coupler," U.S. Patent No., 7,991,255 (2011).
- [36] ITF Labs, <http://www.itflabs.com>.
- [37] Gooch and Housego, <http://www.goochandhousego.com>.
- [38] M. D. Nielsen, M. H. Sørensen, A. Liem, M. Kozak, and P. M. Skovgaard, "High power pcf-based pump combiners," Proc. SPIE **6453**, 64532C (2007).
- [39] M. D. Nielsen, P. M. W. Skovgaard, J. Broeng, and G. Vienne, "Optical coupler devices, methods of their production and use," U.S. Patent No., 7,526,165 (2007).
- [40] P. M. W. Skovgaard and M. D. Nielsen, "Optical coupler, a method of its fabrication and use," U.S. Patent No., 2008/0050069 (2008).
- [41] M. D. Nielsen and P. M. W. Skovgaard, "Optical coupler, a method of its fabrication and use," U.S. Patent No., 2009/0202204 (2009).
- [42] S. G. Leon-Saval, T. A. Birks, J. Bland-Hawthorn, and M. Englund, "Multimode fiber devices with single-mode performance," Opt. Lett. **30**, 2545–2547 (2005).

- [43] B. Saleh and M. Teich, *Fundamentals of photonics* (John Wiley & Sons, Inc., 1991).
- [44] D. Gloge, “Weakly guiding fibers,” *Appl. Opt.* **10**, 2252–2258 (1971).
- [45] G. Keiser, *Optical Fiber Communications* (McGraw Hill, 1991).
- [46] D. Marcuse, “Gaussian approximation of the fundamental modes of graded-index fibers,” *J. Opt. Soc. Am.* **68**, 103–109 (1978).
- [47] NKT Photonics, <http://www.nktphotonics.com/>.
- [48] J. Broeng, D. Mogilevstev, S. E. Barkou, and A. Bjarklev, “Effective area of photonic crystal fibers,” *Optical Fiber Technology* **5**, 305–330 (1999).
- [49] N. A. Mortensen, “Effective area of photonic crystal fibers,” *Opt. Express* **10**, 341–348 (2002).
- [50] N. A. Mortensen, J. R. Folkenberg, M. D. Nielsen, and K. P. Hansen, “Modal cutoff and the v parameter in photonic crystal fibers,” *Opt. Lett.* **28**, 1879–1881 (2003).
- [51] S. Johnson and J. Joannopoulos, “Block-iterative frequency-domain methods for Maxwell’s equations in a planewave basis,” *Opt. Express* **8**, 173–190 (2001).
- [52] A. D. Yablon, *Optical fiber fusion splicing* (Springer, 2005).
- [53] I. Hatakeyama and H. Tsuchiya, “Fusion splices for single-mode optical fibers,” *IEEE J. Quantum Electron.* **QE-14**, 614–619 (1978).
- [54] D. L. Bisbee, “Splicing silica fibers with an electric arc,” *Applied Optics* **15**, 796–798 (1976).
- [55] D. L. Bisbee, “Optical fiber joining technique,” *Bell Syst. Tech. J* **50**, 3153–3158 (1971).
- [56] J. T. Krause and C. R. Kurkjian, “Fibre splices with ‘perfect fibre’ strengths of 5.5 GPa, $v < 0.01$,” *Electron. Lett.* **21**, 533–535 (1985).
- [57] H. Fujita, Y. Suzaki, and A. Tachibana, “Optical fiber splicing technique with a CO₂ laser,” *Applied Optics* **15**, 320–321 (1976).

- [58] Vytran, <http://www.vytran.com>.
- [59] W. B and E. Mies, “Review of fabrication techniques for fused fiber components for fiber lasers,” Proc. SPIE **7195**, 71950A (2009).
- [60] A. W. Snyder and J. D. Love, *Optical waveguide theory* (Kluwer Academic, 1983).
- [61] W. J. Stewart and J. D. Love, “Design limitation on tapers and couplers in single mode fibres,” in Proceedings of European Conference on Optical Communication (1985).
- [62] J. D. Love and W. M. Henry, “Quantifying loss minimization in single-mode fibre tapers,” Electron. Lett. **22**, 912–914 (1986).
- [63] T. A. Birks and Y. W. Li, “The shape of fiber tapers,” Journal of Lightwave Technology **10**, 432–438 (1992).
- [64] M. D. Nielsen, N. A. Mortensen, J. R. Folkenberg, and A. Bjarklev, “Mode-field radius of photonic crystal fibers expressed by the V parameter,” Opt. Lett. **28**, 2309–2311 (2003).
- [65] W. R. McCluney, *Introduction to radiometry and photometry* (Artech House, 1994).
- [66] C. P. Halsted, “Brightness, luminance, and confusion,” Information Display (1993).
- [67] D. N. Payne, Y. Jeong, J. Nilsson, J. K. Sahu, D. B. S. Soh, C. Alegria, P. Dupriez, C. A. Codemard, V. N. Philippov, and V. Hernandez, “Kilowatt-class single-frequency fiber sources,” Proc. SPIE **5709**, 133–141 (2005).
- [68] A. Tünnermann, T. Schreiber, F. Röser, A. Liem, S. Höfer, H. Zellmer, S. Nolte, and J. Limpert, “The renaissance and bright future of fibre lasers,” J. Phys. B: At. Mol. Opt. Phys. **38**, S681–S693 (2005).
- [69] A. Carter and E. Li, “Recent progress in high-power fiber lasers for high-power and high-quality material processing applications,” Proc. SPIE **6344**, 63440F (2006).
- [70] D. Bayart and L. Berthelot, “Optical coupler for a multimode pump,” U.S. Patent No., 6,778,562 (2004).

- [71] J. J. Larsen, C. F. Pedersen, and G. Vienne, "Side-pumping of double-clad photonic crystal fibers," *Proc. SPIE* **5335**, 202–209 (2004).
- [72] J. J. Larsen and G. Vienne, "Side pumping of double-clad photonic crystal fibers," *Opt. Lett.* **29**, 436–438 (2004).
- [73] D. Noordegraaf, M. D. Nielsen, P. M. W. Skovgaard, S. Agger, K. P. Hansen, J. Broeng, C. Jakobsen, H. R. Simonsen, and J. Lægsgaard, "Pump combiner for air-clad fiber with PM single-mode signal feed-through," in *Proceedings of IEEE Conference on Lasers and Electro-Optics* (2009).
- [74] D. Noordegraaf, M. D. Maack, P. M. W. Skovgaard, S. Agger, T. T. Alkeskjold, and J. Lægsgaard, "7+1 to 1 pump/signal combiner for air-clad fiber with 15 μm MFD PM single-mode signal feed-through," *Proc. SPIE* **7580**, 75801A (2010).
- [75] B. G. Ward, D. L. S. Jr., and J. D. Tafoya, "A monolithic pump signal multiplexer for air-clad photonic crystal fiber amplifiers," *Proc. SPIE* **7580**, 75801C (2010).
- [76] S. R. Karlsen, R. K. Price, M. Reynolds, A. Brown, R. Mehl, S. Patterson, and R. J. Martinsen, "100-W, 105- μm , 0.15NA fiber coupled laser diode module," *Proc. SPIE* **7198**, 71980T (2009).
- [77] V. Gapontsev, N. Moshegov, P. Trubenko, A. Komissarov, I. Berishev, O. Raisky, N. Strougov, V. Chuyanov, O. Maksimov, and A. Ovtchinnikov, "High-brightness 9XX-nm pumps with wavelength stabilization," *Proc. SPIE* **7583**, 75830A (2010).
- [78] R. Duesterberg, L. Xu, J. A. Skidmore, J. Guo, J. Cheng, J. Du, B. Johnson, D. L. Vecht, N. Guerin, B. Huang, D. Yin, P. Cheng, R. Raju, K. W. Lee, J. Cai, V. Rossin, and E. P. Zucker, "100W high-brightness multi-emitter laser pump," *Proc. SPIE* **7918**, 79180V (2011).
- [79] V. Gapontsev, D. Gapontsev, N. Platonov, . Shkurikhin, V. Fomin, A. Mashkin, M. Abramov, and S. Ferin, "2 kW CW ytterbium fiber laser with record diffraction-limited brightness," in *Proceedings of IEEE Conference on Lasers and Electro-Optics Europe* (2005).

- [80] V. Gapontsev, I. Berishev, G. Ellis, A. Komissarov, N. Moshegov, A. Ovtchinnikov, O. Raisky, P. Trubenko, V. Ackermann, and E. Shcherbakov, "9xx nm single emitter pumps for multi-kW systems," *Proc. SPIE* **6104**, 61040K (2006).
- [81] D. A. V. Kliner, K. Chong, J. Franke, T. Gordon, J. Gregg, W. Gries, H. Hu, H. Ishiguroa, V. Issier, B. Kharlamov, A. Kliner, M. Kobayashi, K.-H. Liao, J. Lugo, J. Luu, D. Meng, J. J. Morehead, M. H. Muendel, L. E. Myers, K. Nguyen, H. Sakoa, K. Schneider, J. Segall, K. Shigeoka, R. Srinivasan, D. Tucker, D. Woll, D. L. Woods, H. Yu, and C. Zhang, "4-kW fiber laser for metal cutting and welding," *Proc. SPIE* **7914**, 791418 (2011).
- [82] P. Yan, S. Yin, J. He, C. Fu, Y. Wang, and M. Gong, "1.1-kW ytterbium monolithic fiber laser with assembled end-pump scheme to couple high brightness single emitters," *IEEE Phot. Tech. Lett.* **23**, 697–699 (2011).
- [83] J. W. Dawson, M. J. Messerly, R. J. Beach, M. Y. Shverdin, E. A. Stappaerts, A. K. Sridharan, P. H. Pax, J. E. Heebner, C. W. Siders, and C. P. J. Barty, "Analysis of the scalability of diffraction-limited fiber lasers and amplifiers to high average power," *Opt. Express* **16**, 13240–1326 (2008).
- [84] R. H. Stolen, E. P. Ippen, and A. R. Tynes, "Raman oscillation in glass optical waveguide," *Appl. Phys. Lett.* **20**, 62–64 (1972).
- [85] A. V. Smith and B. T. Do, "Bulk and surface laser damage of silica by picosecond and nanosecond pulses at 1064 nm," *Appl. Opt.* **47**, 4812–4832 (2008).
- [86] A. A. Said, T. Xia, A. Dogariu, D. J. Hagan, M. J. Soileau, E. W. V. Stryland, and M. Mohebi, "Measurement of the optical damage threshold in fused quartz," *Appl. Opt.* **34**, 3374–3376 (1995).
- [87] R. Kashyap and K. J. Blow, "Observation of catastrophic self-propelled self-focusing in optical fibres," *Electron. Lett.* **24**, 47–49 (1988).
- [88] R. L. Farrow, D. A. V. Kliner, G. R. Hadley, and A. V. Smith, "Peak-power limits on fiber amplifiers imposed by self-focusing," *Opt. Lett.* **31**, 3423–3425 (2006).

- [89] N. S. Platonov, D. V. Gapontsev, V. P. Gapontsev, and V. Shumilin, "135W CW fiber laser with perfect single mode output," in Proceedings of IEEE Conference on Lasers and Electro-Optics, CPDC3 (2002).
- [90] J. Limpert, A. Liem, H. Zellmer, and A. Tünnermann, "500W continuous-wave fiber laser with excellent beam quality," *Electron. Lett.* **39**, 645–647 (2003).
- [91] C.-H. Liu, A. Galvanauskas, B. Ehlers, F. Doerfel, S. Heinemann, A. Carter, K. Tankala, and J. Farroni, "810W single transverse mode Yb-doped fiber laser," Proc. Advanced Solid-State Photonics, Post-deadline Paper PDP17 (2004).
- [92] Y. Jeong, J. Sahu, D. Payne, and J. Nilsson, "Ytterbium-doped large-core fiber laser with 1.36 kW continuous-wave output power," *Opt. Express* **12**, 6088–6092 (2004).
- [93] D. Gapontsev, "6kW CW single mode Ytterbium fiber laser in all-fiber format," Proc. Solid State and Diode Laser Technology Review (2008).
- [94] T. Y. Fan, "Laser beam combining for high-power, high-radiance sources," *IEEE J: Sel. Top. Quantum Electron.* **11**, 567–577 (2005).
- [95] T. H. Loftus, A. Liu, P. R. Hoffman, A. M. Thomas, M. Norsen, R. Royse, and E. Honea, "522 W average power, spectrally beam-combined fiber laser with near-diffraction-limited beam quality," *Opt. Lett.* **32**, 349–351 (2007).
- [96] C. Wirth, O. Schmidt, I. Tsybin, T. Schreiber, T. Peschel, F. Brückner, T. Clausnitzer, J. Limpert, R. Eberhardt, A. Tünnermann, M. Gowin, E. ten Have, K. Ludewigt, and M. Jung, "2 kW incoherent beam combining of four narrow-linewidth photonic crystal fiber amplifiers," *Opt. Express* **17**, 1178–1183 (2009).
- [97] Y. Shamir, Y. Sintov, and M. Shtaif, "Incoherent beam combining of multiple single-mode fiber lasers utilizing fused tapered bundling," *Proc. SPIE* **7580** (2010).
- [98] M. Muendel, R. Farrow, K.-H. Liao, D. Woll, J. Luu, C. Zhang, J. J. Morehead, J. Segall, J. Gregg, K. Tai, B. Kharlamov, H. Yu,

- and L. Myers, "Fused fiber pump- and signal-combiners for a 4-kW Ytterbium fiber-laser," Proc. SPIE **7914**, 791431-1 (2011).
- [99] JDSU, <http://www.jdsu.com>.
- [100] Oclaro, <http://www.oclaro.com>.
- [101] Laserline, <http://www.laserline.de>.
- [102] T. Schreiber, J. Limpert, H. Zellmer, A. Tünnermann, and K. P. Hansen, "High average power supercontinuum generation in photonic crystal fibers," Opt. Commun. **228**, 71-78 (2003).
- [103] J. Dudley, G. Genty, and S. Coen, "Supercontinuum generation in photonic crystal fiber," Rev. Mod. Phys. **78**, 1135 (2006).
- [104] J. Travers, "Blue extension of optical fibre supercontinuum generation," J. Opt. **12**, 113001 (2010).
- [105] C. Larsen, D. Noordegraaf, P. M. W. Skovgaard, K. P. Hansen, K. E. Mattsson, and O. Bang, "Gain-switched CW fiber laser for improved supercontinuum generation in a PCF," Opt. Express **19**, 14883-14891 (2011).
- [106] C. Larsen, D. Noordegraaf, P. M. W. Skovgaard, K. P. Hansen, K. E. Mattsson, and O. Bang, "Supercontinuum generation in a photonic crystal fiber pumped by a gain-switched high-power fiber laser," in Proceedings of IEEE Conference on Lasers and Electro-Optics (2011).
- [107] D. Carlson, "Dynamics of a repetitively pump-pulsed Nd:YAG laser," J. Appl. Phys. **39**, 4369-4374 (1968).
- [108] L. Zenteno, E. Snitzer, H. Po, R. Tumminelli, and F. Hakimi, "Gain switching of a Nd³⁺-doped fiber laser," Opt. Lett. **14**, 671-673 (1989).
- [109] P. Beaud, W. Hodel, B. Zysset, and H. P. Weber, "Ultrashort pulse propagation, pulse breakup, and fundamental soliton formation in a single-mode optical fiber," IEEE J. Quantum Electron. **23**, 1938-1946 (1987).
- [110] S. T. Sørensen, A. Judge, C. L. Thomsen, and O. Bang, "Optimum fiber tapers for increasing the power in the blue edge of a supercontinuum - group-acceleration matching," Opt. Lett. **36**, 816-818 (2011).

- [111] J. C. Travers, A. B. Rulkov, B. A. Cumberland, S. V. Popov, and J. R. Taylor, “Visible supercontinuum generation in photonic crystal fibers with a 400 W continuous wave fiber laser,” *Opt. Express* **16**, 14435–14447 (2008).
- [112] A. Kudlinski, G. Bouwmans, O. Vanvincq, Y. Quiquempois, A. L. Rouge, L. Bigot, G. Mélin, and A. Mussot, “White-light CW-pumped supercontinuum generation in highly GeO₂-doped-core photonic crystal fibers,” *Opt. Lett.* **34**, 3631–3633 (2009).
- [113] Optoskand, <http://www.optoskand.se>.
- [114] Rofin, <http://www.rofin.com>.
- [115] Primes, <http://www.primes.de>.
- [116] K. B. Sparks, *Optical fiber with low taper induced loss*, vol. 7,046,890 (U.S. Patent No., 2006).
- [117] W. R. Holland and T. F. Taunay, *Fiber based laser combiners*, vol. 12/760,547 (U.S. Patent Appl. No., 2010).
- [118] D. Noordegraaf, M. D. Maack, P. M. W. Skovgaard, M. H. Sørensen, J. Broeng, and J. Lægsgaard, “Mode field diameter preserving fiber tapers,” *Opt. Lett.* (2011).
- [119] B. J. Eggleton, P. S. Westbrook, R. S. Windeler, S. Spälter, and T. A. Strasser, “Grating resonances in air-silica microstructured optical fibers,” *Opt. Lett.* **24**, 1460–1462 (1999).
- [120] J. Koponen, M. Söderlund, H. J. Hoffman, D. Kliner, and J. Koplów, “Photodarkening measurements in large-mode-area fibers,” *Proc. SPIE* **6453**, 64531E (2007).
- [121] K. E. Mattsson, S. N. Knudsen, B. Cadier, and T. Robin, “Photo darkening in ytterbium co-doped silica material,” *Proc. SPIE* **6873**, 68731C (2008).
- [122] S. Barden, L. W. Ramsey, and R. J. Truax, “Evaluation of some fiber optical waveguides for astronomical instrumentation,” *Publ. Astron. Soc. Pac.* **93**, 154–162 (1981).

- [123] P. M. Gray, "Astronomical uses of optical fibres at the anglo-australian observatory," *Proc. SPIE* **374**, 160–164 (1983).
- [124] J. Bland-Hawthorn, J. Bryant, G. Robertson, P. Gillingham, J. O'Byrne, G. Cecil, R. Haynes, S. Croom, S. Ellis, M. Maack, P. Skovgaard, and D. Noordegraaf, "Hexabundles: imaging fibre arrays for low-light astronomical applications," *Proc. SPIE* **7735** (2010).
- [125] J. J. Bryant, J. W. O'Byrne, J. Bland-Hawthorn, and S. G. Leon-Saval, "Hexabundles: first results," *Proc. SPIE* **7735**, 77350O–1 (2010).
- [126] J. Bland-Hawthorn, J. Bryant, G. Robertson, P. Gillingham, J. O'Byrne, G. Cecil, R. Haynes, S. Croom, S. Ellis, M. Maack, P. Skovgaard, and D. Noordegraaf, "Hexabundles: imaging fiber arrays for low-light astronomical applications," *Opt. Express* **19**, 2649–2661 (2011).
- [127] J. J. Bryant, J. Bland-Hawthorn, and S. G. Leon-Saval, "Hexabundles - Imaging fibre bundles for astronomy," in *Proceedings of IEEE Conference on Lasers and Electro-Optics Europe* (2011).
- [128] J. Bland-Hawthorn, M. Englund, and G. Edvell, "New approach to atmospheric OH suppression using an aperiodic fibre bragg grating," *Opt. Express* **12**, 5902–5909 (2004).
- [129] J. Bland-Hawthorn, A. Buryak, and K. Kolossovski, "Optimization algorithm for ultrabroadband multichannel aperiodic fiber Bragg grating filters," *J. Opt. Soc. Am. A* **25**, 153–158 (2008).
- [130] J. Bland-Hawthorn, J. Lawrence, G. Robertson, S. Campbell, B. Pope, C. Betters, S. Leon-Saval, T. Birks, R. Haynes, N. Cvetojevic, and N. Jovanovic, "PIMMS: photonic integrated multimode microspectrograph," *Proc. SPIE* **7735**, 77350N (2010).
- [131] N. Cvetojevic, J. Lawrence, S. Ellis, J. Bland-Hawthorn, R. Haynes, and A. Horton, "Characterization and on-sky demonstration of an integrated photonic spectrograph for astronomy," *Opt. Express* **17**, 18643–18650 (2009).
- [132] D. Noordegraaf, P. M. Skovgaard, M. D. Nielsen, and J. Bland-Hawthorn, "Efficient multi-mode to single-mode coupling in a photonic lantern," *Opt. Express* **17**, 1988–1994 (2009).

- [133] D. Noordegraaf, P. M. W. Skovgaard, M. D. Nielsen, J. Bland-Hawthorn, R. Haynes, and J. Lægsgaard, “Multi-mode to single-mode conversion in a 61 port photonic lantern,” *Opt. Express* **18**, 4673–4678 (2010).
- [134] D. Noordegraaf, P. M. W. Skovgaard, R. S. Helmsby, M. D. Maack, J. Bland-Hawthorn, J. Lawrence, and J. Lægsgaard, “19 port photonic lantern with multi-mode delivery fiber,” Submitted to *Opt. Lett.* (2011).
- [135] T. A. Birks, A. Diez, J. L. Cruz, S. G. Leon-Saval, and D. F. Murphy, “Fibers are looking up: optical fiber transition structures in astrophotonics,” in *Frontiers in Optics, OSA Technical Digest (CD)*, paper FTuU1 (2010).
- [136] R. R. Thomson, T. A. Birks, S. G. Leon-Saval, A. K. Kar, and J. Bland-Hawthorn, “Ultrafast laser inscription of an integrated photonic lantern,” *Opt. Express* **19**, 5698–5705 (2011).
- [137] I. Spaleniak, N. Jovanovic, S. Gross, M. Ireland, J. Lawrence, and M. Withford, “Exploration of integrated photonic lanterns fabricated by femtosecond laser inscription,” in *Proceedings of IEEE Conference on Lasers and Electro-Optics Pacific Rim* (2011).
- [138] D. B. Mortimore and J. W. Arkwright, “Monolithic wavelength-flattened 1x7 single-mode fused coupler,” *Electron. Lett.* **25**, 606–607 (1989).
- [139] S. G. Leon-Saval, A. Argyros, and J. Bland-Hawthorn, “Photonic lanterns: a study of light propagation in multimode to single-mode converters,” *Opt. Express* **18**, 8430–8439 (2010).
- [140] OFS Fitel, <http://www.ofsoptics.com>.
- [141] S. G. Leon-Saval, A. Argyros, and J. Bland-Hawthorn, “Mode evolution in photonic lanterns,” in *Frontiers in Optics, OSA Technical Digest (CD)*, paper FWA4 (2010).
- [142] S. G. Leon-Saval, A. Argyros, and J. Bland-Hawthorn, “Photonic lantern mode evolution: A multicore geometry study,” *Communications and Photonics Conference and Exhibition* pp. 697–698 (2010).

- [143] Corning, <http://www.corning.com>.
- [144] Fiberguide Industries, <http://www.fiberguide.com>.
- [145] S. C. Ellis, J. Bland-Hawthorn, J. S. Lawrence, J. Bryant, R. Haynes, A. Horton, S. Lee, S. Leon-Saval, H.-G. Löhmannsröben, J. Mladenoff, J. O’Byrne, W. Rambold, M. Roth, and C. Trinh, “GNOSIS: an OH suppression unit for near-infrared spectrographs,” *Proc. SPIE* **7735**, 773516 (2010).